

https://dspace.org/

Application of stochastic orebody simulation techniques to assess geological volume and grade uncertainty for gold reef deposits

Chanderman, Lisa

2017

http://hdl.handle.net/10539/23453

Chanderman, Lisa (2017) Application of stochastic orebody simulation techniques to assess geological volume and grade uncertainty for Gold Reef deposits, University of the Witwatersrand <http://hdl.handle.net/10539/23453>

Downloaded from a DSpace repository. https://dspace.org/



Application of Stochastic Orebody Simulation Techniques to assess Geological Volume and Grade Uncertainty for Gold Reef Deposits

Lisa Chanderman

School of Mining Engineering

University of the Witwatersrand

Johannesburg, South Africa

Supervisor (Johannesburg): Professor Richard Minnitt

Supervisor (Canada): Professor Roussos Dimitrakopoulos

A Dissertation submitted to the Faculty of Engineering and the Built Environment, University of the Witwatersrand, in fulfilment of the requirements for the Degree of Masters in Engineering by research only and to the Stochastic Mine Planning Laboratory, McGill University as part of the COSMO scholarship in Mine Planning under uncertainty

Johannesburg, 2017

DECLARATION

I declare that this dissertation is my own unaided work. It is being submitted for the Degree of Master of Science in Engineering in the University of the Witwatersrand, Johannesburg. The work was conducted as part of the requirements for the Consortium Scholarship in Geostatistics and Mine Planning Optimisation with Uncertainty awarded by the COSMO Stochastic Mine Planning Laboratory at McGill University, Canada. This work has not been submitted before for any degree or examination to any other University.

The information used in this research was obtained from AngloGold Ashanti as part of the Scholarship. Information regarded as confidential has been excluded from this dissertation.

_____

Lisa Chanderman

_____ day of _____ 2017

I ABSTRACT

This dissertation discusses the use of stochastic orebody modelling techniques for assessing geological uncertainty associated with gold mineralisation at Geita Gold Mine in Tanzania, and proposes a practical methodology that can be applied to similar studies. As part of the pre-feasibility stage studies for underground mining at Geita, stochastic simulations were required to assess the geological uncertainty associated with isolating (modelled) high grade lenses that occur within the known low grade mineralisation currently targeted for underground mining. Two different simulation techniques are applied in this research: Sequential Indicator Simulation to generate lithofacies realisations from which to assess ore category boundaries and shapes for use in quantifying volumetric uncertainty; and Direct Block Simulations to simulate gold grade realisations from which to assess grade uncertainty. This study identified potential upside and downside mine planning scenarios for volumes and total metal content from the ore category and grade simulations respectively. The findings of the results demonstrated that the high grade zones are much more broken up and discontinuous than the currently modelled high grade shape. The current business case uses a probabilistic high grade shape based on a single grade indicator and a probability choice of 50 percent as the threshold for high grade. The results of the study consider a simulation of possible outcomes based on the same threshold grade indicator and hence quantify the uncertainty or total geological risk. This geological risk may be introduced to mine designs, production schedules and NPV predictions The stochastic workflowdeveloped can be applied to analogous deposit types to assess the risk related to geological uncertainty. The work includes a description of practical considerations to be accounted for when applying the techniques.

Keywords: **stochastic orebody modelling, geological uncertainty, mine planning**

II PREFACE

Parts of this dissertation are in the publication process.

Chapters 1, 2 and 3 are composed in part by Chanderman, L. and Minnitt, R.C.A., *Need for stochastic orebody modelling approaches to assess geological uncertainty and risk in the South African mining industry*, to be submitted to the International Journal of Mining, Reclamation and Environment.

Chapters 4, 5 and 6 are composed in part by Chanderman, L., Minnitt, R.C.A. and Dimitrakopoulos, R., *Application of Stochastic Orebody simulation Techniques to assess Geological Volume and Grade Uncertainty for Gold Reef Deposits*, to be submitted to the Journal of Mathematical Geosciences.

III ACKNOWLEDGEMENTS

I would like to thank my supervisors: Professor R.C.A. Minnitt of the School of Mining Engineering at the University of the Witwatersrand, and Professor Roussos Dimitrakopoulos of the Stochastic Mine Planning Laboratory at McGill University for entrusting me with the Consortium Scholarship in Geostatistics and Mine Planning Optimisation with Uncertainty.

I would also like to thank Mr Vaughan Chamberlain - Senior Vice President: Strategic Technical Group at AngloGold Ashanti for reviewing this research and Datamine for offering their software for use in the study.

A special thank you is given to the technical experts from AngloGold Ashanti who assisted with the validation of this study and provided regular software assistance: Mr Vasu Govindsammy - Senior Manager Resource Evaluation; Mrs Yelena van der Grijp - Specialist Evaluation Geologist, and Mrs Samantha Reid - Specialist Evaluation Geologist.

I would also like to thank the team at the COSMO lab in McGill for making my stay in Montreal wonderful.

Author

Lisa Chanderman

IV LIST OF FIGURES

Figure 2-1: Reality in the ore deposit is partially accessible through drilling information; uncertainty associated with in-situ grade and geological variability is captured in multiple realisations (Dimitrakopoulos, 1998, pp 174). 16
Figure 2-2: Mapping the space of response uncertainty (Dimitrakopoulos, 1998, pp 175)..... 17
Figure 3-1: View of the Geita Hill pits showing the existing interpretation for the location and extent of higher grade lenses (red wireframe) within the known low grade mineralisation (green wireframe). 34
Figure 3-2: East-West section through the Geita Hill pits showing the preliminary mining stope layouts (purple wireframe) targeting higher grade lenses below the pit. 35
Figure 3-3: A simplified geological map for the Lake Victoria Region showing the main geological units. *SU*Sukumaland Greenstone Belt, *NZ*Nzega Greenstone Belt, *SM*Shyninanga-Malita Greenstone Belt, *IS*Iramba-Sekenke Greenstone Belt, *KF*Kilimafedha Greenstone Belt, *MM*Musoma-Mara Greenstone Belt. Super-terrane boundaries include: *ELVST* East Lake Victoria, *MLEST* Mwanza Lake Eyasi, *LNST* Lake Nyanza, *MMST*Moyowosi-Manyoni, *DBST* Dodoma Basement, *MAST*MbuluMasai, *NBT*Nyakahura-Burigi. Inset map of Africa showing the location of Archean blocks (Sanislav, Brayshaw, Kolling, Dirks, Cook, & Blenkinsop, 2016, pp 2). 36
Figure 3-4: Geological map of the Geita Greenstone Belt (Sanislav, Brayshaw, Kolling, Dirks, Cook, & Blenkinsop, 2016, pp 3)..... 37
Figure 3-5: Geological map of the Geita Hill West gold deposit. The background of the map (thin grey lines) represents the pit wireframe. (Sanislav, Brayshaw, Kolling, Dirks, Cook, & Blenkinsop, 2016, pp. 6)..... 38
Figure 3-6: Reef Thrust Geometry. The portion of the reef forming the Geita Hill deposit is highlighted in yellow. The deposit is divided into Geita Hill East and Geita Hill West. Geita Hill East if further differentiated into GHE West and GHE East. .. 39
Figure 3-7: View of the entire study area in relation to the pit and low grade ore wireframe. The drill holes are displayed according to grade values. Holes highlighted in yellow were excluded from the study. 40
Figure 3-8: W-E section through Geita Hill pits showing the sample information available in the GHEE sub area. 41

Figure 3-9: W-E section through Geita Hill pits showing the sample information available in the GHEW sub area. 42
Figure 3-10: East SIS directional variogram models 47
Figure 3-11: West SIS directional variogram models 47
Figure 3-12: East SIS variogram validation. Variograms for data is indicated as solid lines (red, green and blue) for each anisotropic direction. Variogram models for each realisation is indicated by black lines. 51
Figure 3-13: West SIS variogram validation. Variograms for data is indicated as solid lines (red, green and blue) for each anisotropic direction. Variogram models for each realisation is indicated by black lines. 51
Figure 3-14: 3D view of resultant noisy simulation 52
Figure 3-15: Section views showing the effect of using the same model variogram parameters and conditional data composited to 1m (left) and 3m (right). 54
Figure 3-16: Section view through SIS realisations for GHEW run using conditioning data composited to 1m (left) and 3m (right), using the same variogram model parameters 55
Figure 3-17: East SIS variogram validation. Variograms for data is indicated as solid lines (red, green and blue) for each anisotropic direction. Variogram models for each realisation is indicated by black lines. 56
Figure 3-18: West SIS variogram validation. Variograms for data is indicated as solid lines (red, green and blue) for each anisotropic direction. Variogram models for each realisation is indicated by black lines. 56
Figure 3-19: Recommended workflow for simulating grades using DBSim in ISATIS (ISATIS user manual, 2016) 58
Figure 3-20: Raw Gold Grade distributions for conditioning data 59
Figure 3-21: Transformed Grade distributions for conditioning data 60
Figure 3-22: Variogram model fitting for GHEE High Grade Gaussian Gold variables in 3 anisotropic directions. Experimental pairs of data are indicated as green points in each figure. The solid coloured lines represent the variogram models. 62
Figure 3-23: Variogram model fitting for GHEE Low Grade Gaussian Gold variables in 3 anisotropic directions. Experimental pairs of data are indicated as green points in each figure. The solid coloured lines represent the variogram models. 62

Figure 3-24: Variogram model fitting for GHEWHigh Grade Gaussian Gold variablesin 3 anisotropic directions. Experimental pairs of data are indicated as green points in each figure. The solid coloured lines represent the variogram models. 63
Figure 3-25: Variogram model fitting for GHEWLow Grade Gaussian Gold variables in 3 anisotropic directions. Experimental pairs of data are indicated as green points in each figure. The solid coloured lines represent the variogram models. 63
Figure 3-26: Regularised Block Variogram model fit on Gaussian point variables for GHEE High Grade. 65
Figure 3-27: Regularised Block Variogram model fit on Gaussian point variables for GHEE Low Grade. 65
Figure 3-28: Regularised Block Variogram model fit on Gaussian point variables for GHEW High Grade. 66
Figure 3-29: Regularised Block Variogram model fit on Gaussian point variables for GHEW Low Grade 66
Figure 3-30: GHEE high grade data variogram models (red, green and blue lines) against variograms for simulated realisations (black lines) 69
Figure 3-31: GHEE low grade data variogram models (red, green and blue lines) against variograms for simulated realisations (black lines) 69
Figure 3-32: GHEW high grade data variogram model (red, green and blue lines) against variograms for simulated realisations (black lines) 70
Figure 3-33: GHEW low grade data variogram models (red, green and blue lines) against variograms for simulated realisations (black lines) 70
Figure 3-34: Grade tonnage curve comparison for raw data and DBSim point realisations: GHEE HG (top left), GHEE LG (top right), GHEW HG (bottom left) and GHEW LG (bottom right). 71
Figure 3-35: Schematic showing the logic behind combining SIS and DBSim realisations to give an indication of potential joint uncertainty 75
Figure 3-36: Description of a conceptual deterministic workflow for the study area 77
Figure 3-37: Description of the stochastic workflow followed for the study area ... 77
Figure 4-1: Legends used to display gold grades and simulated indicators 78

Figure 4-2: Plan view showing the location of cross sections (E1-E5) through GHEE to compare upside and downside scenarios for the SIS realisations on the 5m x 5m x 3,333m simulation grid. 79
Figure 4-3: Section view (E1) showing the potential downside scenario (left) and upside scenario (right) based on ranked SIS realisations for GHEE using a 5m x 5m x 3,333m simulation grid. IK high grade wireframe for the deposit is depicted by black outlines. 80
Figure 4-4: Section view (E2) showing the potential downside scenario (left) and upside scenario (right) based on ranked SIS realisations for GHEE using a 5m x 5m x 3,333m simulation grid. IK high grade wireframe for the deposit is depicted by black outlines. 80
Figure 4-5: Section view (E3) showing the potential downside scenario (left) and upside scenario (right) based on ranked SIS realisations for GHEE using a 5m x 5m x 3,333m simulation grid. IK high grade wireframe for the deposit is depicted by black outlines. 81
Figure 4-6: Section view (E4) showing the potential downside scenario (left) and upside scenario (right) based on ranked SIS realisations for GHEE using a 5m x 5m x 3,333m simulation grid. IK high grade wireframe for the deposit is depicted by black outlines. 81
Figure 4-7: Section view (E5) showing the potential downside scenario (left) and upside scenario (right) based on ranked SIS realisations for GHEE using a 5m x 5m x 3,333m simulation grid. IK high grade wireframe for the deposit is depicted by black outlines. 82
Figure 4-8: Plan view showing the location of cross sections (W1-W7) through GHEW to compare upside and downside scenarios for the SIS realisations on the 5m x 5m x 3,333m simulation grid. 82
Figure 4-9: Section view (W1) showing the potential downside scenario (left) and upside scenario (right) based on ranked SIS realisations for GHEW using a 5m x 5m x 3,333m simulation grid. IK high grade wireframe for the deposit is depicted by black outlines. 83
Figure 4-10: Section view (W2) showing the potential downside scenario (left) and upside scenario (right) based on ranked SIS realisations for GHEW using a 5m x 5m x 3,333m simulation grid. IK high grade wireframe for the deposit is depicted by black outlines. 83

Figure 4-11: Section view (W3) showing the potential downside scenario (left) and upside scenario (right) based on ranked SIS realisations for GHEW using a 5m x 5m x 3,333m simulation grid. IK high grade wireframe for the deposit is depicted by black outlines. 84
Figure 4-12: Section view (W4) showing the potential downside scenario (left) and upside scenario (right) based on ranked SIS realisations for GHEW using a 5m x 5m x 3,333m simulation grid. IK high grade wireframe for the deposit is depicted by black outlines. 84
Figure 4-13: Section view (W5) showing the potential downside scenario (left) and upside scenario (right) based on ranked SIS realisations for GHEW using a 5m x 5m x 3,333m simulation grid. IK high grade wireframe for the deposit is depicted by black outlines. 85
Figure 4-14: Section view (W6) showing the potential downside scenario (left) and upside scenario (right) based on ranked SIS realisations for GHEW using a 5m x 5m x 3,333m simulation grid. IK high grade wireframe for the deposit is depicted by black outlines. 85
Figure 4-15: Section view (W7) showing the potential downside scenario (left) and upside scenario (right) based on ranked SIS realisations for GHEW using a 5m x 5m x 3,333m simulation grid. IK high grade wireframe for the deposit is depicted by black outlines. 86
Figure 4-16: Plan view showing the location of cross sections (E1-E4) through GHEE to compare upside and downside scenarios for the High and Low Grade DBSim realisations on a 10m x 10m x 3,333m simulation grid. 87
Figure 4-17: Section view (E1) showing the HG potential downside scenario (top left) and upside scenario (top right) and LG potential downside scenario (bottom left) and upside scenario (bottom right) based on ranked DBSim realisations for GHEE using a 10m x 10m x 3,333m simulation grid. IK high grade wireframe for the deposit is depicted by green outlines for the HG simulations. 88
Figure 4-18: Section view (E2) showing the HG potential downside scenario (top left) and upside scenario (top right) and LG potential downside scenario (bottom left) and upside scenario (bottom right) based on ranked DBSim realisations for GHEE using a 10m x 10m x 3,333m simulation grid. IK high grade wireframe for the deposit is depicted by green outlines for the HG simulations 89

Figure 4-19: Section view (E3) showing the HG potential downside scenario (top left) and upside scenario (top right) and LG potential downside scenario (bottom left) and upside scenario (bottom right) based on ranked DBSim realisations for GHEE using a 10m x 10m x 3,333m simulation grid. IK high grade wireframe for the deposit is depicted by green outlines for the HG simulations..... 90
Figure 4-20: Section view (E4) showing the HG potential downside scenario (top left) and upside scenario (top right) and LG potential downside scenario (bottom left) and upside scenario (bottom right) based on ranked DBSim realisations for GHEE using a 10m x 10m x 3,333m simulation grid. IK high grade wireframe for the deposit is depicted by green outlines for the HG simulations..... 91
Figure 4-21: Plan view showing the location of cross sections (W1-W4) through GHEW to compare upside and downside scenarios for the High and Low Grade DBSim realisations on a 10m x 10m x 3,333m simulation grid. 92
Figure 4-22: Section view (W1) showing the HG potential downside scenario (top left) and upside scenario (top right) and LG potential downside scenario (bottom left) and upside scenario (bottom right) based on ranked DBSim realisations for GHEW using a 10m x 10m x 3,333m simulation grid. IK high grade wireframe for the deposit is depicted by green outlines for the HG simulations..... 93
Figure 4-23: Section view (W2) showing the HG potential downside scenario (top left) and upside scenario (top right) and LG potential downside scenario (bottom left) and upside scenario (bottom right) based on ranked DBSim realisations for GHEW using a 10m x 10m x 3,333m simulation grid. IK high grade wireframe for the deposit is depicted by green outlines for the HG simulations..... 94
Figure 4-24: Section view (W3) showing the HG potential downside scenario (top left) and upside scenario (top right) and LG potential downside scenario (bottom left) and upside scenario (bottom right) based on ranked DBSim realisations for GHEW using a 10m x 10m x 3,333m simulation grid. IK high grade wireframe for the deposit is depicted by green outlines for the HG simulations..... 95
Figure 4-25: Section view (W4) showing the HG potential downside scenario (top left) and upside scenario (top right) and LG potential downside scenario (bottom left) and upside scenario (bottom right) based on ranked DBSim realisations for GHEW using a 10m x 10m x 3,333m simulation grid. IK high grade wireframe for the deposit is depicted by green outlines for the HG simulations..... 96

Figure 4-26: Plan view showing the location of cross sections (D1-D4) through GHEW and GHEE to compare upside and downside scenarios for the High Grade DBSim realisations on a 10m x 10m x 3,333m simulation grid against the deterministic estimated model for the study areas. 97
Figure 4-27: The deterministic kriged model for the deposit (top), and section view (D1) showing the potential downside scenario (bottom left) and upside scenario (bottom right) for the joint simulation model 98
Figure 4-28: The deterministic kriged model for the deposit (top), and section view (D2) showing the potential downside scenario (bottom left) and upside scenario (bottom right) for the joint simulation model 99
Figure 4-29: The deterministic kriged model for the deposit (top) and section view (D3) showing the potential downside scenario (bottom left) and upside scenario (bottom right) for the joint simulation model 100
Figure 4-30: The deterministic kriged model for the deposit (top) and section view (D4) showing the potential downside scenario (bottom left) and upside scenario (bottom right) for the joint simulation model 101
Figure 4-31: Plan view showing the location of cross sections (S1-S16) through GHEW and GHEE to compare upside and downside scenarios for the joint uncertainty models on a 10m x 10m x 3,333m simulation grid. 102
Figure 4-32: Section view (S1) showing the potential grade downside scenario (left) and upside scenario (right) for the joint uncertainty model (10m x 10m x 3,333m grid). Proposed location of stope designs are depicted by purple outlines. Resource pit surface is indicated by the brown line. 103
Figure 4-33: Section view (S2) showing the potential grade downside scenario (left) and upside scenario (right) for the joint uncertainty model (10m x 10m x 3,333m grid). Proposed location of stope designs are depicted by purple outlines. Resource pit surface is indicated by the brown line. 103
Figure 4-34: Section view (S3) showing the potential grade downside scenario (left) and upside scenario (right) for the joint uncertainty model (10m x 10m x 3,333m grid). Proposed location of stope designs are depicted by purple outlines. Resource pit surface is indicated by the brown line. 104
Figure 4-35: Section view (S4) showing the potential grade downside scenario (left) and upside scenario (right) for the joint uncertainty model (10m x 10m x

3,333m grid). Proposed location of stope designs are depicted by purple outlines. Resource pit surface is indicated by the brown line. 104
Figure 4-36: Section view (S5) showing the potential grade downside scenario (left) and upside scenario (right) for the joint uncertainty model (10m x 10m x 3,333m grid). Proposed location of stope designs are depicted by purple outlines. Resource pit surface is indicated by the brown line. 105
Figure 4-37: Section view (S6) showing the potential grade downside scenario (left) and upside scenario (right) for the joint uncertainty model (10m x 10m x 3,333m grid). Proposed location of stope designs are depicted by purple outlines. Resource pit surface is indicated by the brown line. 105
Figure 4-38: Section view (S7) showing the potential grade downside scenario (left) and upside scenario (right) for the joint uncertainty model (10m x 10m x 3,333m grid). Proposed location of stope designs are depicted by purple outlines. Resource pit surface is indicated by the brown line. 106
Figure 4-39: Section view (S8) showing the potential grade downside scenario (left) and upside scenario (right) for the joint uncertainty model (10m x 10m x 3,333m grid). Proposed location of stope designs are depicted by purple outlines. Resource pit surface is indicated by the brown line. 106
Figure 4-40: Section view (S9) showing the potential grade downside scenario (left) and upside scenario (right) for the joint uncertainty model (10m x 10m x 3,333m grid). Proposed location of stope designs are depicted by purple outlines. Resource pit surface is indicated by the brown line. 107
Figure 4-41: Section view (S10) showing the potential grade downside scenario (left) and upside scenario (right) for the joint uncertainty model (10m x 10m x 3,333m grid). Proposed location of stope designs are depicted by purple outlines. Resource pit surface is indicated by the brown line. 107
Figure 4-42: Section view (S11) showing the potential grade downside scenario (left) and upside scenario (right) for the joint uncertainty model (10m x 10m x 3,333m grid). Proposed location of stope designs are depicted by purple outlines. Resource pit surface is indicated by the brown line. 108
Figure 4-43: Section view (S12) showing the potential grade downside scenario (left) and upside scenario (right) for the joint uncertainty model (10m x 10m x 3,333m grid). Proposed location of stope designs are depicted by purple outlines. Resource pit surface is indicated by the brown line. 108

Figure 4-44: Section view (S13) showing the potential grade downside scenario (left) and upside scenario (right) for the joint uncertainty model (10m x 10m x 3,333m grid). Proposed location of stope designs are depicted by purple outlines. Resource pit surface is indicated by the brown line. 109
Figure 4-45: Section view (S14) showing the potential grade downside scenario (left) and upside scenario (right) for the joint uncertainty model (10m x 10m x 3,333m grid). Proposed location of stope designs are depicted by purple outlines. Resource pit surface is indicated by the brown line. 109
Figure 4-46: Section view (S15) showing the potential grade downside scenario (left) and upside scenario (right) for the joint uncertainty model (10m x 10m x 3,333m grid). Proposed location of stope designs are depicted by purple outlines. Resource pit surface is indicated by the brown line. 110
Figure 4-47: Section view (S16) showing the potential grade downside scenario (left) and upside scenario (right) for the joint uncertainty model (10m x 10m x 3,333m grid). Proposed location of stope designs are depicted by purple outlines. Resource pit surface is indicated by the brown line. 110
Figure A-1: East SIS histogram reproduction..... 129
Figure A-2: West SIS histogram reproduction..... 130

V LIST OF TABLES

Table 1: Proportion of low and high grade lithologies for GHEE and GHEW 45
Table 2: Description of the simulation grid 45
Table 3: Experimental Variogram parameters for the low-grade ore high-grade lens interface (GHEE)..... 48
Table 4: Experimental Variogram parameters for the low grade ore- high grade lens interface (GHEW) 48
Table 5: Spherical Model Variogram parameters for the low grade ore- high grade lens interface (GHEE and GHEW) 48
Table 6: Model Variogram parameters for Gaussian Gold variables (GHEE and GHEW) 61

VI LIST OF SYMBOLS

z	a (sample) realisation or observation of Z
Z	a random variable
u	coordinate location vector
Z(**u**)	Random variable of Z at location u

VII PHYSICAL QUANTITIES

g/cm^3	density, grams per cubic centimetre
g/t	metal grade, grams per metric ton

VIII NOMENCLATURE

2D	Two dimensional
3D	Three dimensional
Au	Gold
Cdf	Cumulative distribution function
DBMAFSim	Direct Block Simulation with Multiple Correlated Variables
DBSim	Direct Block Simulations
GHE	Geita Hill East study area
GHEE	study area located east of Geita Hill East
GHEW	study area located west of Geita Hill East
GHSZ	Geita Hill Shear Zone
GSGS	Group Sequential Gaussian Simulation
GSLIB	Geostatistical software library
HG	High grade
LG	Low grade
MPS	Multiple-point statistics
NPV	Net present value
Pdf	Probability density function
RF	Random function
RV	Random variable
SA	Simulated Annealing

SGEMS	Stanford Geostatistical Modelling Software
SGS	Sequential Gaussian Simulation
SIS	Sequential Indicator Simulations
SMU	Smallest Mining Unit
SNESim	Single Normal Equation Simulations
TI	Training image
UC model	Uniform Conditioned model

IX TABLE OF CONTENTS

Chapter 1

1 Introduction 1

1.1 Project background 3

1.2 Problem Statement 4

1.3 Assumptions 6

1.4 Research question(s)/Hypotheses 6

1.5 Research Objectives and Methods 6

1.6 Research Limitations 8

1.7 Significance of the research study 8

1.8 Organisation of the dissertation 9

Chapter 2

2 Literature review 10

2.1 Introduction 10

2.2 Geological uncertainty 11

2.3 Spatial statistics 12

2.4 Shortcomings of Kriging 14

2.5 Building a model of Uncertainty 16

2.6 Stochastic simulations as an alternative 16

2.7 Sequential Gaussian Simulation (SGS) 18

2.8 Direct Block Simulation (DBSim) 19

2.9 Sequential Indicator Simulation (SIS) 20

2.10 Multiple Point Statistics (MPS) 20

2.11 Choice of simulation algorithm and relevant software 22

2.12 Conclusion 22

Chapter 3

3 Research methodology 24
3.1 Simulating geological boundaries 25
3.1.1 Simulated Annealing (SA) 25
3.1.2 Single Normal Equation Simulation (SNESim) 26
3.1.3 Sequential Indicator Simulation (SIS) 28
3.2 Simulating grades 30
3.2.1 Direct Block Simulations (DBSim) 31
3.3 Validation 33
3.4 Practical application of the simulation algorithms 34
3.4.1 Geological Setting 35
3.4.2 Description of data 39
3.5 Simulating the study area 43
3.5.1 Simulating lithologies using SIS 44
3.5.2 Simulating grades using DBSim 57
3.5.3 Identifying upside and downside scenarios 72
3.5.4 Model of Joint Uncertainty 74
3.6 Conclusion 76

Chapter 4

4 Results 78
4.1 Conventions applied 78
4.2 SIS Results 79
4.2.1 Comparison between potential upside and downside scenarios 79
4.2.2 Difference in volumes between simulated results and IK wireframe model 86

4.2.3 Ranking of simulated volumes occurring inside proposed stope designs 86

4.3 Results for DBSim 87

4.3.1 Comparison between DBSim Upside and Downside Scenarios 87

4.4 Results for the Model of Joint Uncertainty 97

4.4.1 Comparison between joint simulation upside and downside scenarios against the deterministic estimated ore model for the deposit 97

4.4.2 Comparison between joint simulation upside and downside scenarios against the proposed Stope layout 102

4.5 Conclusion 111

Chapter 5

5 Discussion 112

5.1 Summary of Research Problem 113

5.2 Assessing geological uncertainty 113

5.3 Assessing volumetric uncertainty using SIS 114

5.3.1 Ranking of SIS Realisations 114

5.3.2 Potential upside and downside mine planning scenarios 115

5.3.3 Comparison between the IK model and SIS realisations 115

5.3.4 Calculated volumetric differences 116

5.4 Assessing grade uncertainty using DBSim 116

5.4.1 Ranking of DBSim Realisations 116

5.4.2 Potential upside and downside mine planning scenarios 117

5.4.3 Comparison between the IK model and DBSim realisations 117

5.5 Assessing grade uncertainty from the model of joint uncertainty 117

5.5.1 Ranking of Joint Realisations 118

5.5.2 Comparison between potential upside and downside mine planning scenarios and deterministic kriged model 118

5.5.3 Comparison between potential upside and downside mine planning scenarios and proposed stope layout 119

5.6 Conclusion 121

Chapter 6

6 Conclusions and Recommendations 122

6.1 Research question 1: “Can stochastic simulations of the geological ore body model be used to assess the uncertainty associated with identifying high grade lenses within the known lower grade mineralisation at Geita Mine?” 123

6.2 Research question 2: “Can this knowledge (from 6.1) be used to make a risk-informed decision on whether or not to develop an underground mining operation?” 124

6.3 Research question 3: “Can uncertainty about the ore body model be incorporated in planning and designing stope layouts to access the high grade lenses in the underground mine? 125

6.4 Limitations and Recommendations 126

6.5 Conclusion 127

Appendix A Histogram validation 129

References 131

CHAPTER 1

"Probability is not a mere computation of odds on the dice or more complicated variants; it is the acceptance of the lack of certainty in our knowledge and the development of methods for dealing with our ignorance."

-Nassim Nicholas Taleb (2001), Fooled by Randomness: The Hidden Role of Chance in Life and in the Markets)

1 INTRODUCTION

Regardless of how often geological models are refined based on new sample information, the knowledge of the geological complexity of the deposit is often incomplete due to the high costs and practical constraints associated with drilling. This incomplete knowledge presents risk that translate into the typical geological model that represents the deposit as a 3D array of blocks whose attributes are defined from the nearby sampling data (Chanderman, 2015). Grade estimates are then subsequently interpolated into the model blocks based on the interpreted geological domains in the model and spatial characteristics of the grades displayed in the sample data. To mitigate error arising from imperfect knowledge, it is common practice to allow the a-priori information known about the deposit (geologist's knowledge of the deposit) to support the sample data and thereupon guide the geological modelling. A realistic description of the geology is necessary for accurate grade predictions to be made. Estimation methodologies are subsequently adapted to suit the uniqueness of the deposit.

The problem of constructing accurate geological models to constrain mineral resource estimates is compounded by the considerable uncertainty in the spatial distribution of grades and position of geological boundaries. The topic of geological uncertainty in Mineral Resource Estimates (MREs) is of great interest (Goovaerts, 1997; Chiles & Delfiner, 1999) because of the inherent risk that it poses to mine planning. Despite this uncertainty the mining industry still relies heavily on conventional kriged models for estimating reserves. Kriged models cannot account for geological uncertainty because they are unable to capture the true complexity

and in-situ variability of the geological phenomena under study, resulting in misleading MREs and poorly informed mine planning expectations. Each mineral deposit may be unique, but the outcomes of the random variables occurring in that deposit are not, resulting in estimated grade and volumetric uncertainty, henceforth referred to as geological uncertainty.

Mining companies have traditionally applied deterministic geostatistical methods for geological modelling and estimation whereby the random function is characterised fully on its first two moments (the mean and a spatial correlation function) and uses a single model (single realisation) to estimate values at unsampled locations in the deposit (Myers, 2016). If perfect knowledge of the deposit exists and if the deposit adheres to assumptions of stationarity, this approach is reasonable for making predictions on the extent and spatial continuity of grades. Unless a deposit is drilled sufficiently to provide adequate confidence in terms of grade distribution and the position of geological contacts, there may be many interpretations of the data and geological models of the ore body as there are geologists. Furthermore, a single, often smoothed version of grade distribution is produced from kriged models which by definition cannot account for geological uncertainty. Such models pose risk to mine planning decisions.

The method of stochastic simulation uses all the geological information from drill holes in a recursive manner to produce multiple realisations of the spatial arrangement of the geology, each conditioned by the same data. In this way it is possible to assess the uncertainty associated with the spatial distribution of geological contacts and grades. This alternative approach involves the use of probabilistic or stochastic simulations as a planning tool to generate a range of equiprobable orebody realisations (another “reality”) of a random function from which to assess geological uncertainty. Stochastic models are used in a variety of scientific and engineering applications. Like conventional estimation methods, simulations also require sufficient data to be accurate and the choice of stochastic algorithm and its success require a good practical and theoretical understanding of the underlying assumptions and mathematics of the available methods (Vann et. al., 2002) as well as their applicability to the geology. But unlike conventional models, simulations enhance the variability of the data (deposit) to allow for an assessment of geological uncertainty.

The research will identify suitable stochastic simulation techniques for assessing geological volume and grade uncertainty at the Geita gold mine in Tanzania. This knowledge will help guide mine planning for the proposed underground mining by providing a method for making decisions for which the uncertainty has been quantified.

1.1 Project background

Metal and commodity demand in the minerals industry is affected by volatility in factors such as commodity prices, fluctuating demand, declining metal grades, regulatory policies, and labour unrest. This market instability threatens mining operations, forcing companies to consider new approaches to reducing debts and achieving production targets (Deloitte, 2015). Failure to meet production targets is strongly linked to over-estimation of metal grades and volumes derived from kriged resource models on which mine designs, production schedules and expectations about NPV are based.

"When metal prices are low, it requires change. Some aspects of mining cannot be changed, but others can... the future of the mining industry, can and should adapt and think differently . . . use different techniques to be more efficient…A lack of ingenuity in the industry remains a worry…We keep doing the same things, in the same way, over and over again." - Dr Tony Harwood, CEO of Montero Mining (2016)

As an alternative to the conventional kriged models which do not provide any insights into the uncertainty of estimates, stochastic simulation techniques can assist and guide mine planning under geological uncertainty, by providing a means for quantifying the uncertainty associated with planning decisions. This study proposes the application of stochastic simulation techniquesto the Geita Mine in Tanzania where investigations regarding the planning of an underground mining operation are underway at two of its open pits: Geita Hill and Nyankanga. Geita Hill contains the portion of the gold bearing reef of interest to this study.

A similar study was undertaken at Nyankanga by McNeil (2016) who applied stochastic simulations to develop a risk based approach to evaluate the decision to transition from Open pit to underground mining. McNeil (2016) quantified

geological uncertainty using Single Normal Equation Simulations (SNESim) to simulate lithologies followed by grade simulations within those lithologies. Despite the close proximity of the Geita Hill and Nyankanga pits to each other, the study areas did not share sufficient geological similarity to apply McNeil's (2016) methodology successfully to this study. Extensive historical geological work on the Geita Hill deposit has shown that the gold mineralisation in the study area is not lithologically controlled,and thus demands a different approach.

Stochastic simulations of grade and ore category formed part of the pre-feasibility studies regarding underground mining at Geita. This allowed the geological uncertainty of locating high grade lenses in the low grade background mineralisation, to be assessed. The results for the ore category and grade simulations will be used in conjunction to help the mine consider the business case for the development of an underground mine from a risk-informed perspective.

1.2 Problem Statement

The problem of constructing accurate geological models with which to constrain mineral resource estimates is compounded because of geological uncertainty. Each mineral deposit may be unique, but the outcomes of the random variables occurring in that deposit are not, resulting in estimated grade and volumetric uncertainty. Deterministic estimation models cannot account for this geological uncertainty because they aim to produce an optimal estimate together with an associated error variance and not to evaluate the uncertainty linked to the unknown grade. Where the deterministic resource model carries a high degree of geological uncertainty, geological risk is introduced into mine designs, production schedules and predictions of NPV, resulting in unrealistic expectations about the rates of production. This limitation can be overcome by applying stochastic simulations to fully represent the in-situ variability of metal grades and production volumes. Rather than a single deterministic value, simulation methods provide a range of estimated grades and volumes that reflect the geological uncertainty. In this way expectations about potential upside and downside scenarios are accounted for and allow the problem of associated risk to be quantified.

This research aims to provide a bridge between an in depth understanding of stochastic algorithms and the ability to generate meaningful realisations based on an understanding of the geology.

The study is different to others because it requires the 3D stochastic simulation of a complex gold reef deposit as compared to the commonly encountered 2D case studies covering smaller study areas. Most simulation studies likewise lean towards presenting simulation results rather than developing practical user-friendly methodologies that can be adopted by mining companies.This results in confusion when those new to stochastic ore body modelling attempt to generate similar results. Another observation made from similar studies is the custom of reporting on positive project findings and not on the problems encountered during practical implementation of the techniques. The research also aims to give guidance on these areas to help practitioners avoid encountering common problems identified during implementation as this awareness is as important as the mathematical intricacies underlying the algorithms.

To correctly apply any simulation technique, it is critical that the user understand the fundamentals underlying the algorithm. However, the field of stochastic simulations is still largely dominated by academics, computer programmers, operations research specialists and mathematicians who are not the main users on mine sites. Though these specialists are drivers to advancements in this field of research, the true value lies in the ability to implement stochastic techniques in the mining industry in a way that Resource Geologists and Mining Engineers can apply meaningfully.In this way, the study intends to present theoretical concepts in a way that can be easily implemented:

"Engineers are correct in judging geostatistics by efficiency and practical records rather than by the intricacy of its theoretical developments; if there existed a simpler language leading to the same algorithms and results there is little doubt that it would be adopted" –A.G. Journel, 1985

1.3 Assumptions

It is assumed that sampling data provided by the mine are the most recent and that rigorous system and quality checks were applied to the database. Thus the database is assumed to be free of errors and that the data used in the analyses are representative, accurate, and precise. Furthermore, it is assumed that the only uncertainty in this study arises from the natural geological variability in the deposit and is not due to bias or errors associated with sampling or analytical procedures.

1.4 Research question(s)/Hypotheses

As part of the pre-feasibility stage studies for underground mining at Geita, stochastic grade and ore category simulations were required to assess the geological uncertainty associated with isolating high grade lenses that occur within the known low grade mineralisation currently targeted for underground mining. The current business case supporting underground mining is centred around the interpretation of high grade lenses in the deterministic kriged model for the deposit.

The results derived from the ore category and grade simulations will be used in conjunction to help the mine evaluate the business case for the development of an underground mine from a risk-informed perspective. The three fundamental research questions facing the mine are “Can stochastic simulations of the geological ore body model be used to quantify the uncertainty associated with identifying high grade lenses within the known lower grade mineralisation at Geita Mine?” Secondly, “Can this knowledge be used to make a risk-informed decision on whether or not to develop an underground mining operation?” Finally, “Can uncertainty about the ore body model be incorporated in planning and designing stope layouts to access the high grade lenses in the underground mine?

1.5 Research Objectives and Methods

The objective of this research is to apply the stochastic simulation ore body modelling techniques learned at McGill University, to decision-making about the transition from open-pit to underground mining at the Geita Mine. In addition, this case study will aid the mine in making risk-quantified mine planning decisions that consider geological uncertainty. To achieve this, several stages of learning and testing were required:

Stage 1: Attending a 4 month course in *Linear Programming* in the School of Computer Science and Applied Mathematics at the University of the Witwatersrand as a prerequisite for the lectures and practicals part of the COSMO scholarship (**March – July 2015).**

Attending a 5 month course in *stochastic ore body modelling* and an introductory course in *C++ Programming* at McGill University (**August 2015 – Jan 2016).**

Each course included lectures, assignments and final examinations.

Stage 2: Practical implementation of the stochastic ore body modelling concepts learned at McGill University to the Geita mine case study. Various stochastic simulation techniques were investigated to find a suitable methodology to simulate ore category boundaries including the use of conventional simulation techniques, heuristics as well as Multiple Point Statistics. This stage of work was structured as follows:

- Four months testing FORTRAN code for Simulated Annealing in Microsoft Visual Studio 2015 using a dummy dataset, to verify the suitability of the algorithm to simulate categorical data **(October 2015 – Jan 2016)**;
- Preparation of training images for Single Normal Equation Simulations and testing simulation parameters using Stanford Geostatistical Modelling Software (SGEMS) **(February 2016 – May 2016)** and,
- testing Sequential Indicator Simulations to generate ore category realisations to assess volumetric uncertainty **(June 2016 – September 2016)**.

Stage 3: Direct Block Simulations based on Gaussian Random Function models were applied to simulate grades using ISATIS geostatistical software to assess grade uncertainty **(June 2016 – September 2016)**

Stage 4: Validation of simulations using histograms and variograms **(August 2016- September 2016)**

Stage 5: Ranking of simulations to provide potential upside and downside mine planning scenarios **(August 2016- September 2016)**

The simulations were run on a 64-bit operating system with 2.9GHz processor.

1.6 Research Limitations

The research was conducted as part of the COSMO scholarship using data supplied by AngloGold Ashanti. Stages 1 to 3 from *section 1.5*, focused on different research objectives to those presented in the dissertation. This modification was required by AngloGold Ashanti whose needs changed during the study to focus on areas where this work would provide more value. As a consequence, the project scope was affected by:

- 3 changes in study area;
- 3 changes in simulation techniques;
- 1 change in software used, and
- 2 changes in study objectives.

AngloGold Ashanti finalised the project objectives in May 2016. Multiple-point statistics and Simulated Annealing were explored in the early stages of the research. Because of scope changes mentioned, limited time was available to re-test the applicability of the techniques to the final study area. A brief summary of these investigations are included in the dissertation for the interest of the reader.

Traditional stochastic models may not be the most appropriate methods to fully characterise the spatial nature of the deposit due to their reliance on two point statistics using variograms or covariance functions. Multiple point statistics overcome this limitation but is controlled by a training image. This approach was investigated during the early stages of the project without success and not reinvestigated later due to time constraints.

The choice of simulation software had to be changed from SGEMS to ISATIS geostatistical software mid project due to the coding required to implement the techniques. This was also on recommendation from AngloGold who have a preference to using ISATIS software.

1.7 Significance of the research study

The 3 dimensional geological modelling of gold reefs can be a complicated task due to the erratic behaviour of gold grades and the unavailability of adequate sample data to provide complete information about a deposit. As a result,

reasonable inferences need to be made from the limited available data to give an indication of the spatial behaviour of the gold distribution at unsampled locations. Deterministic models that carry a high degree of geological uncertainty, introduce geological risk into mine designs, production schedules and predictions of NPV, resulting in unrealistic expectations about the rates of production.

The methodology developed in this research will be the first application of stochastic orebody modelling at Geita Hill. The workflow can however be adapted to any similar deposits to produce more realistic models that account for geological uncertainty to allow for risk-informed decision making.

1.8 Organisation of the dissertation

Simulation studies produce a large number of realisations making it impractical to include each result in the dissertation. Therefore, only those results pertinent to the research are presented. The report has been divided into 6 chapters:

Chapter I Introduction: This chapter mainly deals with the rationale, objectives and limitations of the study.

Chapter II Literature Review: This chapter is dedicated to guiding the reader through the relevant literature that has motivated this study as well as recent works related to similar studies.

Chapter III Resources and Methodology: This chapter describes the resources used and methodologies developed for the study and outlines the various tests that were carried out.

Chapter IV Results:The results of the methods are presented as tables and figures in this chapter.

Chapter V Discussion: This chapter contains a description of the interpretations for the results presented in Chapter IV. The discussion is focussed around answering the fundamental research question.

Chapter VI Conclusion and Recommendations: General research conclusions are presented in this chapter which closes with recommendations for future work.

CHAPTER 2

". . . the only way to set up a probability distribution that honestly represents a state of incomplete knowledge is to maximize the entropy, subject to all the information we have. Any other distribution would necessarily either assume information that we do not have, or contradict information that we do have"

-E. Jaynes (1985)

2 LITERATURE REVIEW

2.1 Introduction

The typical block model encountered in industry is a 3 dimensional representation of the orebody as interpreted from available mapping, drill hole and sample data. Each block in the model is commonly assigned an estimate using the available sample information and a conventional geostatistical technique such as kriging. The fate of the block (whether it is deemed waste or ore) depends on the kriged block value. The final destination (low-grade stockpile, waste dump, processing plant) of the block is assessed according to an extraction sequence, constrained to maximise the NPV for future cash flows, over the life of mine. This destination is based on the position of the block and its spatial configuration relative to the value generated by mining and processing surrounding kriged blocks.

Since the available information is not exhaustive, the interpretation of the geological ore body model and the derived block model represent only partial knowledge of the deposit. It has been said that “all models are wrong; some are useful” (Box, Hunter and Hunter, 2005, pp 440). If the geological model is not an accurate representation of the deposit, the cascading effect is that block estimates within the model will be inaccurate, mine designs and production scheduling will be suboptimal and overall mine planning will be poor. Given the importance of the geological model and the block model to optimisation of mining layouts, it is critical to assess decisions based on estimates, in terms of the risk associated with the underlying geological uncertainty. Geological uncertainty in this research refers to the uncertainty associated with spatially distributed estimates of grades as well as the location and complex spatial patterns of 3D geological orebody models that arise from subsequent interpretation (Deutsch, 1992). Thus, geological

uncertainty entails both grade (grade distribution) and volumetric (ore category) uncertainty.

2.2 Geological uncertainty

Conventional orebody modelling and estimation is based on deterministic mathematical models whose output is a single prediction for values at unsampled locations, ignoring random variation of in-situ grade and rock-type distribution (Journel, 1985; Goovaerts, 1997; Chiles and Delfiner, 1999). Since random variation is not incorporated in the models, the risk associated with the uncertainty embedded in the interpretation of geological boundaries and estimated grades, cannot be assessed using deterministic methods. Geological uncertainty arises because of incomplete knowledge about the deposit due to constraints on sample size and drilling density. Generally, the mass of physical samples (hard data) collected from the mineralised zones often represent less than 0.001% of the geological body (Stephenson and Vann, 2001). During deterministic modelling and estimation, practitioners use their a-priori knowledge of the deposit; the geological descriptions and interpretations based on a sound understanding of the grade continuity and geological controls on the grade distribution, to support the available hard data. For the construction of geological boundaries, this practice can greatly reduce the number of possible errors (due to a lack of knowledge) introduced into the orebody model. However, the validity of the model may be eroded if incorrect assumptions are drawn from sparse data. This may result in poor definition of geologically or statistically homogenous domains and misrepresentation of the spatial character and relationship between domains. In the case of implicit orebody modelling performed by an inexperienced user, the software makes predictions about spatial continuity which may not be well understood nor valid (doesn't relate to the a-priori knowledge). This is the first limitation to deterministic modelling and estimation methods: geological boundary (ore category) uncertainty or volumetric uncertainty.

Errors related to incomplete knowledge about the geological model are propagated through the mineral resource estimation process giving rise to potentially biased grade and tonnage estimates. A mining process can be regarded as a transfer function. If descriptors of a deposit, such as grade and tonnage are input through

a sequence of mining processes, the output function generates a distribution of responses which map the space of uncertainty (Dimitrakopoulos, 1998). Because the transfer function is not necessarily linear, the average kriged block model may not provide an average map of the space of uncertainty (Dimitrakopoulos, 1998). This means that biases in the estimates are amplified being grossly higher than the input error itself. The assumption that the data are representative, accurate, and precise, means that geological uncertainty does not arise from the sample data. Deterministic mathematical models such as kriging only provide a single prediction for the value at an unsampled location that ignores sample randomness. This is the second limitation to deterministic modelling and estimation methods: estimated grade uncertainty.

This dissertation is concerned with addressing the uncertainty embedded in estimates of both grade and the location of geological boundaries (ore category allocation) that translate into volumetric uncertainty.

2.3 Spatial Statistics

The discussion on random variables and random functions to follow are summarised from the dissertation by Deutsch (1992). Detailed discussions are also available in Deutsch and Journel (1998), Goovaerts (1997) and Chiles and Delfiner (1999). The text to follow is a rough exposition of the mathematical/probabilistic concepts described in the literature.

Predictive statistics model the uncertainty associated with an unsampled grade *z* as a random variable. The probability distribution of the random variable *Z,* describes the uncertainty associated with z. A random variable takes a certain number of outcome values according to its probability distribution. Commonly, the random variable is denoted with a capital letter and its outcome values with the same letter in lower case. The Random Variable (RV) of *Z* is dependent on its coordinate location vector (**u**) or in notation form: *Z*(**u**). In addition to being dependant on location, the unknown value *Z*(**u**), also relies on the available **information surrounding it to update its probability distribution.**

For continuous RV's such as grades, the cumulative distribution function (cdf) is denoted:

$F(\mathbf{u};z) = Prob\ \{Z(\mathbf{u}) \leq z\}$.....(1)

When the cdf is informed by specific data values, (n), which refers to $n$neighbouringdata values, $Z(\mathbf{u}_\alpha) = z(\mathbf{u}_\alpha)$, α=1,...,n, this is referred to as "conditional to (n)" and the conditional cdf is defined as:

$F(\mathbf{u};z|(n)) = Prob\ \{Z(\mathbf{u}) \leq z|(n)\}$.....(2)

For categorical variables such as lithologies, RV $Z(\mathbf{u})$ also takes on a certain number of outcome values K where k=1,...,K. The RF is a probability density function (pdf) defined as:

$F(\mathbf{u}; k|(n)) = Prob\ \{Z(\mathbf{u}) \in$ category $k|(n)\}$.....(3)

The RV $Y(\mathbf{u})$ can then take on one of the K outcomes depending on the class that $z(\mathbf{u})$ takes.

The cdf (equation 1) and pdf (equation 2) characterise the uncertainty about the unknown random variable. When they are unconditioned to any set of data, they are referred to as prior models. When conditioning data is taken into account, the algorithm updates the prior model of uncertainty and is referred to as a posterior model. Using this information (number of samples, sample values and configuration), optimal estimates for $z(\mathbf{u})$ can be derived from the ccdf mean or expected value according to:

$m(\mathbf{u}) = E\ \{Z(\mathbf{u})\} = \int_0^1 z d\mathrm{F}(\mathbf{u};z|(n))$..... (4)

and for the cpdf, from the mode of classes (k') that has the highest probability:

$F(\mathbf{u}; k'|(n)) \geq F(\mathbf{u}; k|(n)),\ \forall\ k = 1,...,K$.....(5)

Simulated values or outcomes: $z^{(l)}(u)$, l=1,...,L, can be drawn from the ccdf using random numbers. This process is the random function approach to stochastic simulations where the random function (RF) is a set of RV's defined over the area of interest. It is based on Monte Carlo Simulations where probability distributions allow variables to have different probabilities of different outcomes occurring which is essential for risk analysis.

In the same manner that RV $Z(\mathbf{u})$ is characterised by its cdf, the RF $Z(\mathbf{u})$ is characterised by a set of possible N-variate cdf's for any number N and N locations u_i, i= 1,...,N, inside the study area:

$$F(\mathbf{u}_1,...,\mathbf{u}_N;z_1,...,z_N) = Prob\ \{Z(\mathbf{u}_1) \leq z_1,...,Z(\mathbf{u}_N) \leq z_N\} \quad (6)$$

Likewise with the univariate cdf of RV $Z(\mathbf{u})$ that is used to characterise the uncertainty about $z(\mathbf{u})$, the multivariate cdf characterises the joint uncertainty about the N values $z(\mathbf{u}_1),...,z(u_N)$.

2.4 Shortcomings of Kriging

Kriging provides estimates for unsampled values $z(\mathbf{u})$. However, several characteristics render the algorithm ill-suited to studies that are focused on high grade values and that require an assessment of uncertainty. An example from Goovaerts (1997) is used to discuss the limitations of kriging relevant to the study and includes considerations from other authors. It should be noted that where there is sufficient information available and where an assessment of uncertainty is not required, conventional kriging methods provide acceptable results (see Chanderman, 2015). The discussion on the shortfalls of kriging that follows is limited to studies that require an assessment of risk.

Let {z(u), u∈ A} be the set of Kriging estimates of attribute z over study area A. Each estimate z*(u) is taken independently of neighbouring estimates. z*(u') is considered to be the "best" estimate because the local error variance Var{z*(u) - z(u)} is minimum.*

- **Shortfall 1:** Kriged estimates are considered to be “best” because they provide the best linear unbiased estimate for unknown values. However, they do not provide a “best” indication of the distribution of the attribute under study over the study area. Kriged estimates do not correctly represent the local variability due to smoothing.
- **Shortfall 2:** Underlying assumptions regarding the distribution of data distort the understanding of its natural variability. These contribute to conditional bias and resultant misclassification errors, as well as losing the ability to detect spatial patterns in the data. The assumptions on which geostatistics is founded

are not intrinsic properties of the deposit. They are instead intrinsic properties of the probabilistic model, therefore “A model choice and its properties must be judged on its efficiency in capturing and solving the problem at hand” (Journel, A.G., 1985, pp 1).

- **Shortfall 3:** Kriging variance is independent of the data values leading to an incomplete measure of estimation accuracy (Cressie, 1990).
- **Shortfall 4:** Estimation smoothing is not uniform. The local configuration of the data affects the amount of smoothing that occurs. When there is sufficient data to inform the estimate, the effects of smoothing are less noticeable. This results in maps of kriging estimates that show more variability in densely sampled areas and less in sparsely sampled areas. Smoothed maps cannot accurately represent the true spatial pattern of the data. Since spatial variation and the description of underlying spatial patterns drives geostatistics, the inability of the kriged estimate to replicate the prior geological knowledge of the deposit is a major limitation (Srivastava, 2013).
- **Shortfall 5:** Semi-variograms allow for a controlled allocation of sample weights to data based on their locations, assuming that the variogram model used, accurately represents the spatial variation of the data. The interpolation of values between known sampling points, is based on the weights assigned by kriging according to the directions of maximum mineralisation continuity as defined by the variogram. The variogram describes the spatial variation between a pair of data values - “two-point” statistics - which cannot capture complex spatial patterns. A further limitation is the choice of variogram models available and the fitting of model variograms (Webster & Oliver, 2014). Vital statistics derived from variograms based on incomplete measures of the spatial variability of the data do not accurately inform the geological modelling and estimation processes. This results in the generation of high entropy models in which the heterogeneity and connectivity of the variable is misrepresented (Strebelle, 2002 and 2012).

Kriging therefore misrepresents underlying spatial patterns. In the case of stochastic simulations, kriging is still used, but only to build up models of uncertainty about the unknown value $z(\mathbf{u})$ by using its minimum error variance

property to derive the conditional expectation of $z(\mathbf{u})$ by drawing from a series of posterior conditional probability distributions (Deutsch, 1992).

2.5 Building a model of Uncertainty

When the RF model is multivariate Gaussian, the mean and variance of the simple kriged estimate are used to indicate the mean and variance of the posterior ccdf. This is known as the multiGaussian (MG) parametric approach. When applied to indicator data, where the value that needs to be estimated is the expected value of the distribution and not the value for the unsampled location z(**u**), the least squares regression (LS) method is applied. Since this method is aimed at building the ccdf rather than assuming it, the approach is non parametric. This is known as the Indicator Kriging approach. These approaches enable one to build models of uncertainty.

2.6 Stochastic simulations as an alternative

In simple terms, it is better to use alternative versions of reality to describe the potential nature of a deposit rather than a single, possibly incorrect model, of the true distribution. The geological uncertainty can be assessed using stochastic simulations to generate multiple equiprobable realisations of a deposit, as illustrated in Figure 2-1.

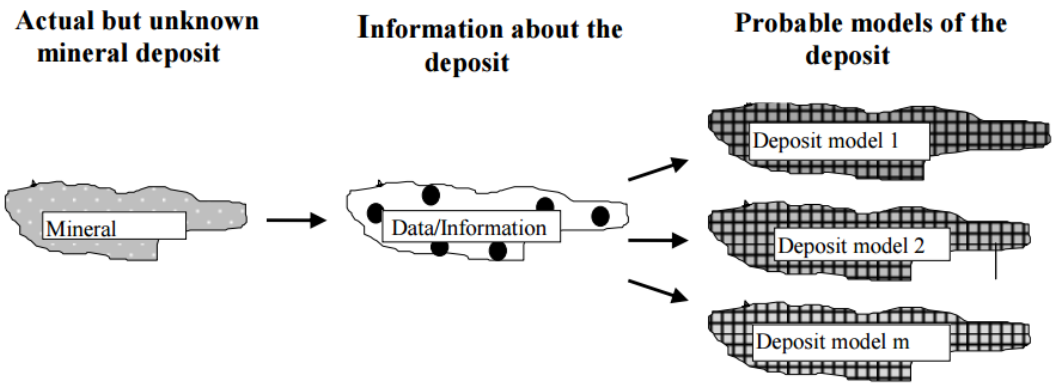


Figure 2-1: Reality in the ore deposit is partially accessible through drilling information; uncertainty associated with in-situ grade and geological variability is captured in multiple realisations (Dimitrakopoulos, 1998, pp 174).

When equiprobable realisations are generated, the simulated technique used is evaluated in terms of its ability to map the response uncertainty as shown in Figure 2-2 (Dimitrakopoulos, 1998).

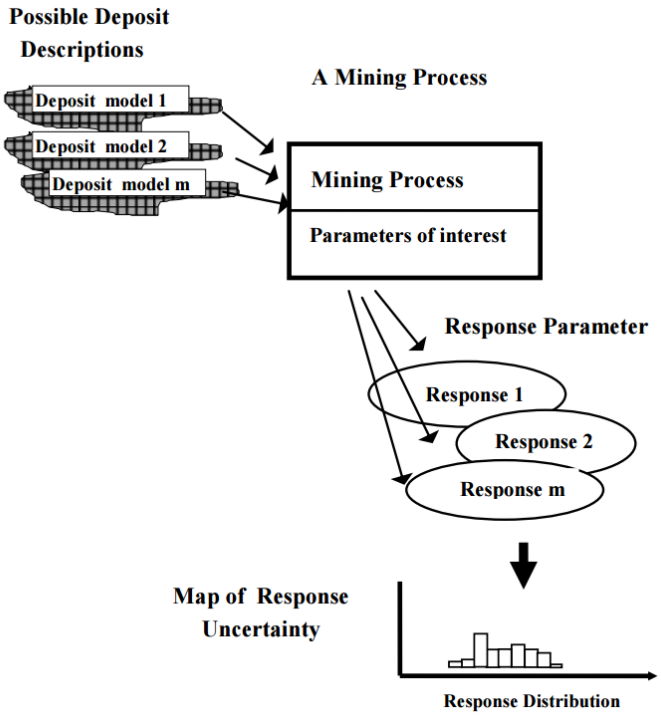


Figure 2-2: Mapping the space of response uncertainty (Dimitrakopoulos, 1998, pp 175)

Numerous stochastic processes exist and to give a full review of the many classes of algorithms and underlying mathematics is beyond the scope of this research. For further information, the reader is referred to Isaaks and Srivastava (1989), Goovaerts (1997), and Chiles and Delfiner (1999) where the conditional simulation subject matter and its derivation are covered extensively. The conditional simulation methods investigated for this study are presented in the remaining sections of this chapter.

For the general problem of assessing geological uncertainty in gold deposits, algorithms belonging to the family of sequential simulation are used. These are based on "the decomposition of the multivariate probability density function of a stationary random function, $Z(x)$, $x \in R^d$, into a product of univariate conditional distribution functions" (Dimitrakopoulos & Benndorf, 2005) citing Rosenblatt (1952). For an excellent review on the use of conditional simulation algorithms for

modeling orebody uncertainty the reader can refer to the paper by Dimitrakopoulos (1998) on Conditional Simulation Algorithms for Modelling Orebody Uncertainty in Open Pit Optimisation.

2.7 Sequential Gaussian Simulation (SGS)

SGS gets its name from the way in which the algorithm runs sequentially from one grid node to the next, following a random path on a predefined simulation grid. A univariate conditional distribution of possible values is calculated at each node on the grid from the surrounding data. The conditional mean and conditional variance of the distribution is defined by Simple Kriging of the estimate at that location. A random value is drawn from this distribution at this location and becomes the simulated value which is then incorporated into the data set. The algorithm then randomly visits the next node to be simulated, and the process is repeated, only this time the previously simulated value is now used as a valid data point to calculate the conditional mean and conditional variance of the distribution at that node. The process reaches completion when all nodes on the grid have been visited and a value simulated at that point. To avoid the incompleteness of the distribution of possible outcomes, the algorithm assumes normality which also allows for the use of Simple Kriging to define the conditional mean and conditional variance. This assumption requires that all data be transformed to normal space before simulating. Since nodes to be simulated tend to share sample neighborhoods with surrounding nodes, the overlap allows for the simulation of groups of nodes simultaneously rather than the traditional node-by-node sequence. This modification of SGS is known as Generalised Sequential Gaussian Simulation (GSGS).

During GSGS, the grid is divided into clusters of nodes called groups. If a group contains all the nodes, GSGS follows the principles of LU-decomposition described by Goovaerts (1997), Chapter 8, section 8.5, pp. 403. If the group only comprises of a single node, it is the same as SGS. The algorithm randomly visits each group and each node on the grid. The local neighborhood of the group visited is defined and used to calculate the conditional mean and conditional variance for the distribution. The distribution is randomly sampled to generate simulated realisations for each node in the group and the process repeated. This time, the

previously simulated group is added to the conditioning data and used to simulate the current group. The process reaches completion when all groups on the grid have been simulated. The effectiveness of applying GSGS depends on the group size.

2.8 Direct Block Simulation (DBSim)

Conditional simulations such as SGS and GSGS have extensive computational demands when attempting to model very large deposits. When millions of nodes need to be simulated, the runtime and storage requirements become impractical. To overcome this challenge, an extension to GSGS known as the DBSim algorithm can be implemented. Instead of simulating and storing node by node, the method generates a single block value from internal groups of nodes which are subsequently discarded. The description of the algorithm is largely taken from (Dimitrakopoulos & Benndorf, 2005).

As an initial step the data are transformed into normal space and the algorithm visits each block to be simulated along a random path. The data is transformed into normal space and for each block, values are simulated in Gaussian space for each node inside the block. The simulated node values internal to the block are then averaged and back transformed to provide a simulated value for the block in data space. All the internal nodes are then discarded and only the block value in Gaussian space added back as part of the conditioning data. The steps are repeated until the process reaches completion when all blocks have been simulated. Dimitrakopoulos and Benndorf (2005), compared the results for DBSim and GSGS for simulating the same deposit and concluded that both methods are good tools to assess geological uncertainty, but that DBSim allows for improved data management and storage requirements. DBSim has also been compared to the uniform conditioning method in a study by Deraisme et. al. (2008). The issue that uniform conditioning does not provide an indication of the confidence levels of estimates was addressed. Deraisme and his co-authors proposed an alternative method that considers the support and information effects at different scales, but also incorporates DBSim to assess uncertainty. Other modifications to DBSim have involved the joint direct block simulation of correlated variables using minimum/maximum autocorrelation factors (DBMAFSIM). This method, presented

by Boucher and Dimitrakopoulos (2009), confirms that the method reproduces the spatial connectivity of high grade values using the Walker Lake data set.

2.9 Sequential Indicator Simulation (SIS)

Like estimation, many simulation techniques are founded on an assumption of multivariate Gaussianity. SIS caters for deviations from normality because it is nonparametric. SIS works in a similar manner to SGS, but it involves categorical data and the derivation of a conditional probability distribution from which to draw values. SIS is considered to be a reasonable approach when dealing with natural features that do not display the definitive genetic shapes required for object-based models (Deutsch, 2006).

2.10 Multiple Point Statistics (MPS)

As mentioned in Section 2.4 a complete understanding of underlying spatial patterns cannot be fully represented by two-point statistics. Studies by Journel, (1993), Caers and Journel (1998), Strebelle (2002) and Caers and Zhang (2004), also point out that curvilinear geometries are not well reproduced using two-point statistics especially when working with categorical variables such as rock-types.

In cases where we are required to make predictions of spatial patterns with little hard data, multiple point statistics can be used. MPS considers the *n* conditioning data closest to the grid node **u** to be simulated. These conditioning data form a data event d_n that is characterized by its geometrical configuration around the data values, which provides more information than traditional variograms. This template searches through a training image, sharing similar geological patterns, to find replicates of d_n.For each replicate found, the value at the central location of the grid node in the training image, that corresponds to the same relative location as **u** in the data event d_n is recorded. Next, an estimated conditional probability of each facies at **u** is computed, as the proportion of training d_n replicates that have this facies at their central locations. Strebelle (2002, pp 7) provides the following definition for a training image:

“Training images depict the patterns of geological heterogeneities deemed relevant to the application under study. They need not carry any locally accurate information on the actual phenomenon; they merely reflect a prior

geological/structural concept. Thus, a training image can be an unconditional realisation generated by an object-based algorithm, or a simulated realisation of an analogous field, or simply a geologist's sketch processed with CAD algorithms and properly digitized".

The training image is a conceptual 2D or 3D depiction of the spatial continuity of the deposit (Caers & Arpat, 2007) from which multiple-point geostatistics gets its repository of repetitive patterns by searching the training image (Boucher et. al., 2014). It is similar to the act of specifying a variogram model except now, the training image is used to determine the conditional expectation, conditional variance and conditional probability (Van den Boogaart, 2006). Issues of stationarity, the critical dependency on a training image to borrow information for MPS and the validity of a training image have made the application of MPS difficult. (Mirowski, et al., 2009). Mirowski, et. al. (2009) define "statistical validity" as requiring stationarity, to allow for the derivation from the training image an average template pattern. Studies by Strebelle (2002 and 2012), have also concluded that the training images should display the heterogeneities relevant to the phenomenon studied, but that control on the geometry of the data events are not always reliable. In addition, the criteria for how to create a training image and what represents a good training image are not well understood. Despite this, training images deserve more research because they serve as an additional source from which to draw information in areas with limited sample data (Strebelle, 2012). The most popular MPS algorithm for uncertainty studies is SNESim. Less commonly applied MPS algorithms include the heuristic Simulated Annealing algorithm.

In cases where a valid training image can be limiting, cumulant maps have been used instead. Dimitrakopoulos et al, 2010, compared second-order statistics with cumulant maps, in terms of multiple point configurations in the context of connectivity, and found that more information about geological patterns can be derived using cumulants. The study by Mustapha and Dimitrakopoulos (2010) further highlights the usefulness of high-order spatial cumulants when working with limited data sets. High order statistics allow geological aspects to be related to the properties of cumulants. This area of study requires considerable experience for successful implementation.

2.11 Choice of simulation algorithm and relevant software

When selecting a simulation technique, the user should first assess their experience with the technique. If a technique is not well understood, bias realisations may be produced. Another important consideration is the familiarity and ease of the user with selected software. The user must be aware of default settings in software that could impact the results. Other deciding factors include: selecting a simulation technique that maximises the entropy of the response function of the simulation, as well as practical implementation considerations such as the size of the model; number of realisations to be generated as well as the runtime and storage requirements to generate simulations.

2.12 Conclusion

Estimation and simulation methods both provide a means of predicting values at unsampled locations. However, only stochastic simulations account for random variation which makes them more suitable for risk analysis studies involving geological uncertainty. Conventional kriged models are useful for estimation, but where the local scale variations are key considerations to projects, conditional simulations should be applied. Simulations reproduce the in situ variability of grades and lithotype allowing for an assessment of geological uncertainty and underlying risk. There is some loss in accuracy with conditional simulations, but they are more useful than locally smoothed kriged maps in risk assessment. The two methods should therefore be viewed as complimentary since they provide different kinds of information which together help to build a better understanding of a deposit.

Kriging produces a “unique” repeatable output if the same parameters are applied. This feature means kriging hasretained its popularity in mining applications since unique and repeatable answers can allow for quick decision making. Simulations on the other hand, provide a series of equiprobable outcomes (realisations) expressed as probabilities. The generation of multiple equiprobable realisations of the deposit (conditioned to the same sample data and variogram) or alternative versions of reality each describe what is potentially the true character of the deposit. The very existence of multiple equiprobable realisations of the same deposit explains why using deterministic models is risky. Many important decisions

based on deterministic models rely on assumptions and one's own judgment of continuity and stationarity without adequate supporting information. Stochasticorebody modelling is therefore more useful for assessing geological uncertainty.

As with kriging, the choice of stochastic approach rather must be carefully considered to cater to the needs of the study at hand. Each deposit is unique and one should not assume that if a stochastic method is successful in one deposit, that it will be successful in the next.

Based on the review of literature, the gap in knowledge in using deterministic methods for risk analysis studies to assess geological uncertainty can only be overcome using stochastic simulations for Geita mine. The stochastic approach developed has not been applied before to Geita. Previous studies applied by McNeil (2016) for a neighbouring pit quantified the geological uncertainty using SNESim to simulate lithologies followed by simulation of the grade within those lithologies. The study areas do not share sufficient geological similarity to apply McNeil's (2016) methodology requiring this research to provide alternative means to quantify estimated grade and volumetric uncertainty.

CHAPTER 3

"…beware that uncertainty is not intrinsic to the phenomenon under study: rather it arises from our imperfect knowledge of that phenomenon, it is data-dependent and most importantly model-dependent, that model specifying our prior concept (decisions) about the phenomenon. No model, hence no uncertainty measure, can ever be objective: the point is to accept that limitation and document clearly all aspects of the model"

-Pierre Goovaerts, Geostatistics for Natural Resource Evaluation, Chapter 9, pp 442

3 RESEARCH METHODOLOGY

A suitable workflow for assessing geological uncertainty at Geita mine is developed in this chapter after recapitulating the central research questions and subsidiary problems. The range of approaches that were explored in reaching a final and practical workflow are described. The research design is built around a descriptive and interpretive case study evaluating the technical feasibility of a surface-to-underground transition in mining operations using quantitative methods.

The proposed workflow can be applied to analogous deposits to generate stochastic grade and ore category simulations to assess geological uncertainty. The idea that incomplete geological knowledge of the depositcan lead to non-representative 3D geological models of gold bearing reefs, has been discussed in Chapter 2.As a result, inferences about the spatial distribution of gold at unsampled locationsare made from limited available data. Stochastic simulations produce numerous equiprobable realisations of the same deposit that can be used to measure underlying geological risk. Multiple, equiprobable stochastic realisations of the ore body are used in research around this case study to evaluate a business case for the development of an underground mine.

In reaching this decision, three fundamental research questions can be answered using the methodology developed: “Can stochasticsimulations of the geological ore body modelbe used to quantify the uncertainty associated with identifying high grade lenses within the known lower grade mineralisation at Geita Mine?” Secondly, “Can this knowledge be used to make a risk-informed decision on

whether or not to develop an underground mining operation?" Finally, "Can uncertainty about the ore body model be incorporated in planning and designing stope layouts to access the high grade lenses in the underground mine?

3.1 Simulating geological boundaries

To simulate ore category boundaries, two multiple-point statistical (MPS) approaches and one conventional simulation technique were tested. The MPS methods did not fall into the scope of the final study and are only presented for the interest of the reader. They include Simulated Annealing (SA) and Single Normal Equation Simulation (SNESim). The conventional technique, Sequential Indicator Simulation (SIS) was implemented for the final workflow, and therefore forms the bulk of the discussion on simulating geological boundaries.

3.1.1 Simulated Annealing (SA)

The heuristic SA algorithm introduces variograms for sample data and a related training image, into an objective function that minimises the differences between the variograms to produce a resultant training image that is more representative of the sample data (Deutsch & Journel, 1998). SA is therefore used to modify prior rough stochastic images that may be generated using any other simulation method, or it can be used to modify prior locations to ensure that the local data are correctlyhonoured (Deutsch & Journel, 1998). SA was investigated to create a more representative training image for input into SNESim, to simulate lithologies. GSLIB provides two codes for this process: "SASIM", which generates realisations of continuous variables that honour the data variogram and histogram, and "ANNEAL" which "finishes" prior realisations by imposing transition probabilities as obtained from a training image.

The GSLIB SA code was compiled using a Fortran 90 compiler, in Microsoft Visual Studio 2015 and tested on a continuous GSLIB dataset. The code was verified to be error free because the experiments reproduced the results provided for a test dataset in GSLIB. Next, the code was used to perform SA for a dataset originating from an unknown copper deposit. This time, the input data comprised of categorical variables i.e. ore = 1 and waste = 0. The simulated results did not reproduce the data statistics and variogram. The SA code provided in GSLIB was

found to be limited to simulations using continuous input data. Personal communication with the coder, Dr Clayton Deutsch, confirmed that for projects requiring the simulation of categorical data using SA, a full modification of the subroutines embedded in the code is required. This was however beyond the scope of the study.

3.1.2 Single Normal Equation Simulation (SNESim)

The SNESim algorithm was proposed by Strebelle (2002), to scan through a training image (TI), and obtain conditional probability values for the central node to belong to a predefined category - based on a multiple point conditioning data event. As a consequence of failing to produce an input training image for SNESim using SA, a TI was instead generated using interpretations of the geology in Datamine. SNESim was run in SGEMS software, and involved first confirming whether or not the input simulation parameter settings were suitable to reproduce the spatial patterns and statistics of the conditioning data and training image used. After extensive testing, it was found that the resultant realisations were not comparable to the TI and conditioning data. The possible reasons for this are summarised below:

• Inability to reproduce the input TI: Strebelle (2012) states that a training image is a purely conceptual geological model that encompasses only relative spatial information. To ensure that SNESim was correctly set up, unconditional realisations were generated to compare the result to the input TI, to obtain a new possible 3D training image for generating more realisations. The resultant image contained numerous artefacts, hence hard data was introduced to subsequent runs. However, the resulting realisations were still non demonstrative of the geological knowledge and understanding of the deposit, nor were the statistics representative of the input data. Next, the numerous input parameters required to run SNESim were tested and assessed independently in accordance to the study by Liu (2006) including: target global probability distribution function (pdf); servosytem parameter, maximum number of conditioning data; minimum number of replicates; number of multiple grids, maximum search radii; angles for search ellipsoid; affinity and rotation angles; hard data conditioning and soft data conditioning. Despite this, the TI could not be reproduced.

• Uncertainty in the TI: The TI was created in Datamine using a deterministic ore wireframe defined using an economic cut-off grade. The conditioning data comprised of all the available data and was used without applying a cut-off. This may have caused the large deviations of expected local geometry and spatial distribution of grades, especially in sparsely drilled areas. This behaviour was investigated to verify if the problems were data related, or due to a potential inability of the algorithm to capture the complex spatial patterns in the deposit. To test this, all sample data falling inside the ore wireframe was coded as ore and all other samples as waste. The simulations were re-run. Even though it was expected that the realisations would reproduce the TI (due to coding the sample data according to the wireframe, instead of conditioning the TI to the input data) the result did not change – large deviations from expected local geometry. The uncertainty with regards to the suitability of SNESim to the deposit was deemed too high to continue with. Without additional time for testing, it was considered more reasonable to work with a more common and well understood technique.

• Runtime: The runtime required to simulate the study area was in the order of 20hrs to generate a single realisation. This was found to be impractical, therefore, the simulation regions were constrained by imposing a calculated moving average. The resultant model contained a thin “skin” of waste blocks around the ore. All other blocks falling outside of the moving average window were deleted. However, the constraint ignored other areas that contained sample information and could therefore not be used.

Another important observation made regarding SGEMS, is the extra coding required to carry out tasks that are easily performed in commercially available software. This made it difficult to make slight modifications for testing purposes. Based on these observations, it was concluded that generating an appropriate TI is challenging in limited time. The intention of the research methodology was to provide an efficient user-friendly workflow, to allow mine personnel to generate meaningful results, in a reasonable amount of time. It was therefore decided that another more commonly applied technique, such as SIS be investigated. In the absence of additional testing, there was insufficient evidence to suggest that the technique was ill-suited to the deposit. Rather, SNESim was impractical for the objectives of the research during the initial phase of the project, and suffered

severe implementation drawbacks. The technique was therefore not revisited after final study objectives and data was provided by AngloGold.

3.1.3 Sequential Indicator Simulation (SIS)

Sequential indicator simulation (SIS) is a reasonable alternative to object-based modelling when there is difficulty in identifying genetic shapes (Deutsch, 2006). However, it is important to use soft geological interpretations to constrain the process. The method accounts for class-specific patterns of spatial continuity through different indicator semi-variogram models (Goovaerts, 1997). For the research, categorical indicator variables were derived from the underlying continuous gold grades based on a predefined grade cut-off. Using this approach, lower and higher grade domains were distinguished as ore category facies, each representing a mutually exclusive and exhaustive category. For the SIS model to be valid, only one categorical variable may exist at any particular location in the model and a category must exist in all locations in the model. The SIS simulations and conditioning data were constrained to lie within the identified low grade mineralisation, and then the conditioning data used to detect higher grade lenses within it. The similar principles of sequential simulations, as with SGS, applies to SIS. The only difference is that indicator facies are used, therefore the conditional distribution is defined by conditional expectations. The SIS realisations were generated using ISATIS geostatistical software. A rough exposition of the mathematical concepts describing the the algorithm is presented below, and summarised from the study by Hansen (1992):

SIS requires strict stationarity assumptions because it is based on the principle that it is possible to completely specify the joint probability of a collection of *N* dependent events, $\{A_j, j=1, \ldots, N\}$ as the product of *N* conditional probabilities. Grid nodes to be simulated are randomly visited and the conditional distribution for a particular node derived according to:

$$P[Z(u_1) \leq z \mid (n)] = P[Z(u_1) \leq z \mid Z(u_\alpha) = z_\alpha, \alpha \in (n)] \quad \ldots\ldots(7)$$

A random value is drawn from the distribution to become the simulated value. The algorithm then moves to the next location to be simulated. The previously simulated value is then included in the distribution at the new node to be simulated

and the process repeated until all gridnodes are simulated. Deriving the conditional distribution of Z at a particular node is considered to be the most difficult part of implementing SIS. Hansen (1992) citing Journel and Alabert (1989) describes how the conditional distributions are derived using binary indicator random variables as follows:

The event [Z(u) ≤ z] can be characterized using indicator variables as:

$$I(u;z) = \{\frac{1, if Z(u) \le z,}{0, otherwise} \quad \text{..... (8)}$$

Any conditional probability for Z(u) can be written in terms of the conditional expectation:

$$P[Z(u) \le z \mid (n) = E[I(u;z) \mid (n)] \quad \text{..... (9)}$$

When K threshold values for attribute Z are considered, {z_k, k=1,...,K}, each conditioning data point gets coded into an indicator class according to the K thresholds to take on a value of 0 or 1:

$$\{Z(u_\alpha) = z_\alpha\} \rightarrow \{i(u_\alpha; z_k), k = 1,..., K\} \text{..... (10)}$$

The conditional probability distribution for Z(u) is then expressed conditional to the n indicator columns:

$$\begin{aligned} &P[Z(u) \le z_{k_0} \mid Z(u_\alpha) = z_\alpha, \alpha \in (n)] \\ &\approx E[I(u; z_{k_0}) \mid I(u_\alpha; z_k) = i(u_\alpha; z_k), k = 1,..., K; \alpha \in (n)] \end{aligned} \quad \text{..... (11)}$$

A detailed description of the implementation of the algorithm is presented at the end of the Chapter where the practical workflow followed is presented.

3.1.3.1 Summary of SIS Algorithm inputs

The most important inputs for running SIS in ISATIS include: the conditioning data, facies definition, output grid, model, neighbourhood and definition of simulation parameters.

Conditioning Data

The conditioning data is the available sample data coded as categorical indicator variables derived from the underlying continuous gold grades.

Facies definition

The facies definition allows the categorical input data to be transformed into facies.

Output grid

The output grid is a 3D grid where the conditional simulations are stored.

Model

SIS requires an indicator variogram model from which to apply simple kriging. The indicator variogram is derived from the conditioning data. More advanced options are also available including: Rescaled Ordinary Co-kriging; Filtering Model components; Factorial kriging and Deconvolution.

Neighbourhood

Neighbourhood definition is required for estimation to be performed in the kriging step of the algorithm. This assists the algorithm in identifying the samples that are to be used for estimating or simulating values at a target grid node.

Simulation Parameters

This step allows the user to choose the number of realisations to be generated and usually depends on the capabilities of the computer being used to run the simulations. A seed number is also defined to generate random numbers for the simulations. Another parameter to define is, how many already simulated nodes should be used (in the selected neighbourhood) for successive simulations. Finally, the user can choose between performing each simulation using the same (algorithm visits nodes to be simulated in a fixed order) or independent paths (algorithm visits nodes to be simulated at random).

3.2 Simulating grades

Several stochastic conditional simulation algorithms were considered for grade simulations: SGS, GSGS, DBSim and DBMAFSim. Of these, the DBSim algorithm was selected due to its superior computational efficiency (relative to SGS and GSGS) both in terms of storage requirements and simulation time. DBMAFSim

was deemed inappropriate for the study, because the grade of mineralisation and distribution was structurally rather than ore categoryly controlled (refer to Sanislav, et. al., 2016, pp. 21).

3.2.1 Direct Block Simulations (DBSim)

The workings of the DBSim algorithm are described by Dimitrakopoulos and Benndorf (2005, pp. 62-63).The authors use a stationary random function to describe conditional simulation on a grid, based on sampling from the N-variate distribution conditioned to the available data set. The decomposition of the multivariate probability function into a product of univariate conditional distribution functions, is then presented, because it makes sequential conditional simulation possible. From the formulation presented in the paper, the GSGS algorithm is derived by considering the use of groups of nodes for simulation rather than node-by-node as in SGS through the decomposition of the conditional density function into groups of conditional densities. This allows for groups of nodes to be simulated. The authors then extend this formulation (Dimitrakopoulos & Benndorf, 2005, pp. 63) to DBSim. The nodes that are simulated in one group in the GSGS formulation corresponds to simulating the internal nodes discretising the block. The group of nodes is then backtransformed and a simulated block value calculated as the average of the point values both in data and gaussian space. Point values are discarded and only the simulated block value added back as conditioning data and the block value in data space kept as a result.

The operation of the algorithm involves:

• A random path visits each block to be simulated;

• Transform the data into Gaussian space;

• For each block visited in the random path, values for internal nodes discretising the block are simulated;

• The simulated nodes in one group are averaged to give a simulated block value in Gaussian space, then back transformed to give the block value in data space;

• The simulated block value in Gaussian space is added back as conditioning data and the block value in data space retained as the result. The other internal nodes are discarded.

The algorithm repeats the process of visiting each block in the random path until all the blocks are simulated. A description of the implementation of the algorithm is presented in Chapter 4, where the application and practical workflow followed is presented.

3.2.1.1 Summary of DBSim inputs

The most important inputs required to run DBSim in ISATIS include: the conditioning data, auxiliary centred file, output grid, block anamorphosis, block Gaussian model, neighbourhood and definition of simulation parameters.

Conditioning Data

The conditioning data is the available sample data separated into higher and lower grade domains.

Auxiliary centred file

The auxiliary centred file is a file created to store new samples that are moved to the centre of the blocks in the output simulation grid.

Output grid

The output grid is a 3D grid where the conditional simulations are stored. Additional variables may be defined in the output grid but are limited to the variable definition of the conditioning data. The output grid can store both point and block support simulated values.

Block Anamorphosis

The block anamorphosis is a form of Gaussian support correction, to generate at the grid locations, simulated values that can be comparable to the data at the same support i.e. from point to block scale.

Block Gaussian model

This refers to the Block Gaussian variogram model obtained from the block anamorphosis.

Neighbourhood

Neighbourhood definition is required for estimation to be performed in the co-kriging step of the algorithm. This assists the algorithm in identifying the samples that are to be used for estimating or simulating values at a target grid node.

Simulation Parameters

In this step, the number of simulations to be generated can be defined. There is no rule of thumb for the number to be generated. Generally, the limit depends on the capabilities of the computer being used to run the simulations. A seed number is also defined under simulation parameters to generate random numbers for the simulations. Other definitions include the number of already simulated grid nodes in the neighbourhood to be used in the successive simulations.

3.3 Validation

The validation of simulated realisations is achieved through visual assessment, statistics, histograms and variogram reproduction of the input conditioning data.

3.4 Practical application of the simulation algorithms

The SIS and DBSim algorithms were applied to a data set from the world-class Geita Hill gold deposit in Tanzania (Figure 3-1). The Geita Hill gold mineralisation largely occurs along the Geita Hill Shear Zone. The known gold mineralization refers to that part of the mineralisation which is well mapped and understood. The known gold mineralisation envelope referred to in this dissertation is based on a cut-off grade of 0.5 g/t (also referred to as the low grade envelope). This is defined along the length of the Geita Hill pit, which trends NE-SW, dips moderately NW.The high-grade ore lenses that occur along the Geita Hill Shear Zone were defined using grade control drilling available in the top portion of the deposit, and exploration drilling that targeted the underground extensions of the mineralization and plunge NW (Sanislav, et al., 2016).

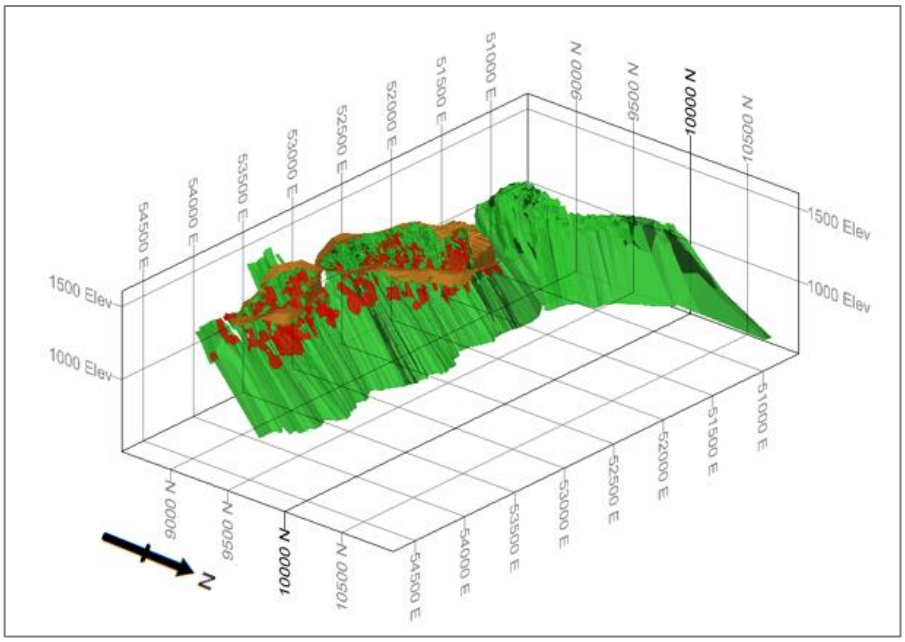


Figure 3-1: View of the Geita Hill pits showing the existing interpretation for the location and extent of higher grade lenses (red wireframe) within the known low grade mineralisation (green wireframe).

As part of the pre-feasibility studies, several underground mining stope layouts are being designed to access the interpreted high grade areas in the resource model (Figure 3-2). The definition of the high grade ore in the resource model is based on a single grade indicator approach which considered modelling of samples from grade control and deeper exploration drilling, targeted around the underground

extensions of the mineralisation, below the current pit. The current stope layout is designed around the interpreted high grade blocks in the resource model. It is important to make realistic interpretations to ensure that stope designs are optimal. Failing to do so may result in incorrect expectations of grades and tonnage which may increase risk to business case studies. To quantify this risk, resultant realisations for the study, will be ranked in terms of potential upside and downside scenarios based on total volume and metal content.

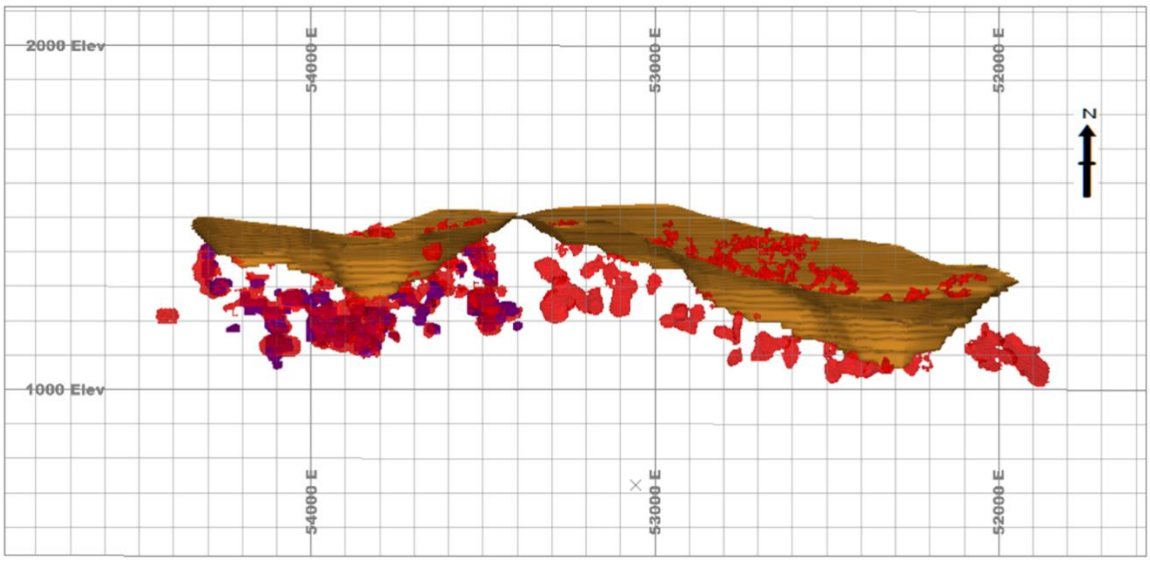


Figure 3-2: East-West section through the Geita Hill pits showing the preliminary mining stope layouts (purple wireframe) targeting higher grade lenses below the pit.

3.4.1 Geological Setting

The description of geological structures and mineralisation to follow, is taken from Sanislav et. al., 2016, whose work is the most recent geological study undertaken at Geita. The data presented by Sanislav et. al., 2016, thus represents the current geological understanding of the deposit as derived from field mapping and structural interpretations, as well as, mapping, core logging and underground mine plans provided by Geita Mine.

The Geita Hill (GH) deposit is located south of the Lake Victoria region in Tanzania and is hosted within the Archean Geita Greenstone Belt (Figure 3-4). Several other major deposits are located within the Geita Greenstone Belt: Lone Cone, Nyankanga, Area3, Kukiluma, Matandani, Chipaka, Pit 30, Ridge 8, Star & Comet, and Roberts as shown in Figure 3-4.

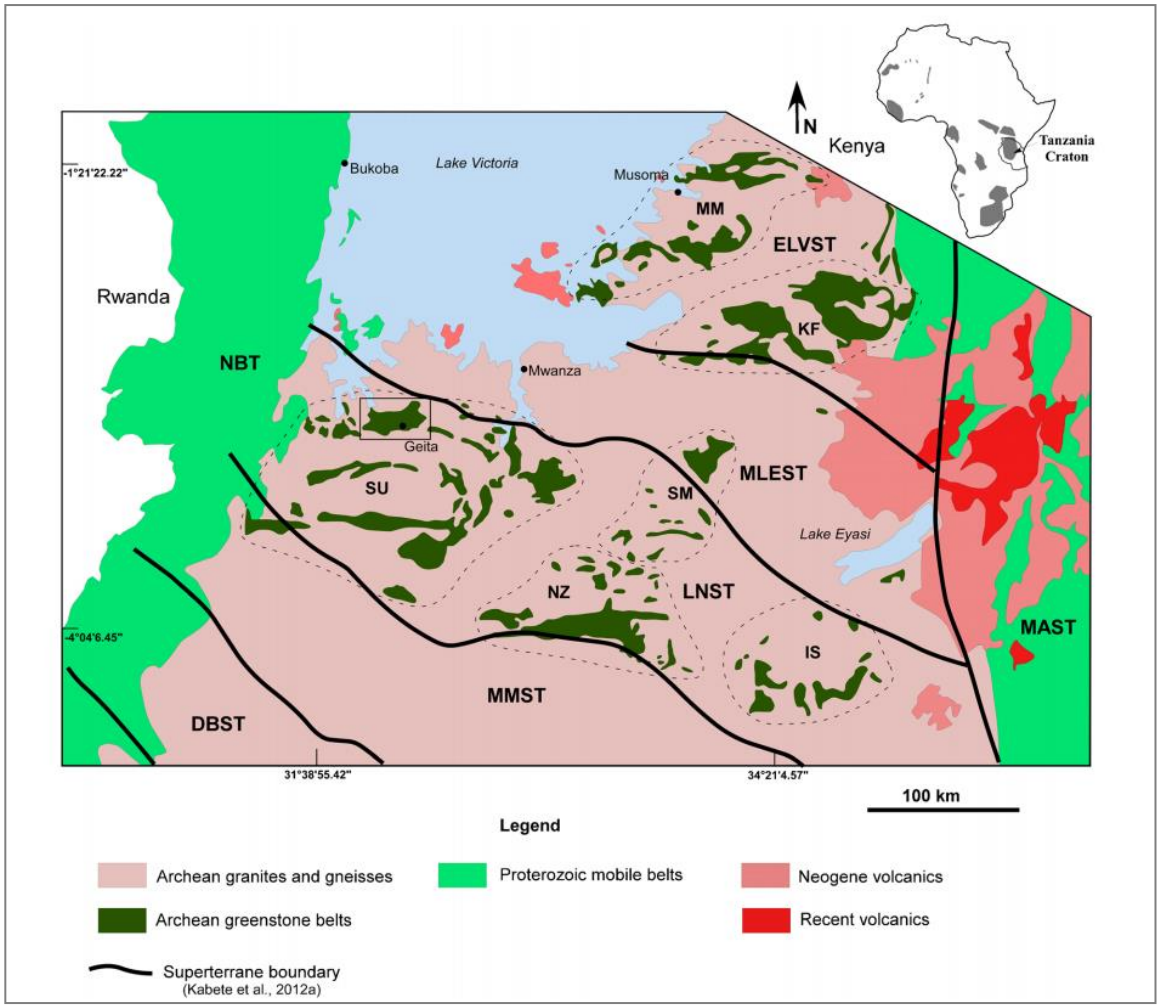


Figure 3-3: A simplified geological map for the Lake Victoria Region showing the main geological units. *SU*Sukumaland Greenstone Belt, *NZ*Nzega Greenstone Belt, *SM*Shyninga-Malita Greenstone Belt, *IS*Iramba-Sekenke Greenstone Belt, *KF*Kilimafedha Greenstone Belt, *MM*Musoma-Mara Greenstone Belt. Super-terrane boundaries include: *ELVST* East Lake Victoria, *MLEST* Mwanza Lake Eyasi, *LNST* Lake Nyanza, *MMST*Moyowosi-Manyoni, *DBST* Dodoma Basement, *MAST*MbuluMasai, *NBT*Nyakahura-Burigi. Inset map of Africa showing the location of Archean blocks (Sanislav, Brayshaw, Kolling, Dirks, Cook, & Blenkinsop, 2016, pp 2).

Figure 3-4 shows the general ENE-WSW trend of the Geita Hill mineralisation that occurs within the nose of a regional fold structure that closes in the SE.

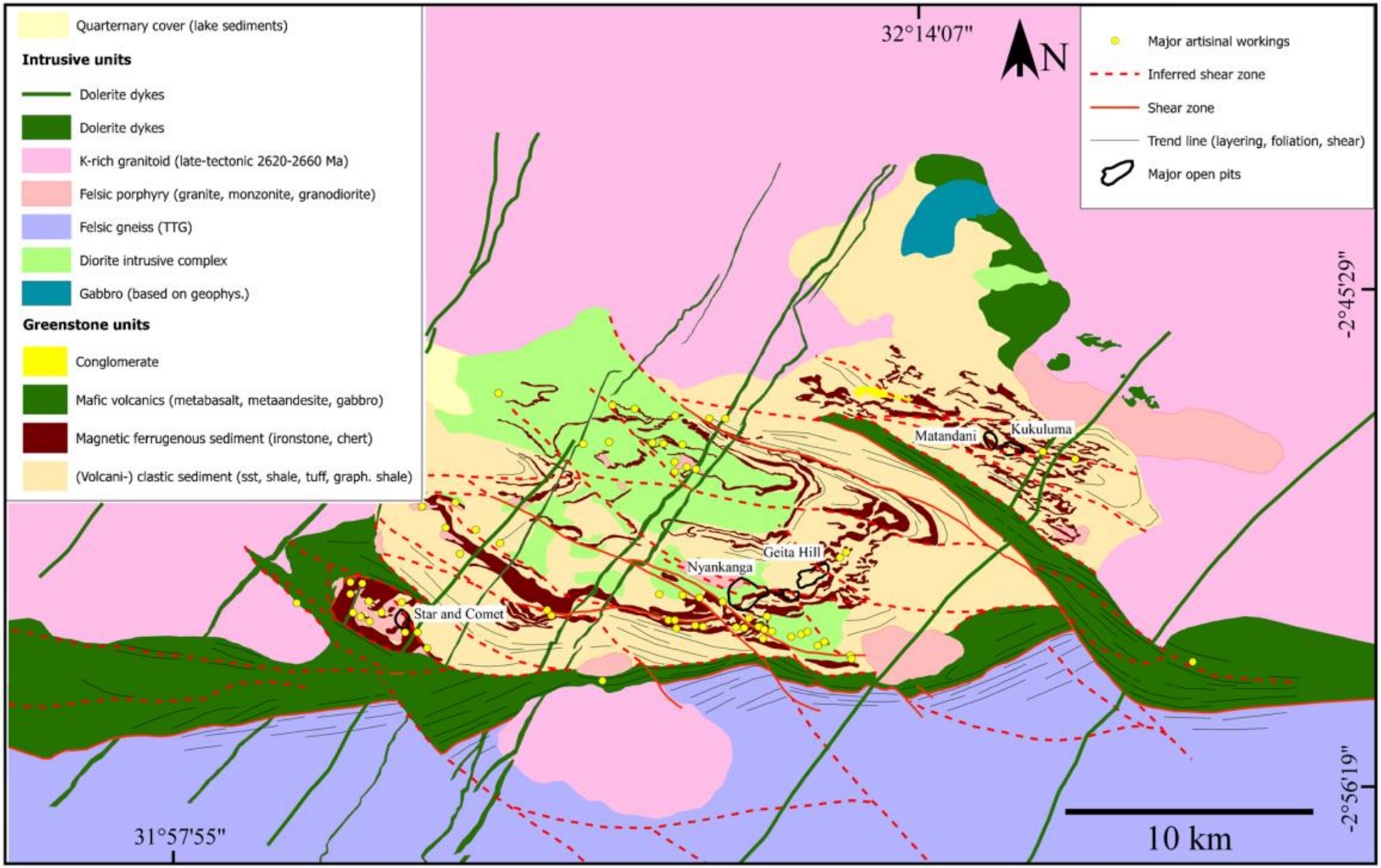


Figure 3-4: Geological map of the Geita Greenstone Belt (Sanislav, Brayshaw, Kolling, Dirks, Cook, & Blenkinsop, 2016, pp 3)

The geology of the deposit is dominated by ironstones intruded by diorite sills and dykes and subordinate lamprophyres and minor quartz-porphyries of granodiorite composition. The geological map of the Geita Hill deposit (Figure 3-5) shows the overall distribution of the lower grade mineralisation (Au≥0.5g/t), along the length of the Geita Hill West pit. The gold mineralisation is spatially related to the Geita Hill Shear Zone (GHSZ) comprising of fault segments that terminate in splays of minor faults and fractures.

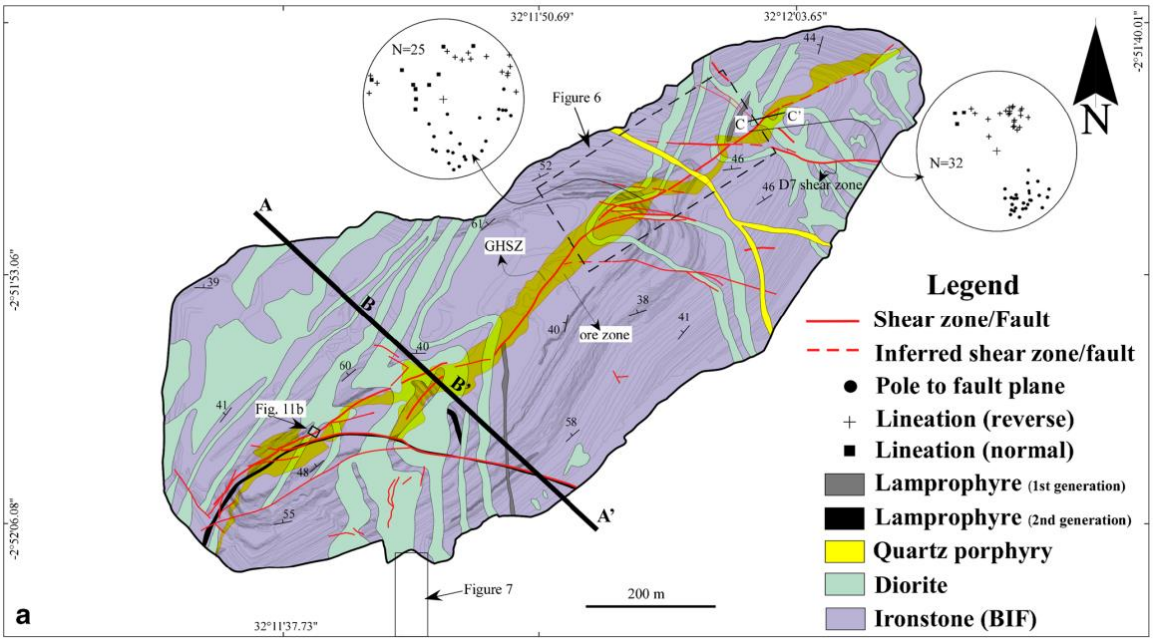


Figure 3-5: Geological map of the Geita Hill West gold deposit. The background of the map (thin grey lines) represents the pit wireframe. (Sanislav, Brayshaw, Kolling, Dirks, Cook, & Blenkinsop, 2016, pp. 6)

The mineralisation forms part of a trend that has an overall interpretation of an imbricate fan and is located along unique thrusts within this fan. The geological model for the entire reef deposit is shown in Figure 3-6. The study area is distinguished into two stationary domains i.e. GHE west (GHEW) and GHE east (GHEE) based on historical mine studies (Figure 3-6). Due to the dependence on the simulations on stationarity (as with kriging) the GHEW and GHEE domains were simulated separately.

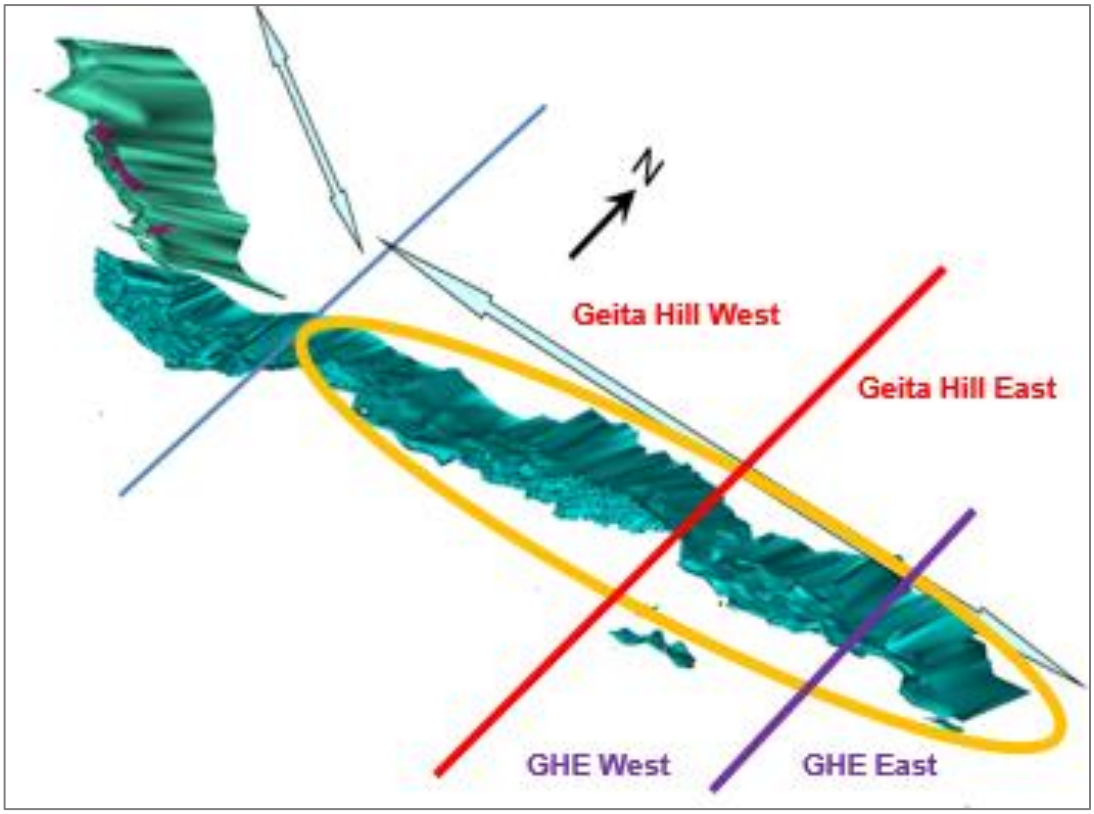


Figure 3-6: Reef Thrust Geometry. The portion of the reef forming the Geita Hill deposit is highlighted in yellow. The deposit is divided into Geita Hill East and Geita Hill West. Geita Hill East if further differentiated into GHE West and GHE East.

3.4.2 Description of data

Simulations were run for the eastern portion of Geita Hill (GHE) because of the following constraints:

- Mining: Access to the underground is planned from the East as a separate portal to current open pit mining making this area an immediate priority; the bulk of underground stopes occur here.
- Sampling: the dense drilling in this portion provides sufficient information to inform the simulations, and
- Practical: for testing the applicability of the techniques, the run time for simulations should be short to allow for quick assessments. Any methodology successfully developed for the east can be applied for studies in the western portion of the study area.

The drillhole dataset for GHEW comprised of 249 drill holes and for GHEE, 205 drillholes. The drill holes were predominantly sampled at 1m intervals. Figure 3-7 shows the location of the study area and available drill hole information, in relation to the operating pit limit and low grade mineralisation. This is shown in closer detail in Figure 3-8 and Figure 3-9 that focus on the GHEE and GHEW sub areas independently.

Only the samples falling within the low grade ore wireframe were used as conditioning data. This data was further separated out into its higher and lower grade domains using a cut-off grade of Au =2g/t.

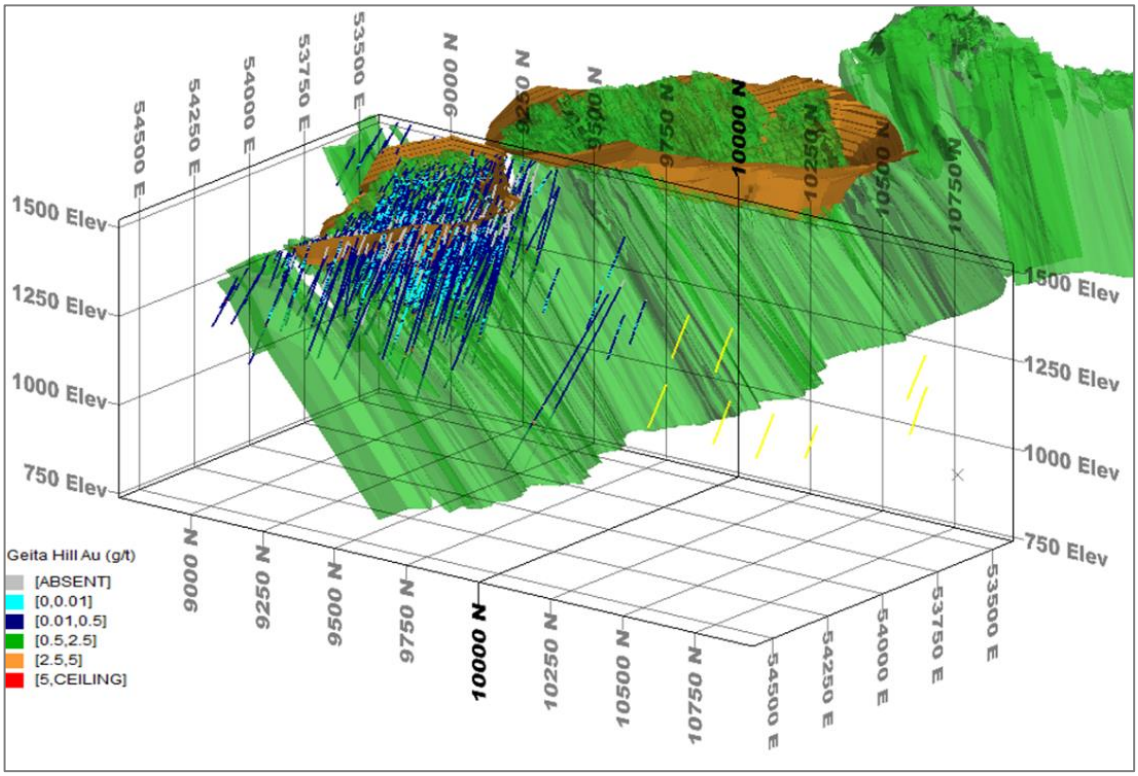


Figure 3-7: View of the entire study area in relation to the pit and low grade ore wireframe. The drill holes are displayed according to grade values. Holes highlighted in yellow were excluded from the study.

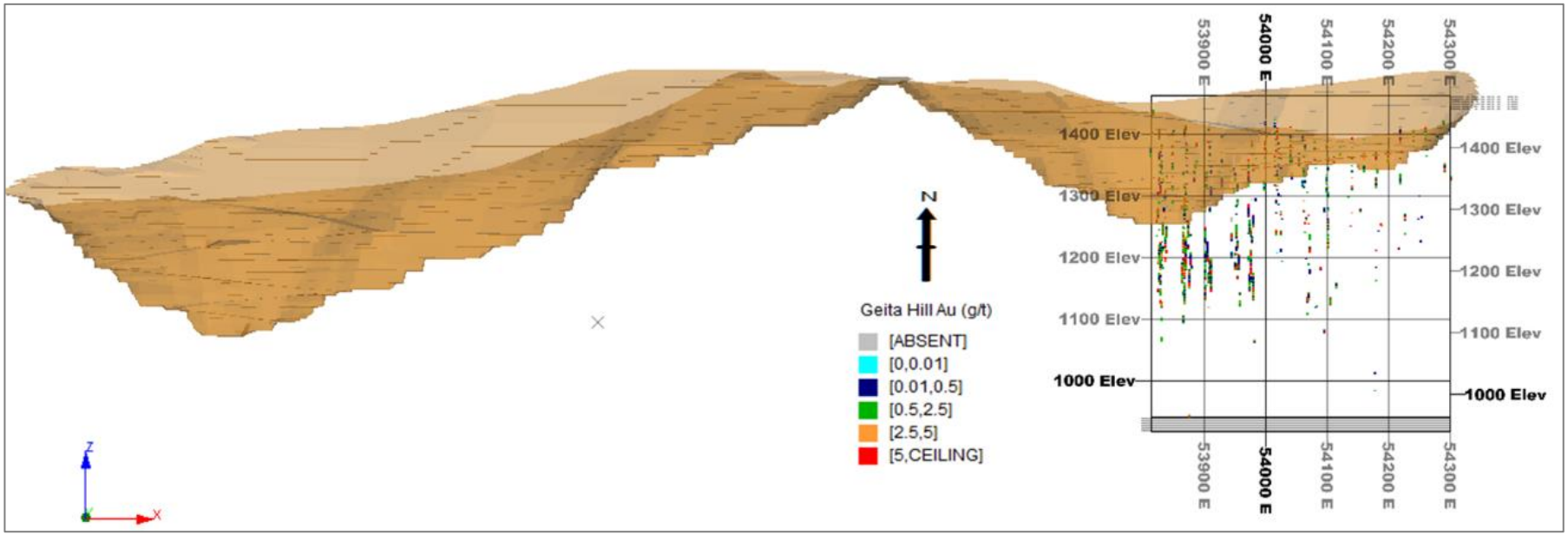


Figure 3-8: W-E section through Geita Hill pits showing the sample information available in the GHEE sub area.

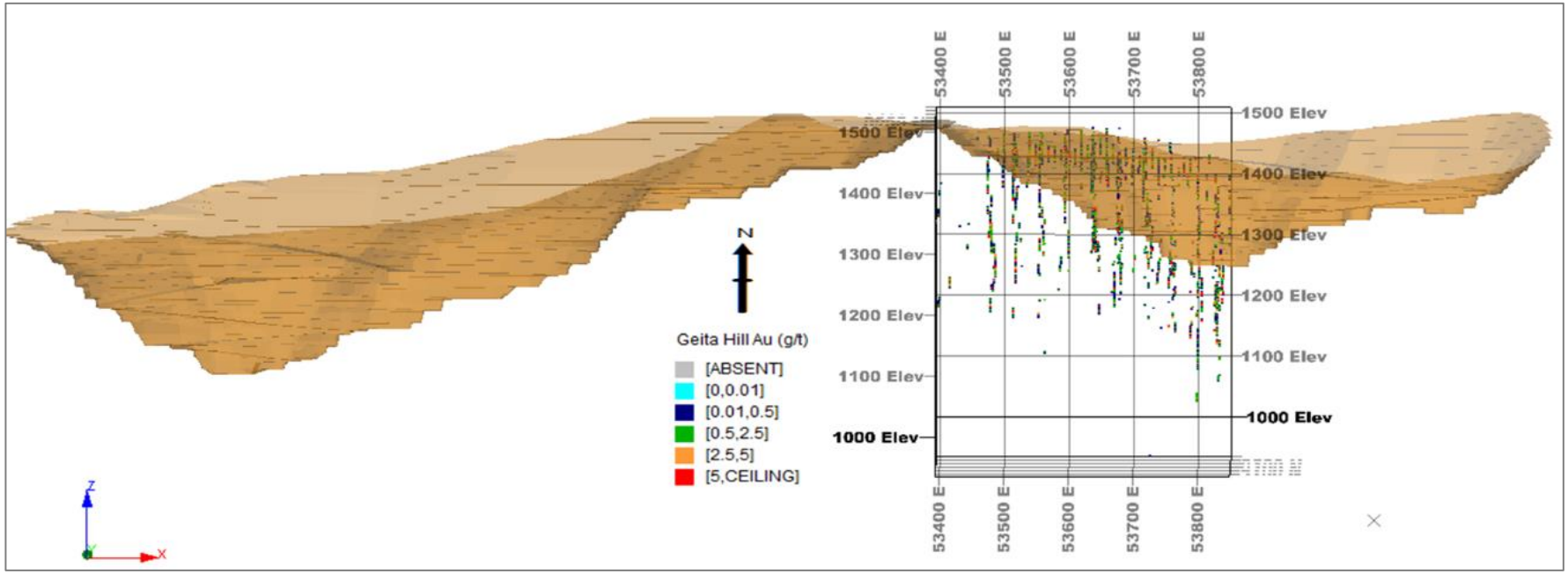


Figure 3-9: W-E section through Geita Hill pits showing the sample information available in the GHEW sub area.

3.5 Simulating the study area

Numerous simulation inputs were tested, to assess the sensitivity of the simulations. The realisations from the tests were evaluated in terms of how well each represented the current geological understanding of the deposit. This included the following:

- Simulating the entire study area using the 1m composited raw data (not split into high and low grade zones) to confirm the current interpretation for the shear zone;
- Simulating the shear zone using 1m composited conditioning data split into high and low grade zones;
- Simulating the shear zone using 1m composited conditioning raw data (not split into high and low grade zones);
- Simulating the shear zone using conditioning data composited to 1m;
- Simulating the shear zone using conditioning data composited to a bench height of 3m;
- Simulating using variogram models based only on the conditioning data, and
- Simulating using variogram models based on the conditioning data and also information borrowed from the well informed top portions of the deposit to better represent the known interpretation of the geology.

Based on the tests, the final simulation process generated 200 grade simulations and 100 ore category simulations as follows:

- 50 sequential indicator simulations conditioned to all the available information composited to 3m in GHEE
- 50 sequential indicator simulations conditioned to all the available information composited to 1m in GHEW

- 50 direct block simulations conditioned to 1m composited high grade samples (Au≥2g/t) in GHEE
- 50 direct block simulations conditioned to 1m composited low grade samples (Au<2g/t) in GHEE
- 50 direct block simulations conditioned to 1m composited high grade samples (Au≥2g/t) in GHEW
- 50 direct block simulations conditioned to 1m composited low grade samples (Au<2g/t) in GHEW

The simulated realisations were ranked and assessed independently to identify potential upside and downside mine planning scenarios. Through a process of combining ranked simulations, a joint uncertainty model was derived. However, it must be noted that the ranking depends on global volumes and total metal and does not consider the joint configuration of blocks.

3.5.1 Simulating ore categories using SIS

SIS realisations were run in ISATIS to obtain indicator maps for stochastic realizations of values higher than the selected 2g/t cut-off. The maps were then compared to the IK wireframe for the deposit, to constrain the shapes and positions of geological boundaries separating higher grade lenses from lower grade mineralisation.

3.5.1.1 SIS Algorithm inputs

The inputs used are summarised below:

Conditioning Data

The available sampling information occurring within the known low grade mineralisation wireframe was used as conditioning data for each sub-domain. The gold grades were coded as lithofacies with an integer value = 1 (higher grade ore, Au≥2g/t) or 0 (lower grade ore, Au<2g/t).

Facies definition

The proportion of each facie in the conditioning data was calculated and is presented in Table 1.

Table 1: Proportion of low and high grade lithologies for GHEE and GHEW

Area	Category	Value	Proportion (%)
GHEE	1 (Au<2g/t)	0	70
GHEE	2 (Au≥2g/t)	1	30
GHEW	1(Au<2g/t)	0	66
GHEW	2 (Au≥2g/t)	1	34

Output grid

The 3D output grid covers the full extent of the Geita Hill study area (Table 2) and comprised of 29,494,080 grid nodes. The simulation region was constrained to fall within the low grade wireframe for the deposit.

Table 2: Description of the simulation grid

X origin (mE)	350
Y origin (mN)	8640
Z origin (mElev)	505
Node spacing along X (m)	5
Node spacing along Y (m)	5
Node spacing along Z (m)	3,33
Number of nodes along X	266
Number of nodes along Y	336
Number of nodes along Z	330

Model

Indicator variogram models were used to establish the interface between the lower grade ore and higher grade lenses (transition ranges). The rotations and directions describing the anisotropy of the deposit, followed the Mathematician's convention in ISATIS: using one angle around the Z axis, counted positive counter clockwise from East to North (+Z) and bounded by -180 and +180 deg. The orientation for strike was measured to be 0 degrees and dip -30 degrees. The resultant indicator variograms for each subdomain is presented in Figure 3-10 and Figure 3-11.

Table 4 and Table 5 provide a summary of model and experimental variogram parameters.

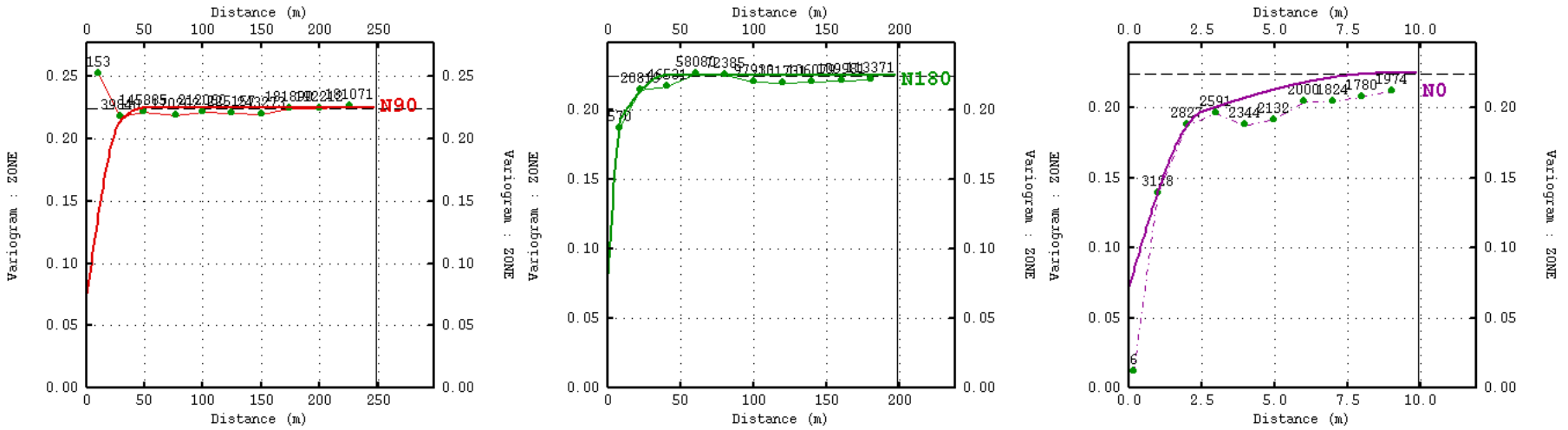


Figure 3-10: East SIS directional variogram models

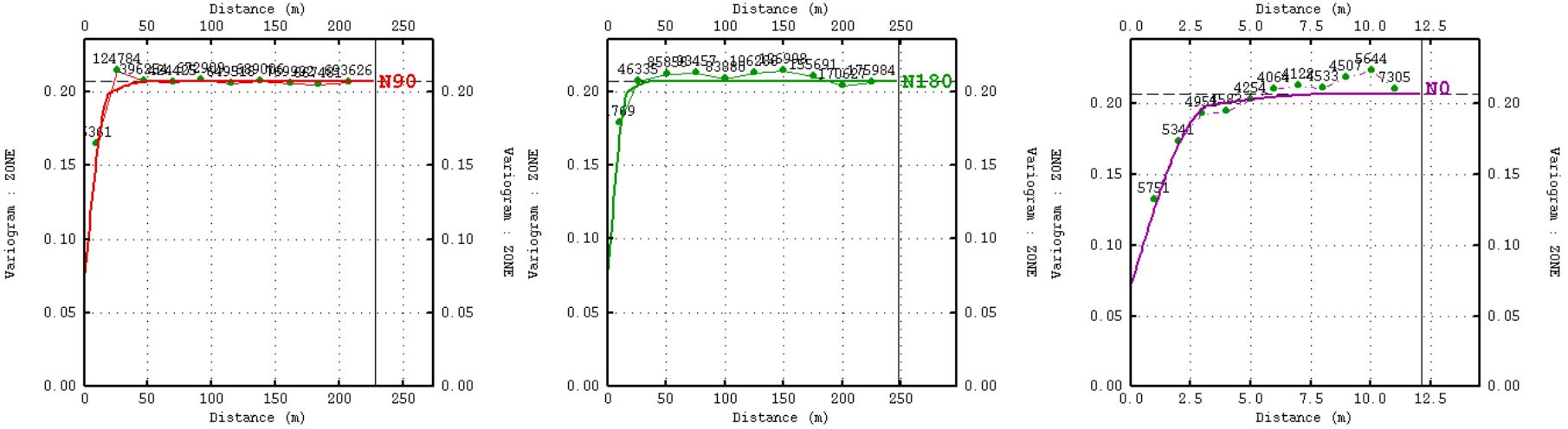


Figure 3-11: West SIS directional variogram models

Table 3: Experimental Variogram parameters for the low-grade ore high-grade lens interface (GHEE)

Parameter	**Downhole**	**Along Strike**	**Across Strike**	**Down Dip**
Direction		N90	N180	N0
Lag distance (m)	1.0	25	20	1.0
Number of lags	10	10	10	10
Angular tolerance (degrees)	90	45	30	90

Table 4: Experimental Variogram parameters for the low grade ore- high grade lens interface (GHEW)

Parameter	**Downhole**	**Along Strike**	**Across Strike**	**Down Dip**
Direction	**N0**	**1: N90**	**2: N180**	**3: N0**
Lag distance (m)	1.0	23	25	1.0
Number of lags	12	10	10	12
Angular tolerance (degrees)	90	45	20	90

Table 5: Spherical Model Variogram parameters for the low grade ore- high grade lens interface (GHEE and GHEW)

Domain	**Nugget**	**Structure number**	**Structure Sill**	**Range in Dir. 1 (m)**	**Range in Dir. 2 (m)**	**Range in Dir. 3 (m)**
GHEE	0.07	1	0.1190	20	18	3.3
		2	0.0179	50	40	8.5
GHEW	0.07	1	0.1078	30	10	2.5
		2	0.0468	50	40	9.0

Neighbourhood

A moving search neighbourhood was defined for each domain, using a search ellipsoid orientated along Azimuth = N0 and dip= -30 degrees. For a sample to be considered as conditioning information (kept in the search ellipsoid), the distance between the target node and the sample must be less than the 3 maximum distances (axes) describing the ellipsoid. The maximum ellipsoid distances were selected to honour the maximum ranges of the variogram model in each direction. After rotation, the X, Y and Z directions of the ellipsoid are referred to as maximum distances U, V and W respectively. In addition to defining these distances, the user needs to choose an optimum number of samples to use in the simulation. A node is only simulated, if the algorithm detects the optimum number of samples, as it sequentially searches the neighbourhood. Due to the sparseness of data, only 10 samples were used. This number can be increased if more conditioning data is available. The maximum distances for GHEE and GHEW were: U=50m, V=40m and W=10m.

The maximum direction along W was adjusted to 20m to account for the varying thickness of the low grade ore wireframe.

Simulation Parameters

The maximum number of test simulations generated for each domain was set to 50. There was no need to generate additional realisations due to stabilisation of the realisations after 50 realisations. The optimum number of already simulated nodes was set to 10 which means that ISATIS loads the original conditioning data and the 10 closest already simulated nodes in the search neighbourhood algorithm. The impact of varying neighbourhood parameters can also be assessed using the TEST window in ISATIS. The seed for the random number generator was set to 423141 and the simulations run using independent paths to guarantee that the resultant realisations would be strictly independent.

3.5.1.2 SIS validation

The variogram models for the SIS realisations generated, were plotted with the variogram model of the input conditioning data (Figure 3-12 and Figure 3-13). This is done to verify that the spatial structure and proportions represented by the realisations, honour that described by the conditioning data. Overall, the

realisations were able to reproduce the data variograms. Due to the categorical nature of the data, interest was only on the range reproduction since the nugget has no significance when dealing with arbitrary categorical variable definition.

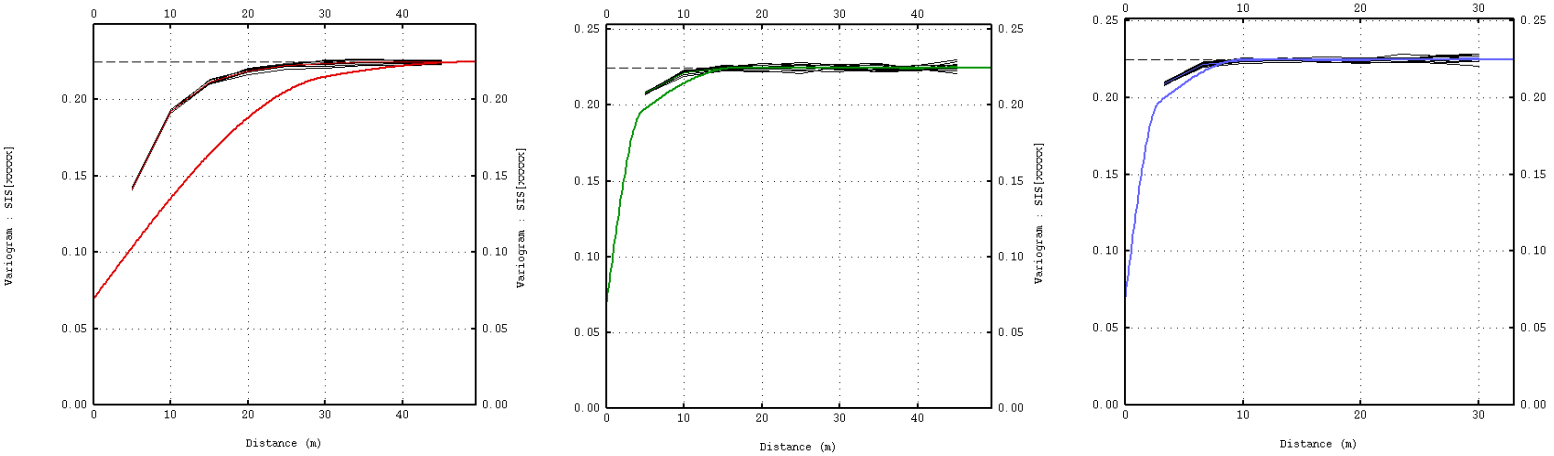


Figure 3-12: East SIS variogram validation. Variograms for data is indicated as solid lines (red, green and blue) for each anisotropic direction. Variogram models for each realisation is indicated by black lines.

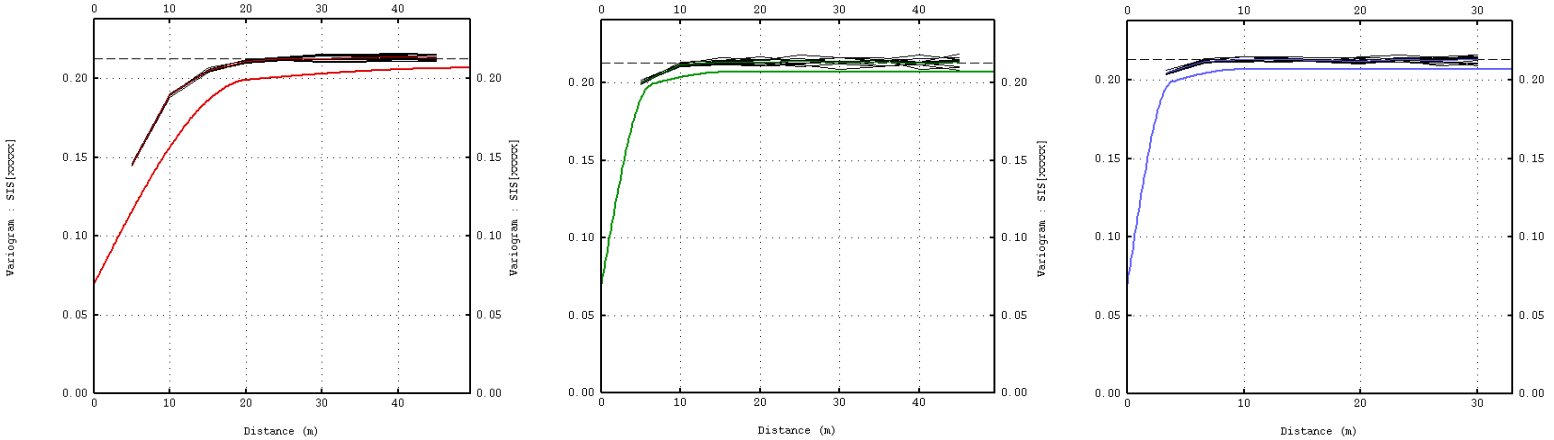


Figure 3-13: West SIS variogram validation. Variograms for data is indicated as solid lines (red, green and blue) for each anisotropic direction. Variogram models for each realisation is indicated by black lines.

In addition to verifying the variogram reproduction, the ability of the simulations to reproduce the data statistics was also tested. This was done by comparing the output simulated proportions of each facies against the input data (Figure A-1 and A-2, Appendix A). Each resultant histogram reproduced the global proportions of material: lower grade (64%) and higher grade (34%) for GHEE and lower grade (70%) and higher grade (30%) for GHEW.

The final check, involved viewing each realisation to ensure that the simulated geology matched the geological understanding of the deposit. Although the simulations passed the variogram and histogram validation, the geologically unrealistic noise in the realisations rendered them unacceptable for use in the research. If an unlikely type is drawn randomly from the cdf during SIS, and used to subsequently condition realisations, the resultant simulated model will contain relics that are geologically unrealistic (Yamamoto et. al., 2015).

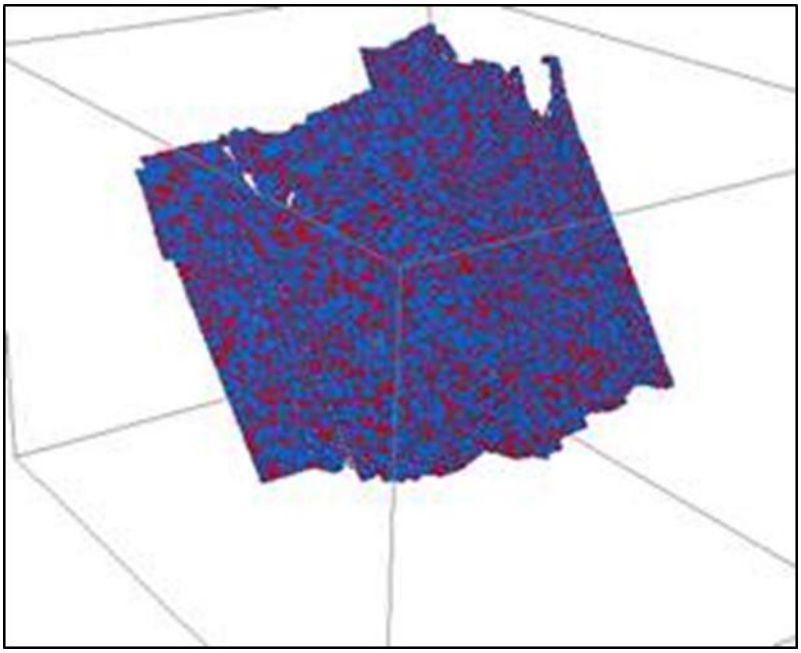


Figure 3-14: 3D view of resultant noisy simulation

Another possible reason for the noisy realisations was that the variogram model ranges for GHEE and GHEW were too short, when in reality stronger continuity exists. To better identify the connectivity of the high grade indicators in the simulations, the variograms were modelled from information borrowed from the densely drilled upper portions of the deposit, to honour the knowledge of the continuity of the high grade lenses, as understood by the on-site geologists, and

new realisations generated. The new realisations were still noisy, showing poor connectivity along the Z-direction. The conditioning data was then composited to a bench height of 3m and re-run with the modified variogram model parameters. The resultant realisations were validated and deemed to be acceptable.

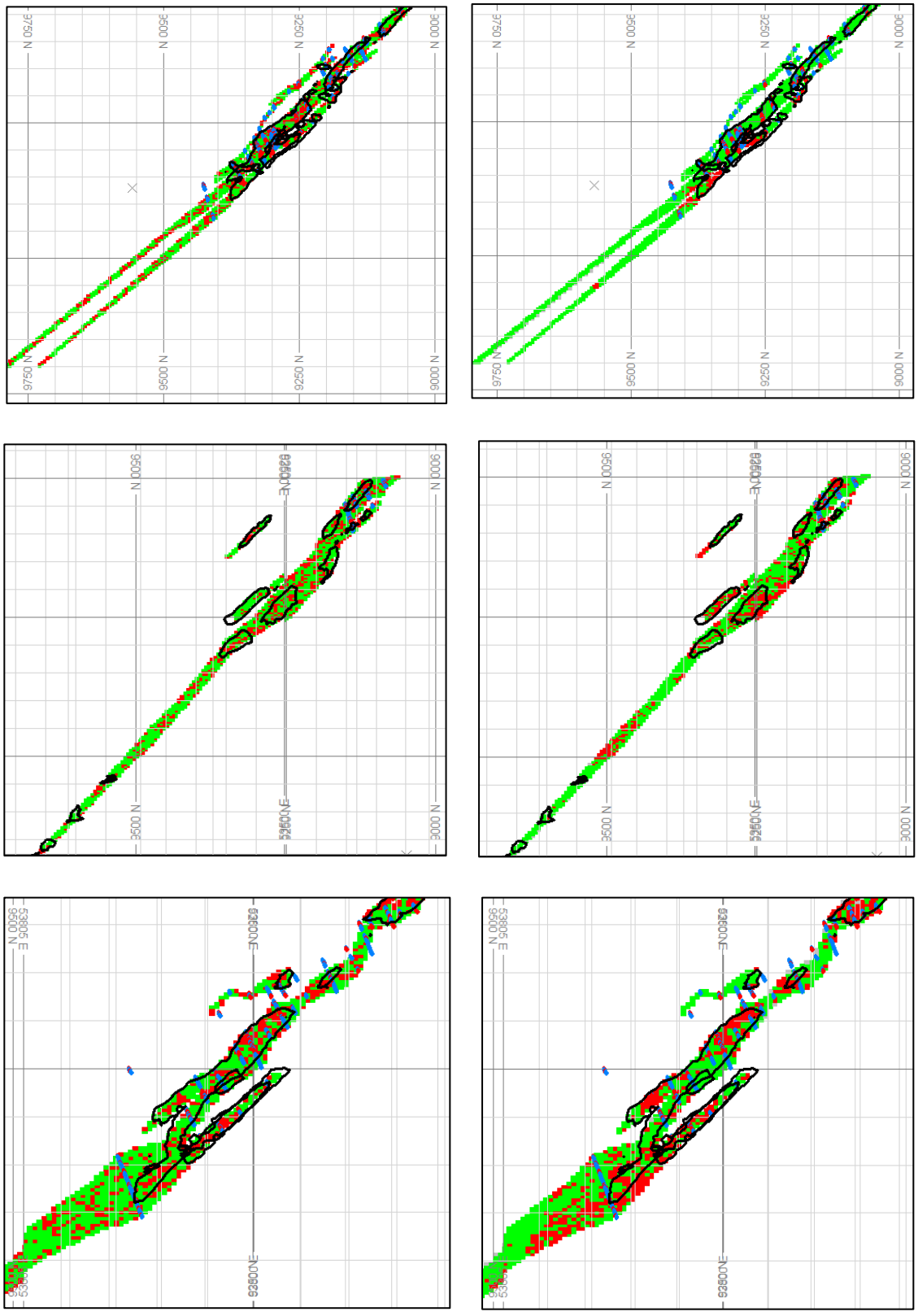


Figure 3-15: Section views showing the effect of using the same model variogram parameters and conditional data composited to 1m (left) and 3m (right).

The same process of modifying the model variogram ranges was applied to GHEW and the conditioning data composited to 3m. However, the realisations for GHEW were noisier than expected (Figure 3-16). The simulations were then run on conditioning data composited to 1m and the resultant realisations validated and deemed acceptable for use in the study.

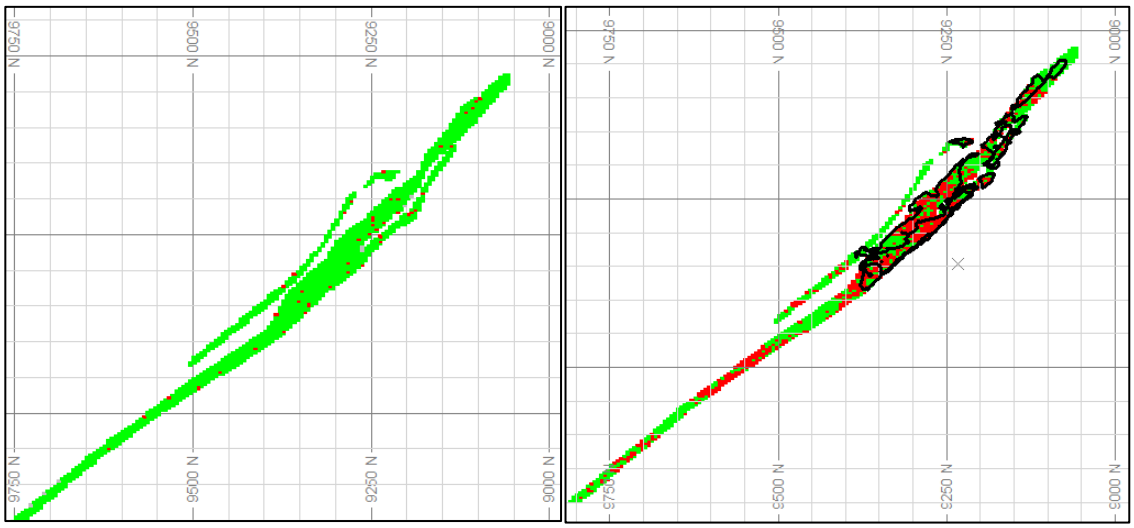


Figure 3-16: Section view through SIS realisations for GHEW run using conditioning data composited to 1m (left) and 3m (right), using the same variogram model parameters

The variogram validation for the final 50 realisations follow. The new variograms models show longer ranges of continuity (>100m) which correlate with the knowledge of the geology of the deposit. Variogram models based on partial datasets (Figure 3-10 and Figure 3-11) showed shorter ranges of continuity (approximately 40m) which misrepresented the spatial structure of the higher grade lenses.

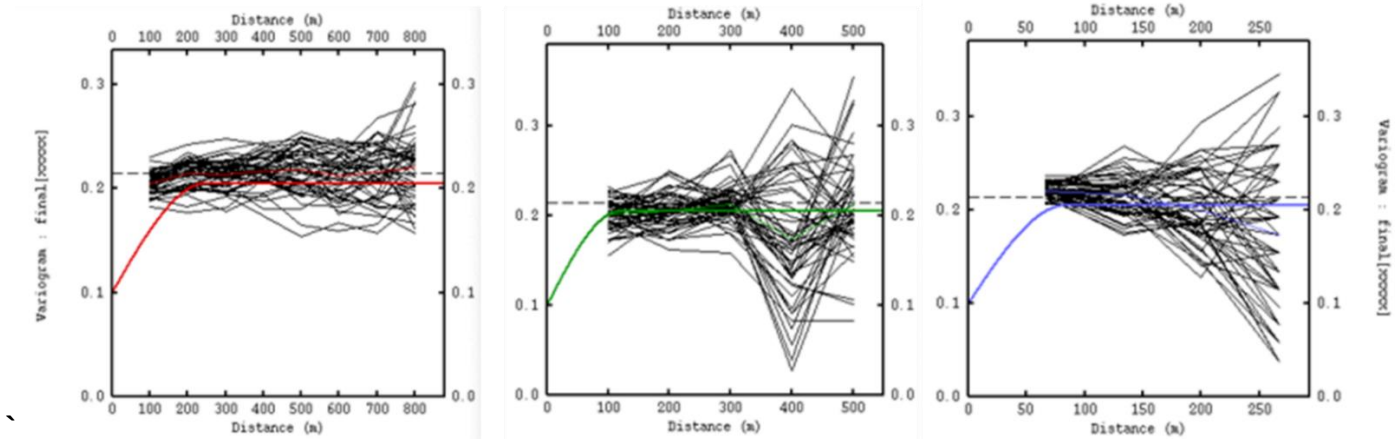


Figure 3-17: East SIS variogram validation. Variograms for data is indicated as solid lines (red, green and blue) for each anisotropic direction. Variogram models for each realisation is indicated by black lines.

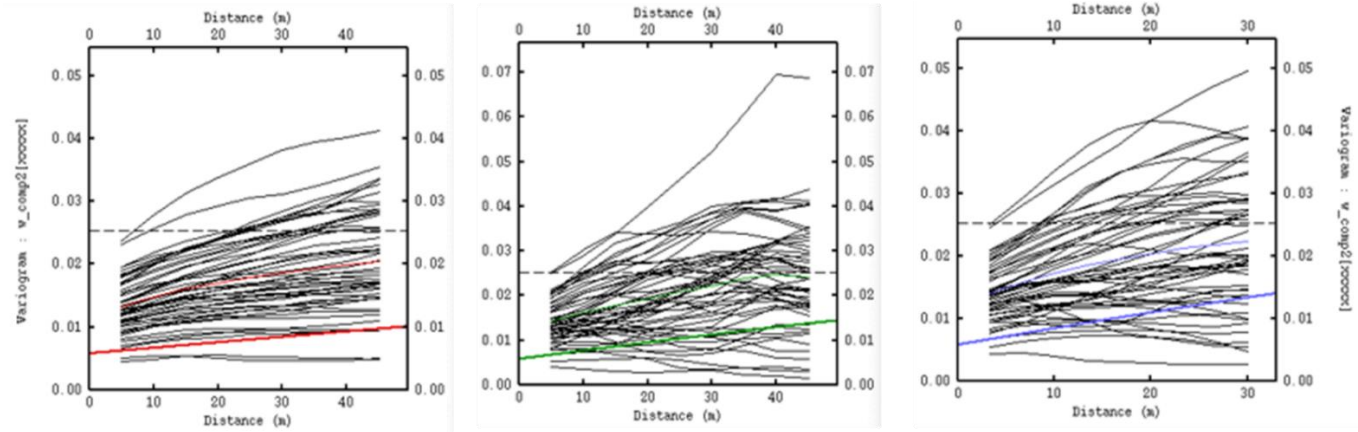


Figure 3-18: West SIS variogram validation. Variograms for data is indicated as solid lines (red, green and blue) for each anisotropic direction. Variogram models for each realisation is indicated by black lines.

3.5.2 Simulating grades using DBSim

DBSim was performed using ISATIS software. The drill hole data was separated into 4 domains:

- GHEW low grade (Au<2g/t);
- GHEW high grade (Au≥2g/t);
- GHEE low grade (Au<2g/t), and
- GHEE high grade (Au≥2g/t).

The simulation region was constrained within the low grade mineralisation envelope. The conditioning data was then used to detect the higher grade lenses. The algorithm relies on a model of the Gaussian variable regularized to the block support. ISATIS software integrates the X. Emery method to achieve the change of support (Emery, 2008) where the variogram model for the “point” Gaussian variables are regularized. The simplified DBSim workflow followed in ISATIS is illustrated in Figure 3-19.

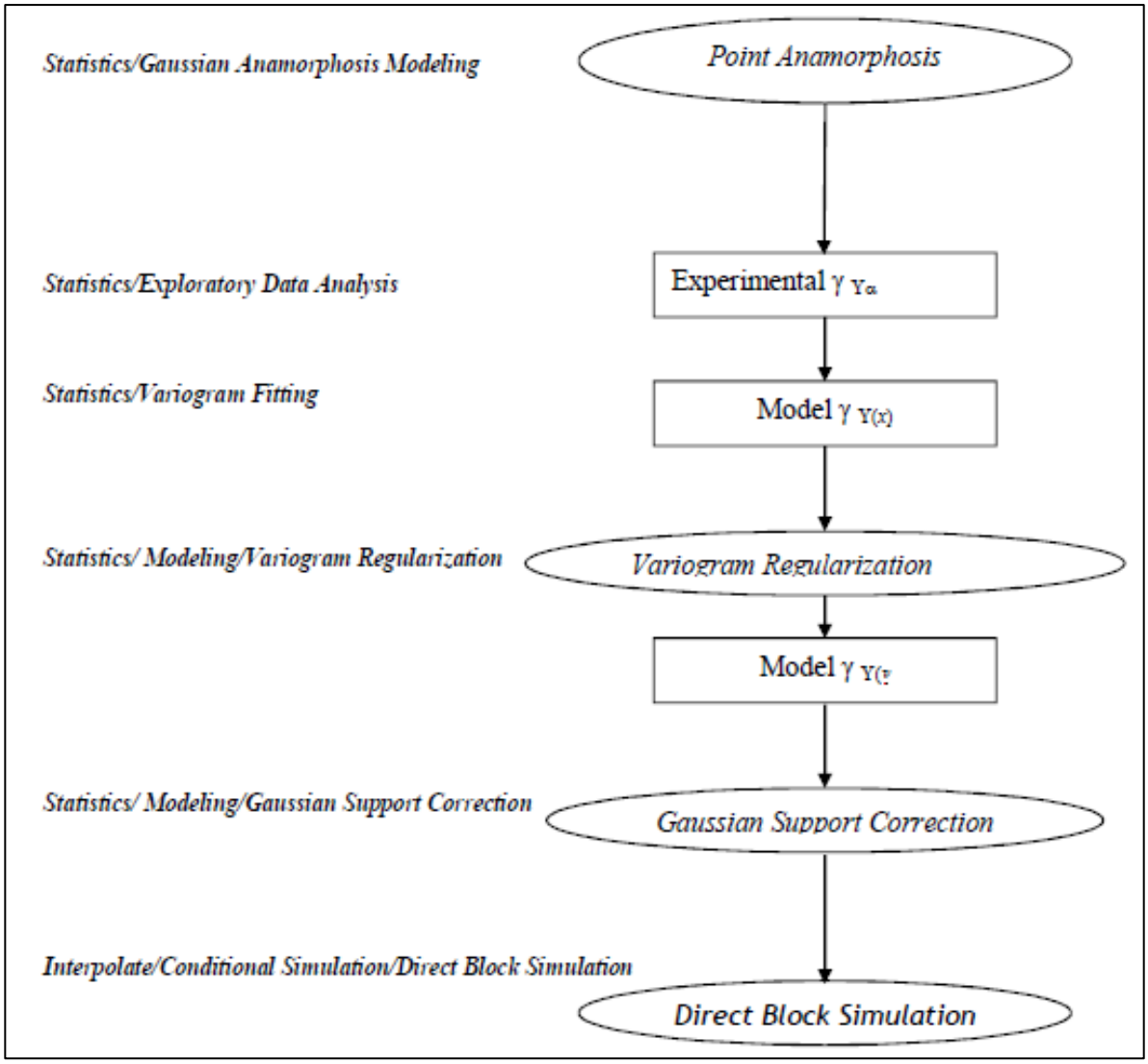


Figure 3-19: Recommended workflow for simulating grades using DBSim in ISATIS (ISATIS user manual, 2016)

3.5.2.1 DBSim Algorithm inputs

The inputs used to run DBSim are summarised below:

Conditioning Data

The conditioning data comprised of the samples occurring inside the low grade mineralisation envelope and separated into lower and higher grade populations, for GHEE and GHEW domains. The data was also declustered and composited to 1m for simulations. Histograms for the resultant datasets are given in Figure 3-20.

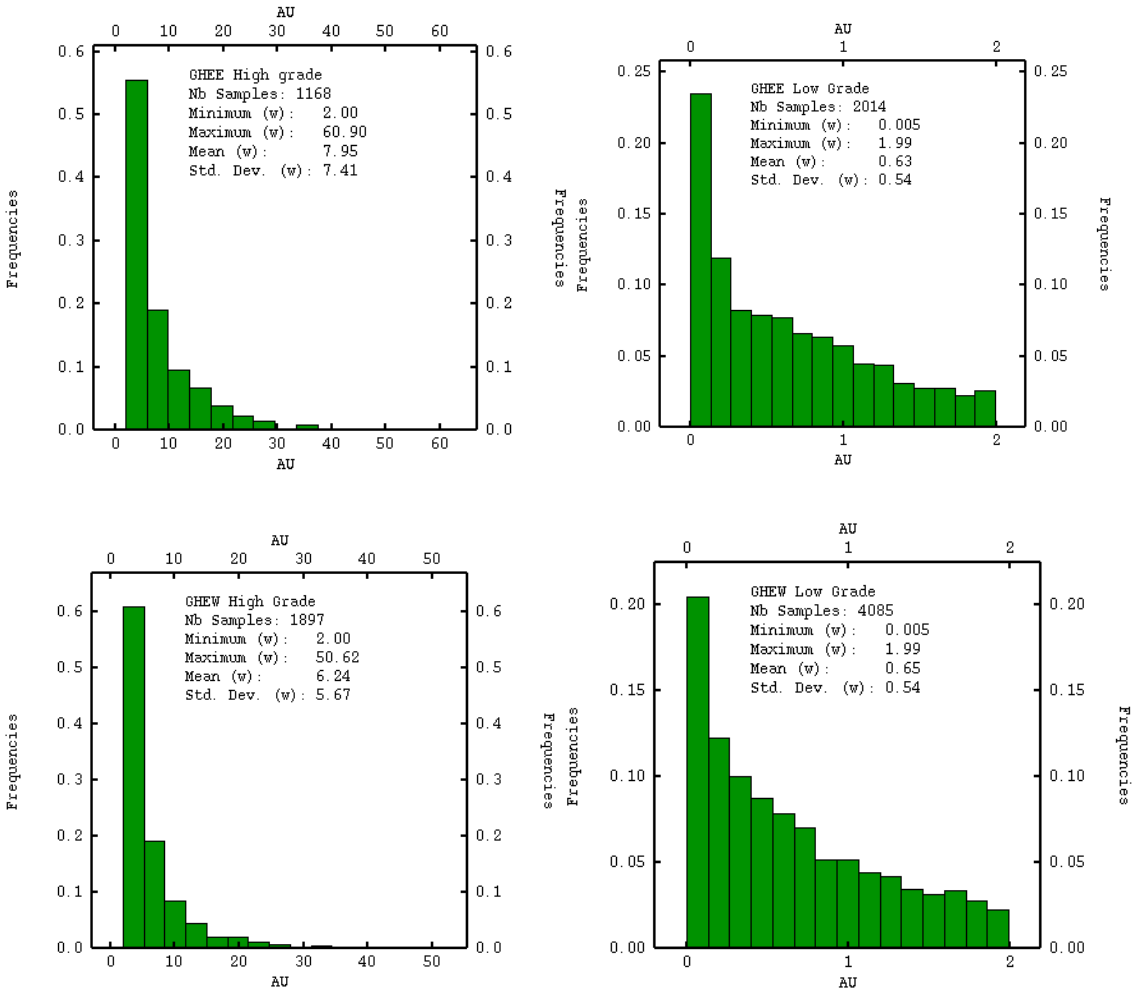


Figure 3-20: Raw Gold Grade distributions for conditioning data

Gaussian Anamorphosis Modelling

Gaussian Anamorphosis Modelling was performed to transform the raw gold grade variables into Gaussian variables so that they can be used in the simulations. The transformed distributions are presented in Figure 3-21.

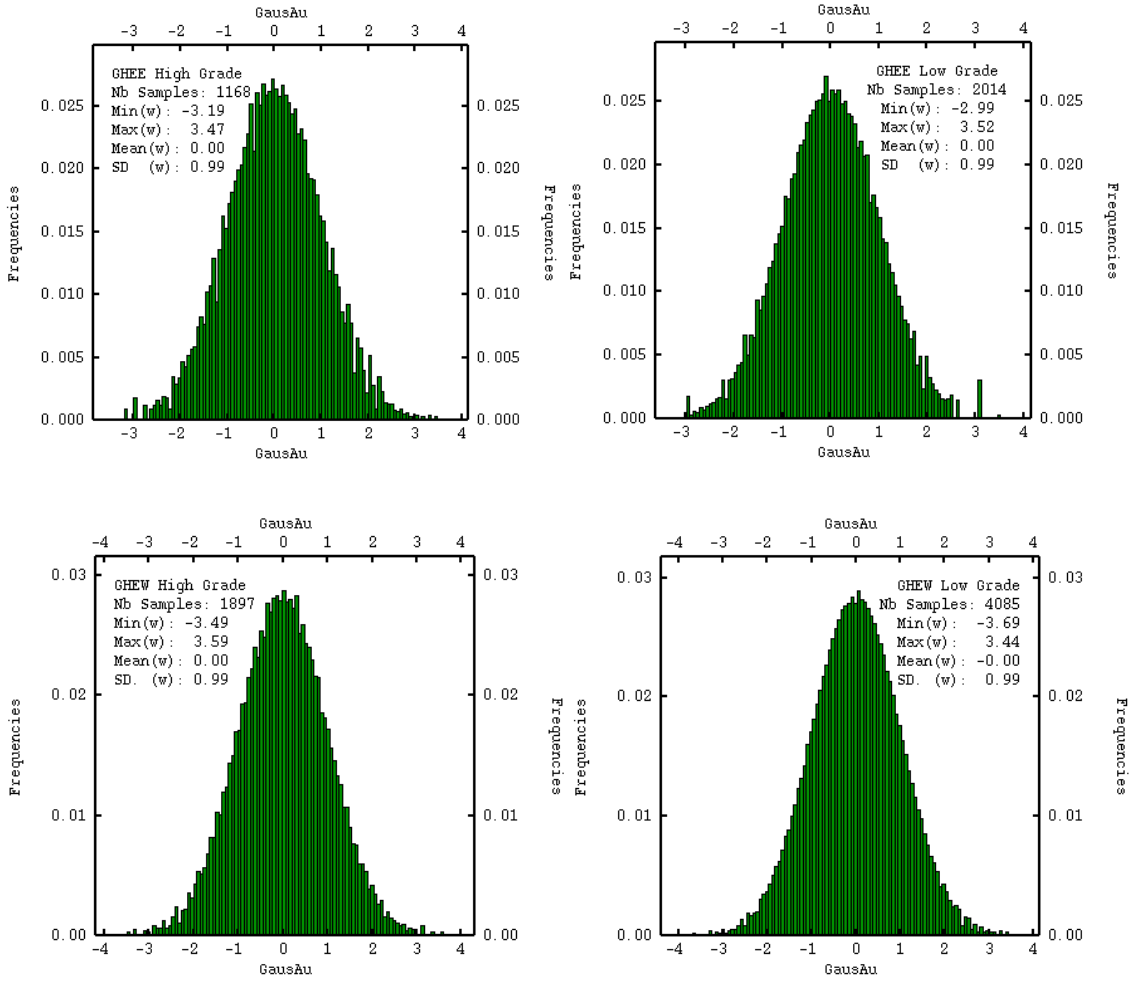


Figure 3-21: Transformed Grade distributions for conditioning data

Variogram Fitting

Exploratory data analysis was undertaken for the transformed gold variables and corresponding experimental variograms calculated. The experimental Gaussian gold variograms were then fit with models (Table 6 and Figure 3-22 to Figure 3-25).

Table 6: Spherical Model Variogram parameters for Gaussian Gold variables (GHEE and GHEW)

Domain	Nugget	Structure ID	Structure Sill	Range in Dir. 1 (m)	Range in Dir. 2 (m)	Range in Dir. 3 (m)
GHEE HG	0.25	1	0.59	20	15	5.20
		2	0.16	80	75	6.00
GHEE LG	0.25	1	0.29	20	10	1.33
		2	0.46	40	30	9.00
GHEW HG	0.25	1	0.57	22	20	2.50
		2	0.18	70	60	4.00
GHEW LG	0.25	1	0.59	20	15	5.20
		2	0.16	80	75	6.00

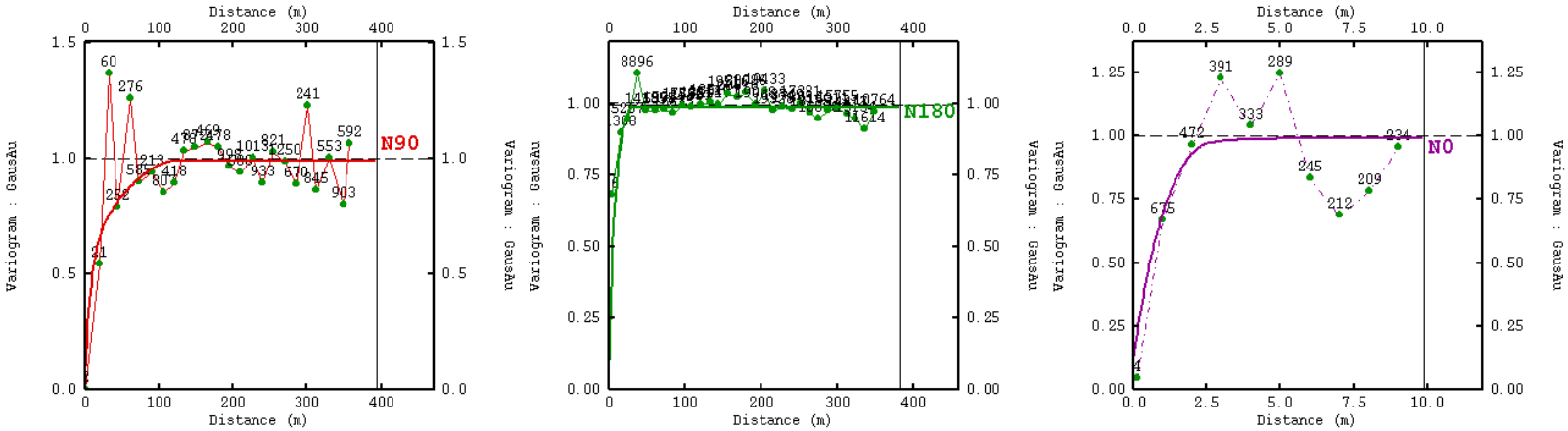


Figure 3-22: Variogram model fitting for GHEE High Grade Gaussian Gold variables in 3 anisotropic directions. Experimental pairs of data are indicated as green points in each figure. The solid coloured lines represent the variogram models.

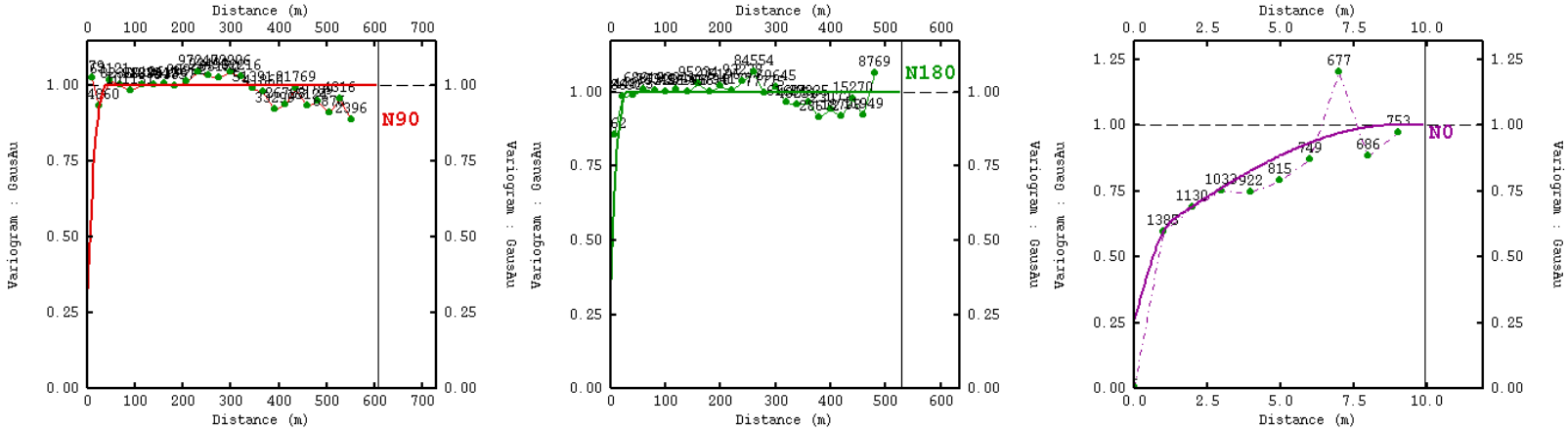


Figure 3-23: Variogram model fitting for GHEE Low Grade Gaussian Gold variables in 3 anisotropic directions. Experimental pairs of data are indicated as green points in each figure. The solid coloured lines represent the variogram models.

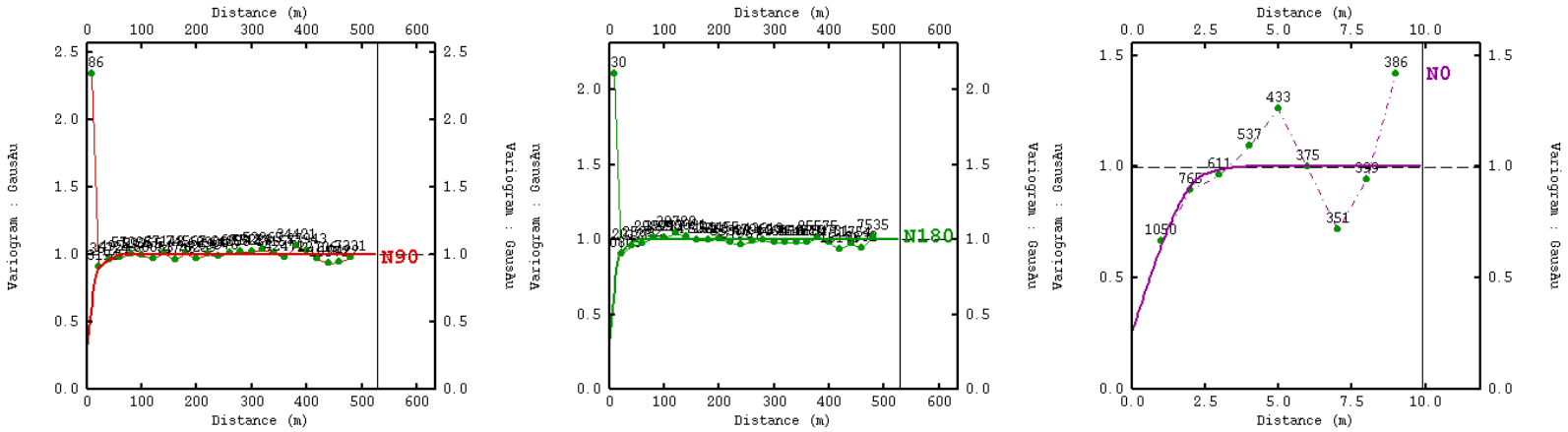


Figure 3-24: Variogram model fitting for GHEWHigh Grade Gaussian Gold variablesin 3 anisotropic directions. Experimental pairs of data are indicated as green points in each figure. The solid coloured lines represent the variogram models.

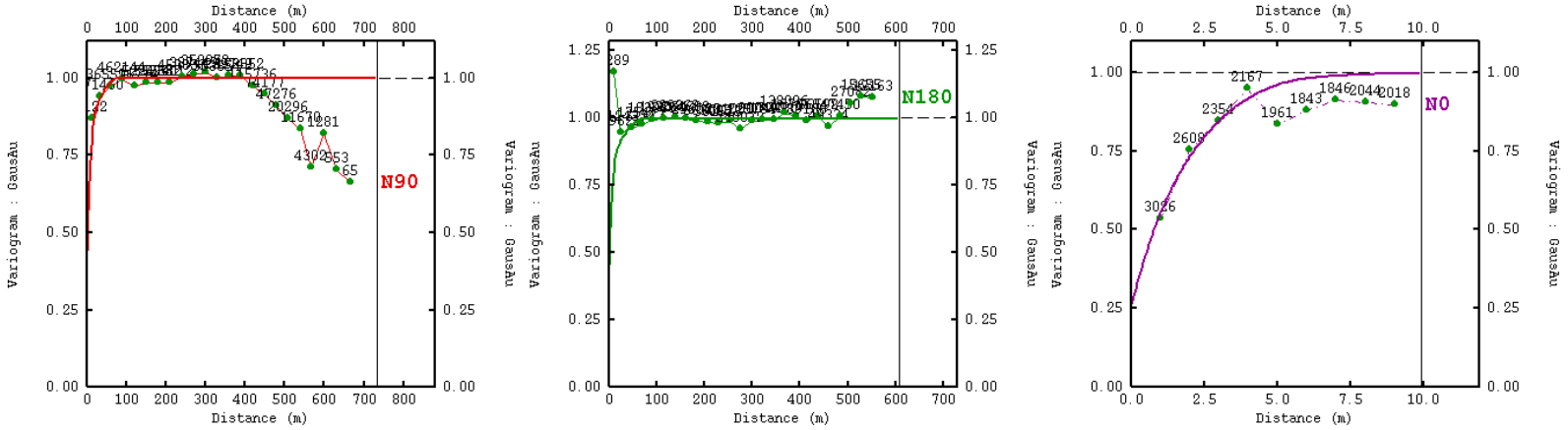


Figure 3-25: Variogram model fitting for GHEWLow Grade Gaussian Gold variables in 3 anisotropic directions. Experimental pairs of data are indicated as green points in each figure. The solid coloured lines represent the variogram models.

Variogram Regularisation and Block Variogram Modelling

To transform the point variogram models (fit on Gaussian point variables) to corresponding variograms on block support, the variogram regularisation function in ISATIS was applied. The aim of this process is to retrieve “pseudo-experimental” directional variograms that can be modelled for use in the simulations. Three orthogonal directions were specified and discretised using the size of the blocks to be simulated i.e. 10mE x 10mN x 3.33mElev. The resultant variograms were saved and fit with variogram models as illustrated in Figure 3-26 to Figure 3-29.

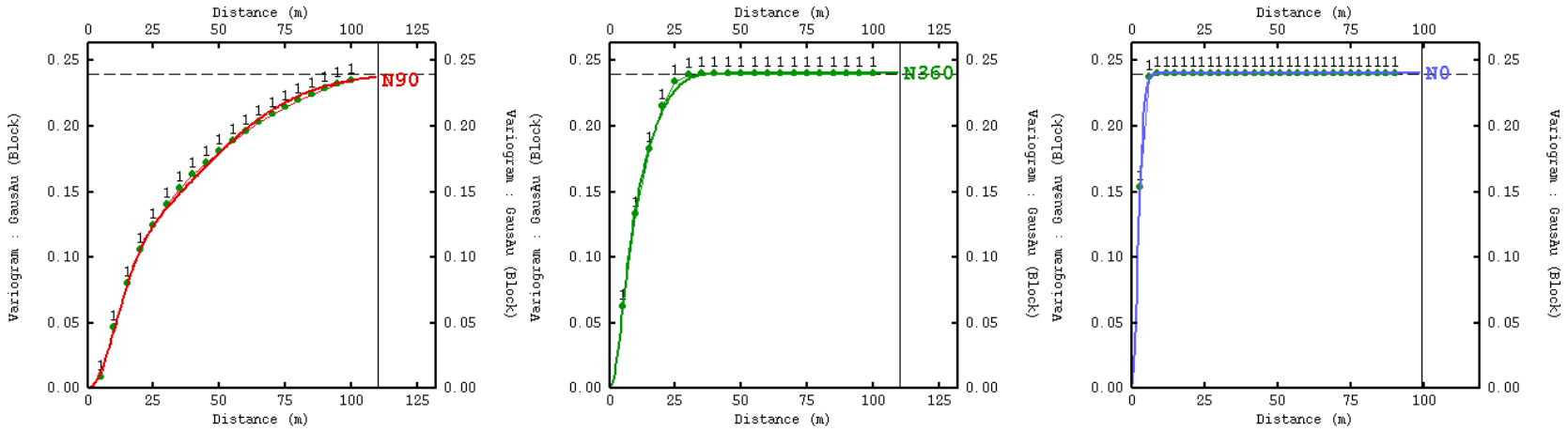


Figure 3-26: Regularised Block Variogram model fit on Gaussian point variables for GHEE High Grade.

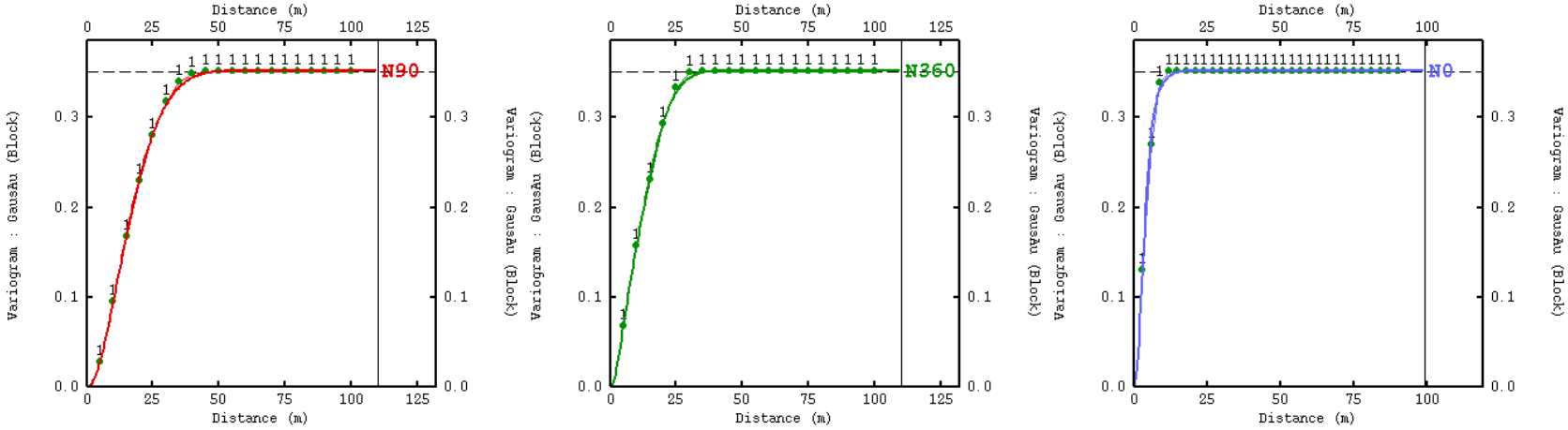


Figure 3-27: Regularised Block Variogram model fit on Gaussian point variables for GHEE Low Grade.

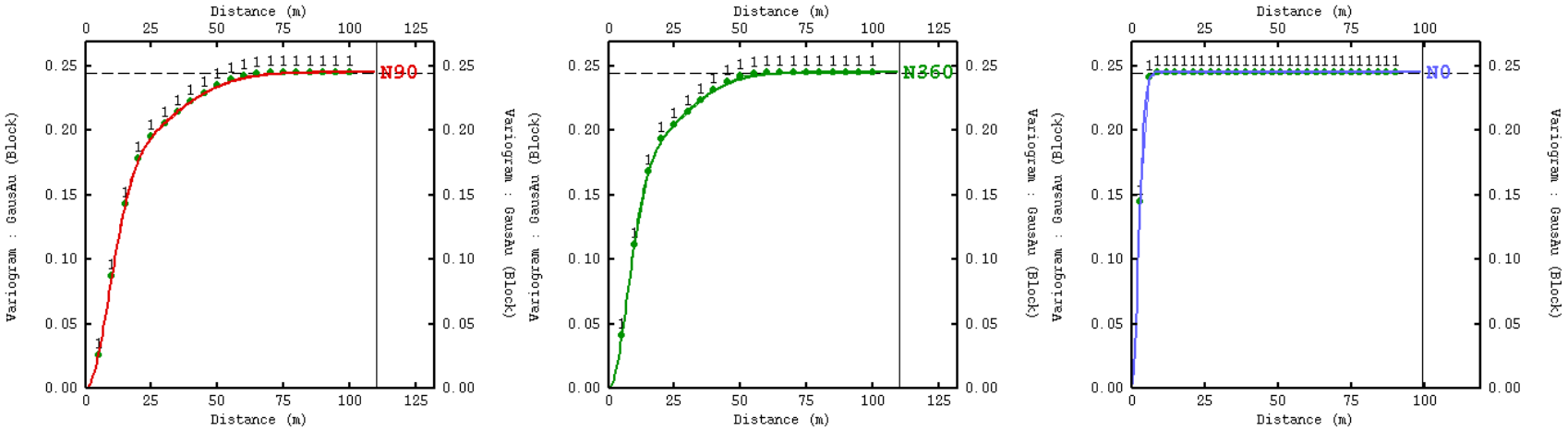


Figure 3-28: Regularised Block Variogram model fit on Gaussian point variables for GHEW High Grade.

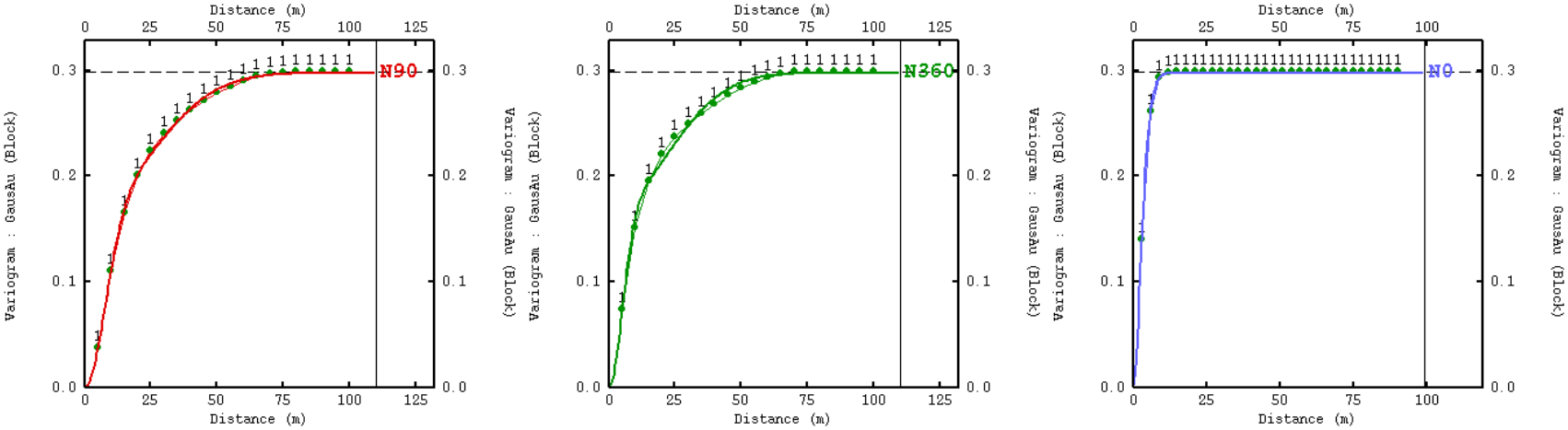


Figure 3-29: Regularised Block Variogram model fit on Gaussian point variables for GHEW Low Grade

Gaussian Support Correction

The first step of DBSim begins with a Discrete Gaussian Support Correction to transform the variogram model based on the regularised transformed Gaussian variable, into a Gaussian variogram on the block support. This represents the second Anamorphosis, only this time at block support which is used together with the Block variogram model (automatically fit for the user) for the simulation procedure.

Neighbourhood

A moving search neighbourhood was defined for each domain using a search ellipsoid orientated along Azimuth = N0 and dip= -30 degrees. A sample is only kept in the search ellipsoid if the distance between the target node and the sample is less than the 3 maximum distances (axes) defining the ellipsoid which represent the 3 main axes of the ellipsoid. The maximum distances were selected based on the maximum ranges of the variogram in each direction. After rotation, the X, Y and Z directions of the ellipsoid are referred to as maximum distances U, V and W respectively. In addition to defining these distances, the optimum number of samples was selected as 10. As the algorithm searches different sectors in the neighbourhood sequentially, it looks for the 10 samples before simulating. This number can be adjusted upward if more conditioning data is available. The maximum distances were defined as follows:

- GHEE HG: U=40m, V=30m and W=20m;
- GHEE LG: U=40m, V=30m and W=20m;
- GHEW HG: U=70m, V=60m and W=20m;
- GHEW LG: U=80m, V=75m and W=20m;

The maximum direction along W was adjusted to 20m to account for the varying thickness of the low grade ore wireframe.

Simulation Parameters

The maximum number of realisations set per domain was 50, to correspond to the number of realisations generated for SIS. The optimum number of already simulated nodes was set to 10, meaning that ISATIS loads the original conditioning data and the 10 closest already simulated nodes in the search neighbourhood

algorithm. The seed for the random number generator was set to 423141 and the simulations run using independent paths. The simulations were then back-transformed into raw data space for interpretation and analysis of results.

3.5.2.2 DBSim validation

The variograms for the DBSim realisations is plotted against the variogram model for the Gaussian variogram model regularised to block support. Overall, the reproduction of the variograms was acceptable for all domains (Figure 3-30 to Figure 3-33). The highest degree of entropy was reported for the intermediate direction of continuity most likely due to the behaviour of the shear zone. Another important observation was that the simulations did not capture the short range structure of the data (range of 10m). The validation results were deemed acceptable because the 10m range was negligible in comparison to the SMU in the planning model (40m x 40m x 10m). Further work is however required to investigate the cause of this behaviour.

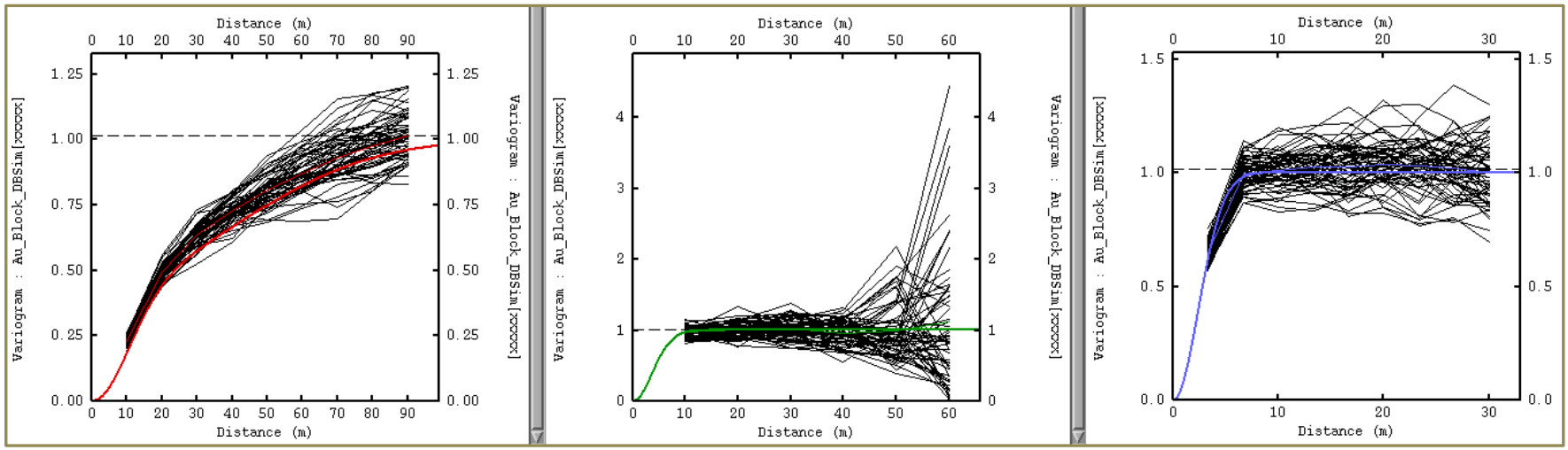


Figure 3-30: GHEE high grade data variogram models (red, green and blue lines) against variograms for simulated realisations (black lines)

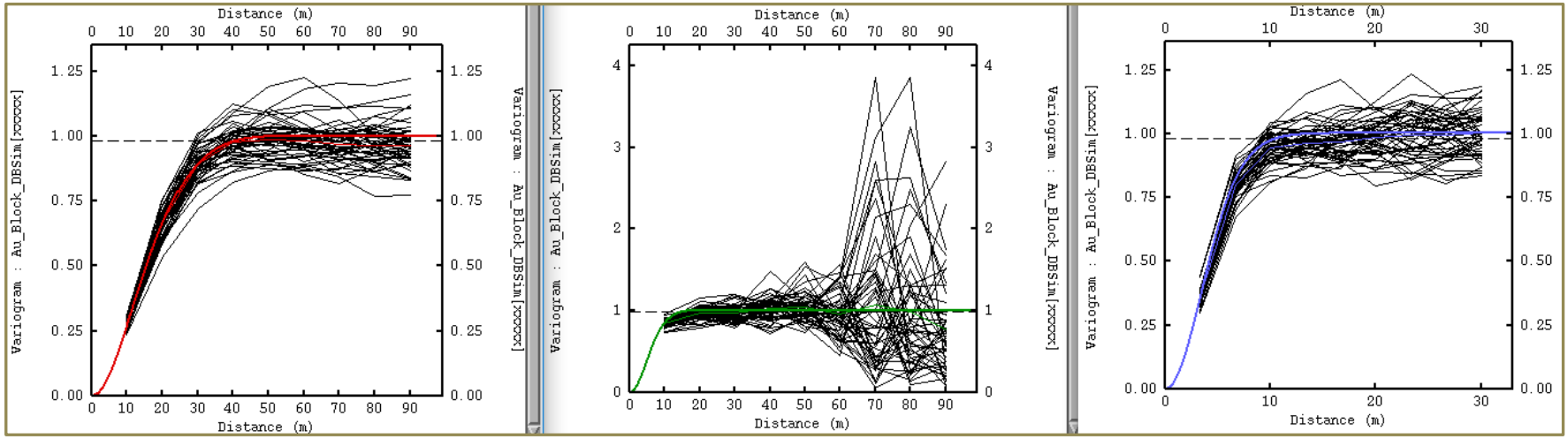


Figure 3-31: GHEE low grade data variogram models (red, green and blue lines) against variograms for simulated realisations (black lines)

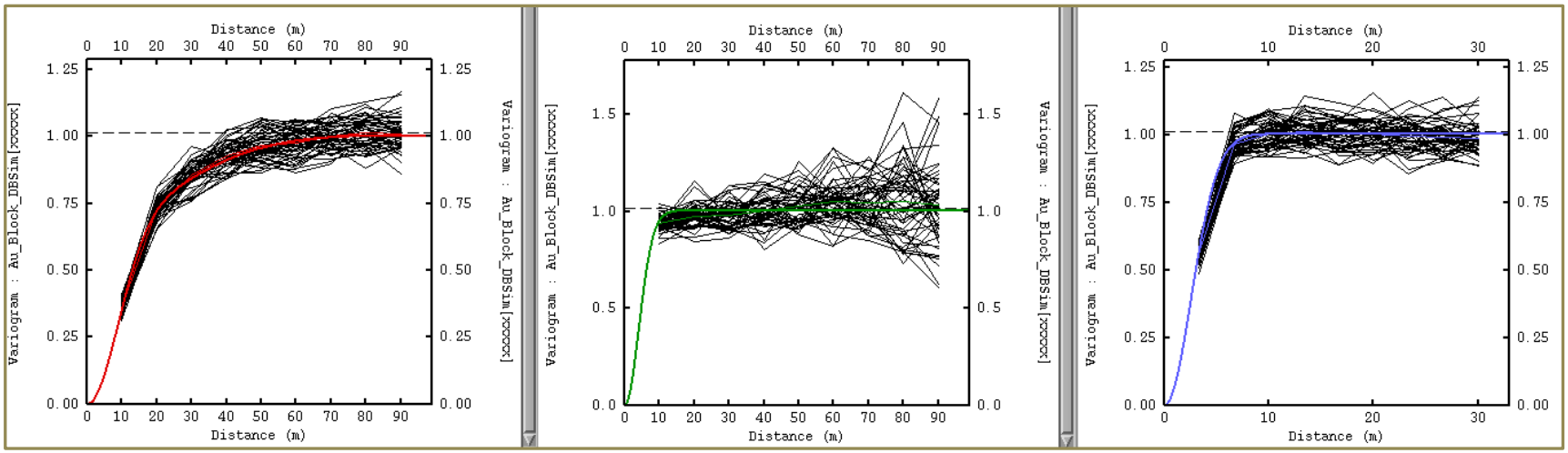


Figure 3-32: GHEW high grade data variogram model (red, green and blue lines) against variograms for simulated realisations (black lines)

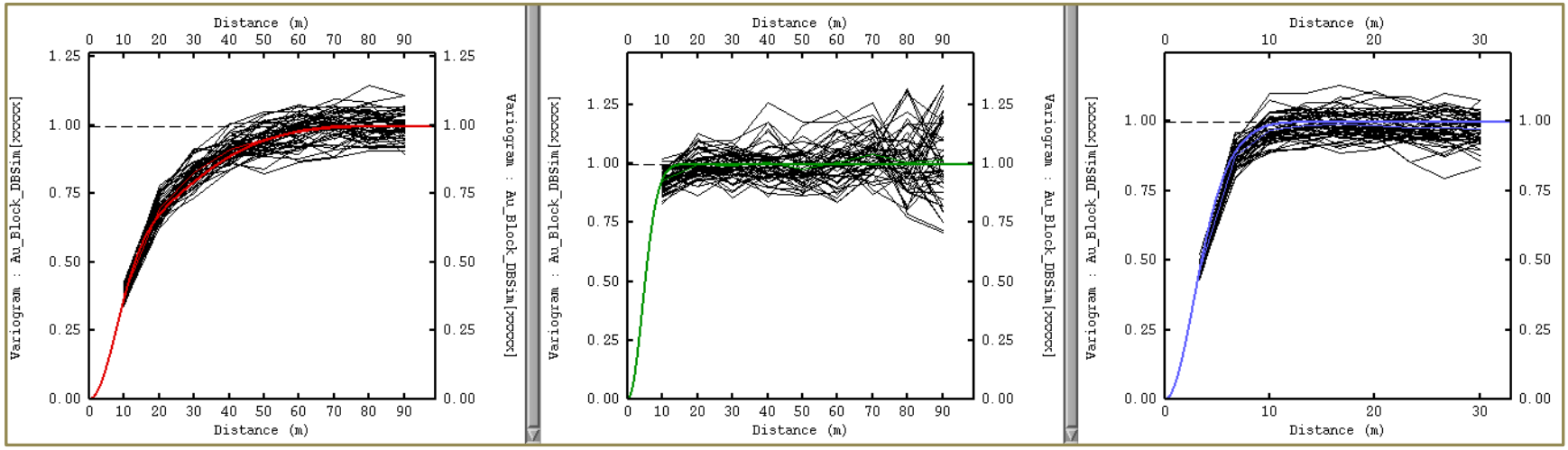


Figure 3-33: GHEW low grade data variogram models (red, green and blue lines) against variograms for simulated realisations (black lines)

The back transformed simulated points were next compared against the raw sample data using grade-tonnage curves and reproduced the data statistics (Figure 3-34). The DBSim point data is used to allow for comparison at the same support. Each grade-tonnage curve is generated by averaging nodes into block grades and accumulating the respective tonnages above a series of cut-off grades. The average grades are then plotted against the tonnages at each cut-off. A single grade-tonnage curve is produced for each simulated realisation (Coombes, Thomas, Glacken, & Snowden, 2016).

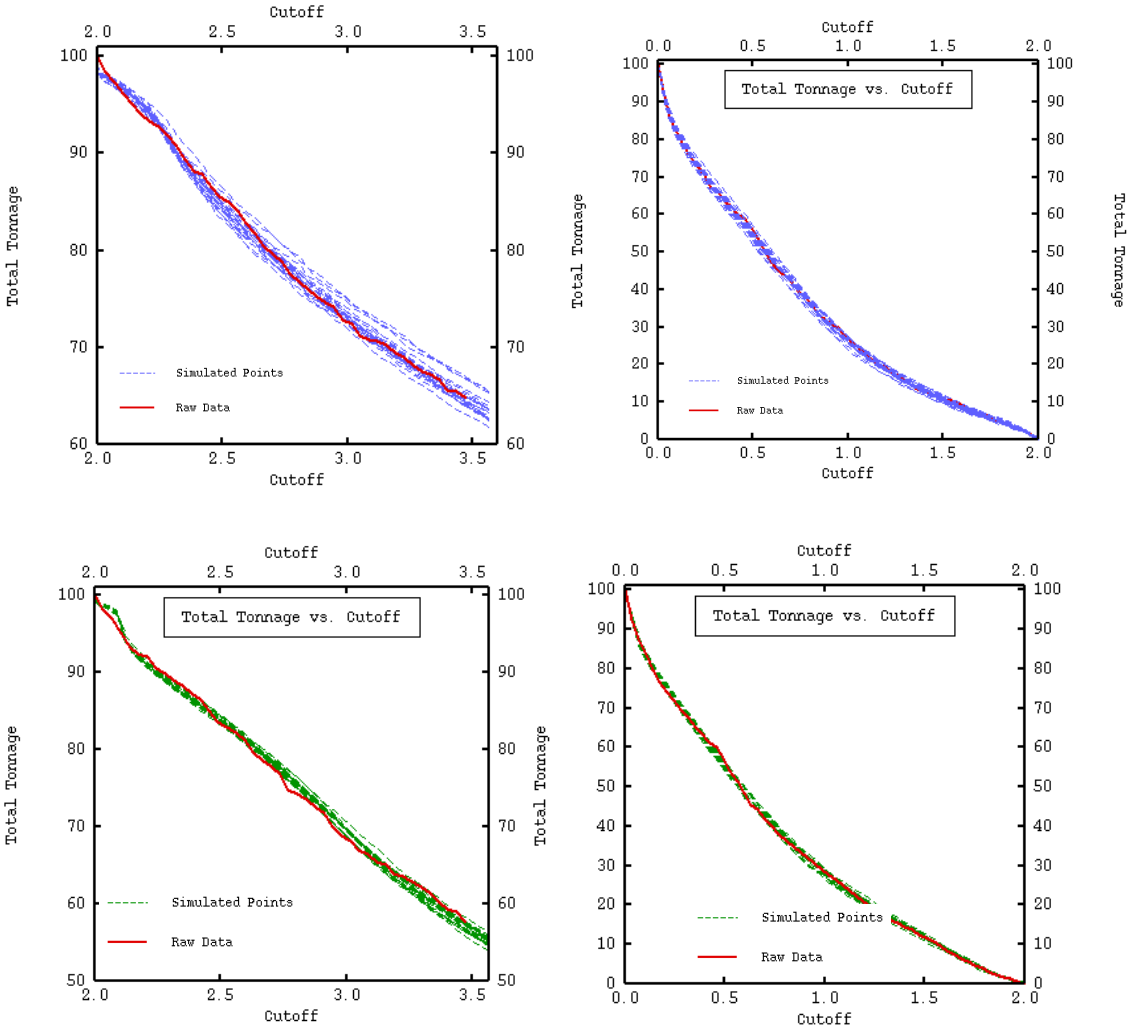


Figure 3-34: Grade tonnage curve comparison for raw data and DBSim point realisations: GHEE HG (top left), GHEE LG (top right), GHEW HG (bottom left) and GHEW LG (bottom right).

The DBSim realisations were deemed acceptable and valid due to variogram reproduction and the ability to reproduce the underlying statistics of the data.

3.5.3 Identifying upside and downside scenarios

It is not possible to select a “best” realization from the many that are generated, regardless of what criteria is applied. The realisations identified as being the most appropriate to the study, were selected in terms of potential upside and downside criteria. All studies involving an assessment of uncertainty are concerned with potential upside and downside scenarios as these give an indication of the risk associated. In mining the potential scenarios show the risk in expected grades and tonnage.For the research, potential upside and downside scenarios were identified as follows:

- ore category simulations (SIS realisations) were ranked in terms of the total simulated volume of material with an indicator value = 1, and
- grade simulations were ranked in terms of the total simulated metal content.

Higher ranking realisations represent potential upside scenarios for mining, and contain the largest total metal content (for DBSim), or volume of high grade material (for SIS). The Lower ranking realisations, on the other hand, represent potential downside scenarios for mining.

3.5.3.1 Ranking of SIS Realisations

The SIS realisations were ranked in ascending order of the volumetric ratio of high to low grade ore. The potential upside scenario was identified as the realisation with rank=50 (containing the largest volume of high grade material), and the potential downside scenario as the realisation having rank=1 (containing the smallest volume of high grade material). The upside scenario was identified as SIS_35 and the downside scenario, SIS_17 for GHEE. For GHEW, realisation SIS_33 was identified as the potential upside scenario and realization SIS_49 as the potential downside scenario. Due to confidentiality clauses, this data is not presented in the research.

Geological uncertainty may then be characterised, by observing the variation between simulated scenarios, and comparing it to the kriged model at the same support. The SIS realisations can be compared to the IK wireframe to better understand the shapes and boundaries of the higher grade lenses. Both methods, can then be used to assess proposed stope layouts, designed to target the high grade lenses. To relate the SIS and DBSim realisations, the simulated models were regularised to the block SIS support i.e. 5mE x 5mN x 3. 33mElev.

3.5.3.2 Ranking of DBSim Realisations

The DBSim realisations were ranked in ascending order of total metal content. The potential upside scenario was identified as the realisation with rank=50 (containing the largest metal content), and the potential downside scenario as the realisation with rank=1 (containing the smallest metal content). The scenarios presented are developed for each domain i.e. GHEE higher and lower grade simulations.

3.5.4 Model of Joint Uncertainty

The model of joint uncertainty developed, is based on ranked combinations of SIS and DBSim realisations (Figure 3-35). The process involves first combining lower and higher grade DBSim realisations (per domain) in Datamine, according to order of ranking. Next, the combined DBSim realisations are added to the corresponding order or ranking SIS realization. The SIS simulated indicator values are then used to constrain the allocation of grades from DBSim, to produce a final model of joint uncertainty:

- If the SIS realisation for a block is a high grade indicator, a final grade is assigned to the block in accordance to the grade value in the corresponding (order of rank) higher grade DBSim realisation for that block;
- If the SIS realisation for a block is a low grade indicator, a final grade is assigned to the block in accordance to the grade value in the corresponding (order of rank) lower grade DBSim realisation for that block;
- If the SIS realisation has an absent simulated indicator, the block is considered as waste and gets assigned a default value of 0.01g/t.
- If the SIS realisations contains a simulated indicator, but the corresponding (order of rank) lower or higher grade DBSim realisation has an absent

simulated grade, the block is considered as waste and gets assigned a default value of 0.01g/t. This however is unlikely, if block regularisation from finer to coarser support is carried out correctly.

3.5.4.1 Ranking of realisations for the model of joint uncertainty

To combine the SIS and DBSim realisations simulation grid for SIS was regularised to fit into the 10m x 10m x 3,33m grid blocks established for DBSim.

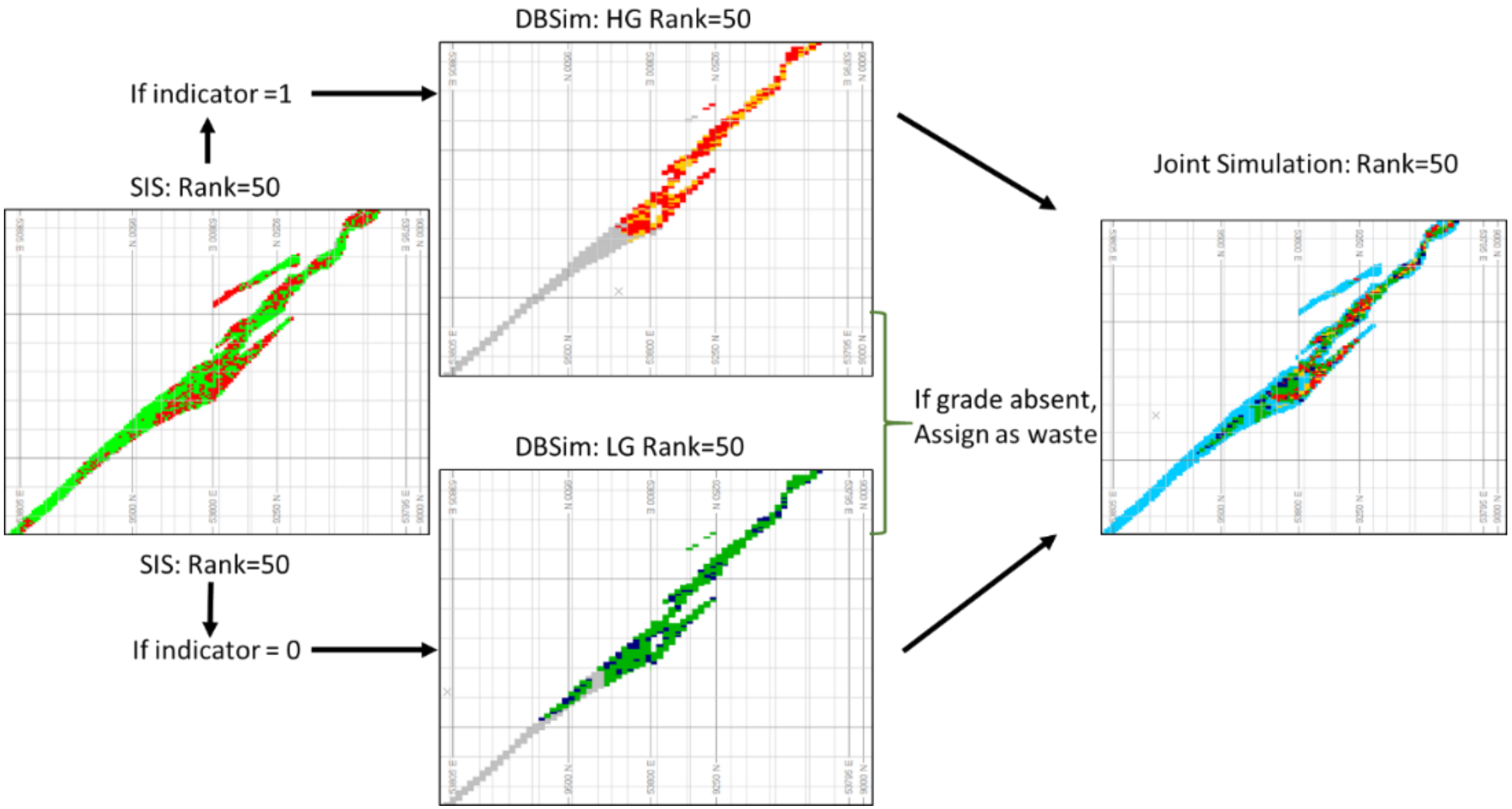


Figure 3-35: Schematic showing the logic behind combining SIS and DBSim realisations to give an indication of potential joint uncertainty

3.6 Conclusion

The aim of this chapter was to find a suitable methodology to assess geological uncertainty for Geita Hill. Deterministic models do not allow for a characterisation of the risk relating to geological uncertainty because a single realisation is produced (Figure 3-36).

The methodology outlined options for stochastic ore body modelling and discussed the several common problems encountered during attempted implementation. The suggested methodology involves using SIS to characterise volumetric uncertainty associated with the domain boundaries and DBSim for characterising grade uncertainty in the study. Stochastic modelling of ore bodies involves the use of the available sample data to generate a range of equiprobable realisations of the deposit. The multiple realisations allow one to assess geological uncertainty (Figure 3-37).

In total, 300 final realisations were generated: 100 grade simulations and 50 ore category realisations per domain. The resultant SIS and DBSim realisations were validated, and deemed acceptable for use in the study. Since it is not possible to select a “best” realization from the many that were generated, only the realisations identified as being the most appropriate to the study were used. These were identified as potential upside and downside mine planning scenarios. For this study, these scenarios provide an indication of the risk associated with grade and tonnage expectations. Finally, a method to model joint uncertainty was presented, based on ranked combinations of SIS and DBSim realisations. The process involves first combining lower and higher grade DBSim realisations per domain, according to order of ranking. Next, the combined DBSim realisations are added to the corresponding order or ranking SIS realization. The SIS simulated indicator values are then used to constrain the allocation of grades from DBSim, to produce a final model of joint uncertainty. The results of the methods are presented in Chapter 4.

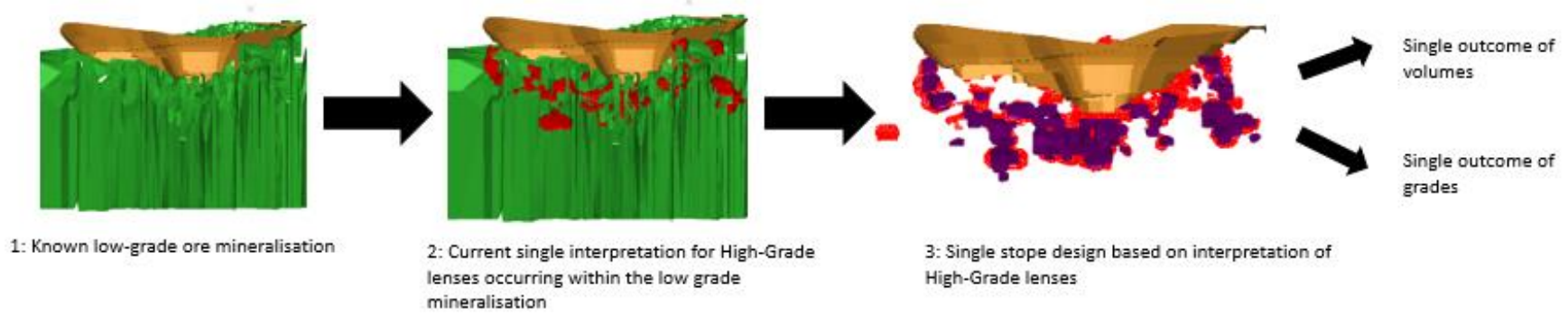


Figure 3-36: Description of a conceptual deterministic workflow for the study area

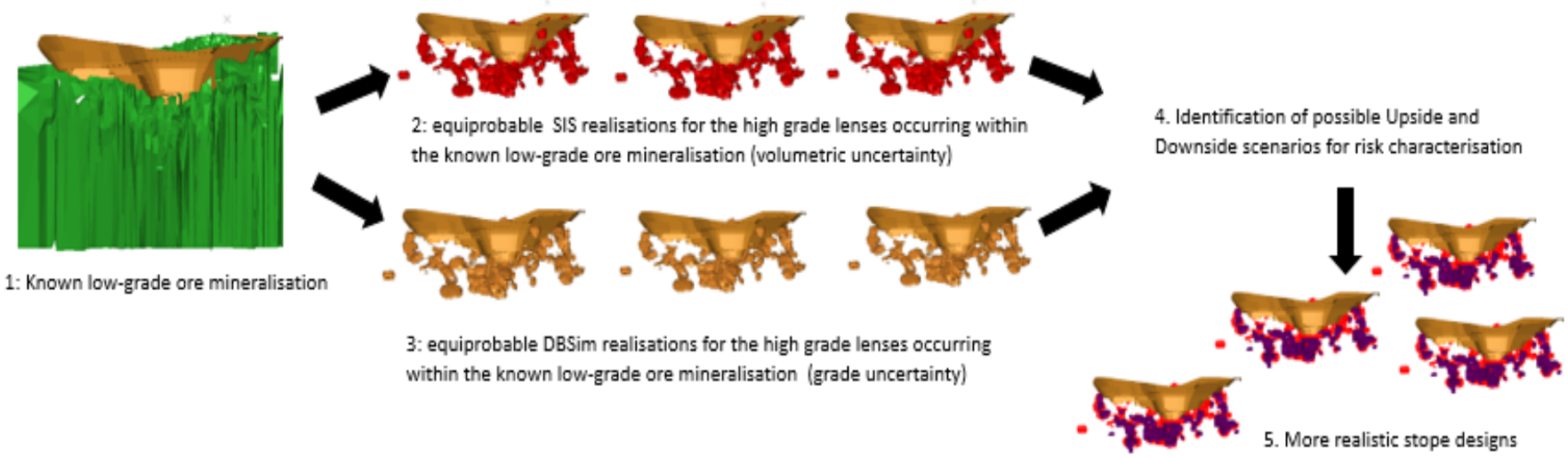


Figure 3-37: Description of the stochastic workflow followed for the study area

CHAPTER 4

"The scientist has a lot of experience with ignorance and doubt and uncertainty, and this experience is of very great importance, I think. When a scientist doesn't know the answer to a problem, he is ignorant. When he has a hunch as to what the result is, he is uncertain. And when he is pretty damn sure of what the result is going to be, he is still in some doubt. Scientific knowledge is a body of statements of varying degrees of certainty -- some most unsure, some nearly sure, but none absolutely certain".

-Physicist and Nobel Laureate Richard Feynman

"The Value of Science," address to the National Academy of Sciences (Autumn 1955)

4 RESULTS

This chapter contains the findings of the simulated realisations generated using the methodology described in Chapter 3. Only the potential upside and downside mine planning scenarios are covered, as they are pertinent scenarios for risk analysis studies with geological uncertainty. However, no interpretations are included. A detailed discussion on the results is provided in Chapter 5.

4.1 Conventions applied

The display convention used for drill holes and model blocks are illustrated below:

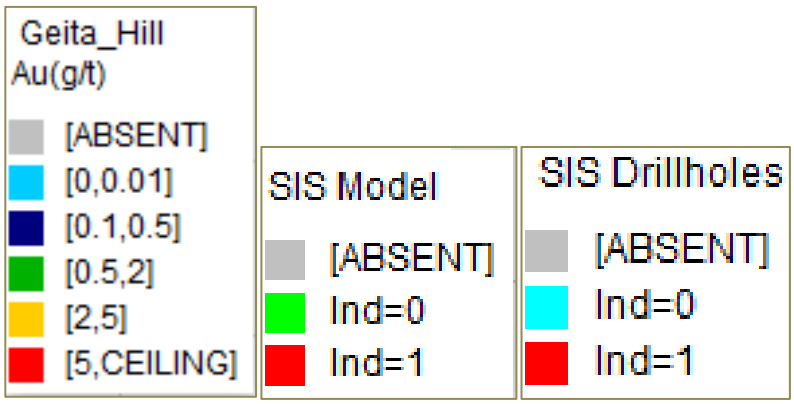


Figure 4-1: Legends used to display gold grades and simulated indicators

4.2 SIS Results

For ease of reading, the findings for SIS will be presented in the same order that was followed (Chapter 3) to generate the final results:

- Potential upside and downside scenarios will be compared to the Indicator Kriged high grade wireframe (provided by the mine) for the deposit to understand the shapes and occurrence of high grade lenses;
- The calculated volumetric differences between simulated scenarios and the IK wireframe will be presented to highlight volumetric risk, andfinally;
- The simulated blocks occurring inside planned stope designs will be ranked to identify potential upside and downside scenarios.

4.2.1 Comparison between potential upside and downside scenarios

SIS and IK are used to provide information on the shapes of the high grade lenses. The IK wireframe is defined as a single 50% probability of the material being high grade. The following figures show how the shape of the high grades vary between potential upside and downside SIS scenarios. They are displayed alongside the IK wireframe.

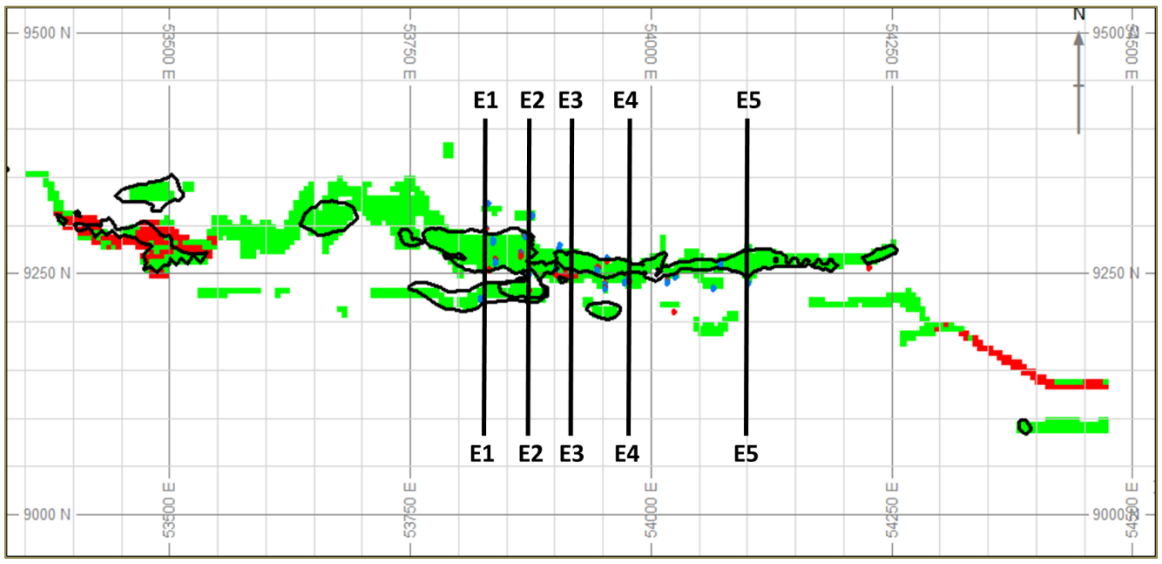


Figure 4-2: Plan view showing the location of cross sections (E1-E5) through GHEE to compare upside and downside scenarios for the SIS realisations on the 5m x 5m x 3,333m simulation grid.

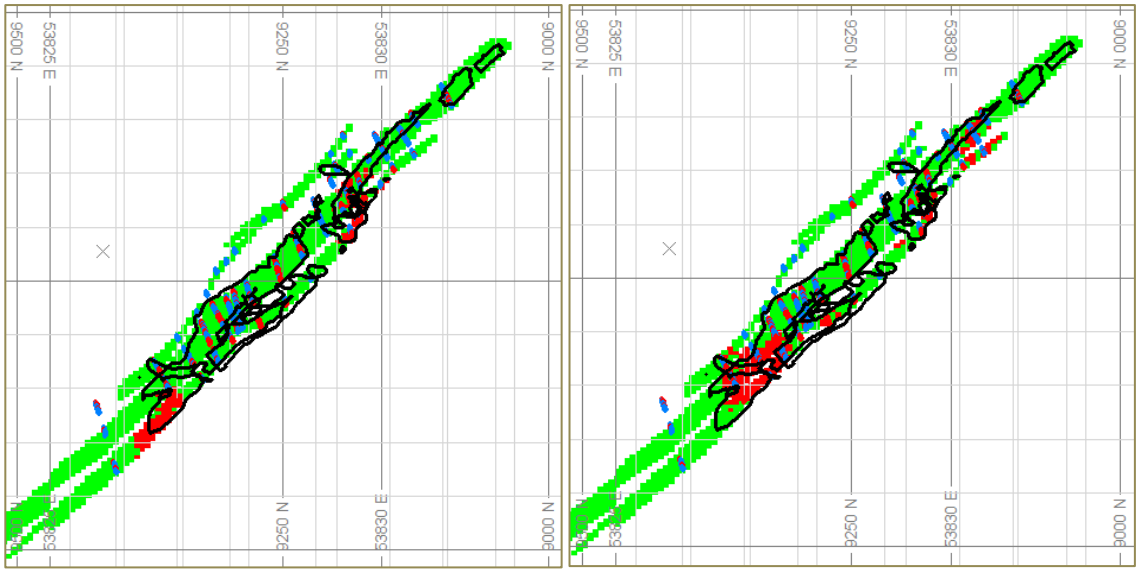


Figure 4-3: Section view (E1) showing the potential downside scenario (left) and upside scenario (right) based on ranked SIS realisations for GHEE using a 5m x 5m x 3,333m simulation grid. IK high grade wireframe for the deposit is depicted by black outlines.

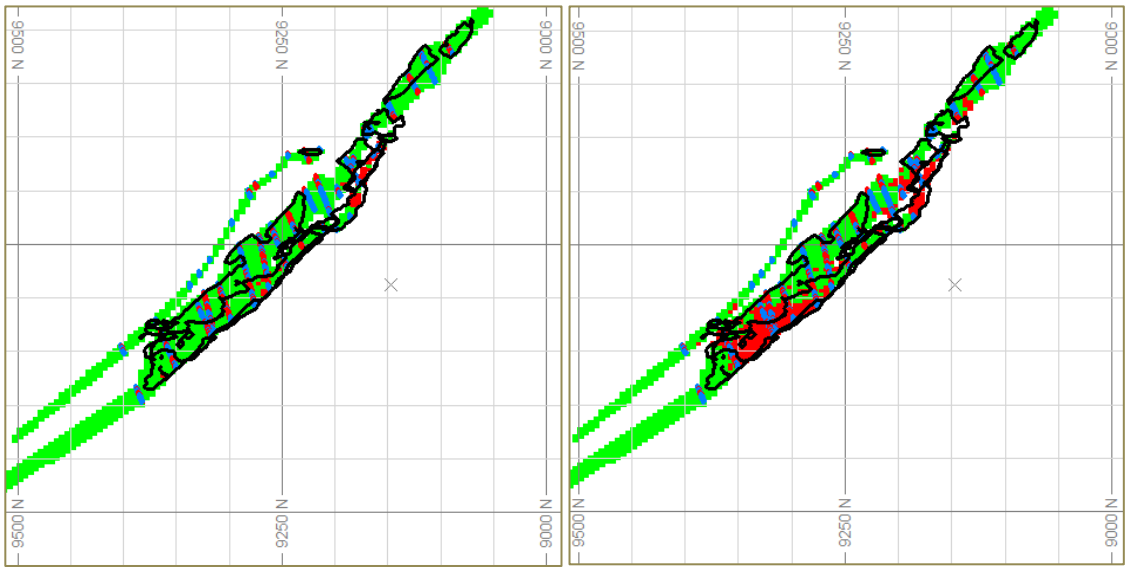


Figure 4-4: Section view (E2) showing the potential downside scenario (left) and upside scenario (right) based on ranked SIS realisations for GHEE using a 5m x 5m x 3,333m simulation grid. IK high grade wireframe for the deposit is depicted by black outlines.

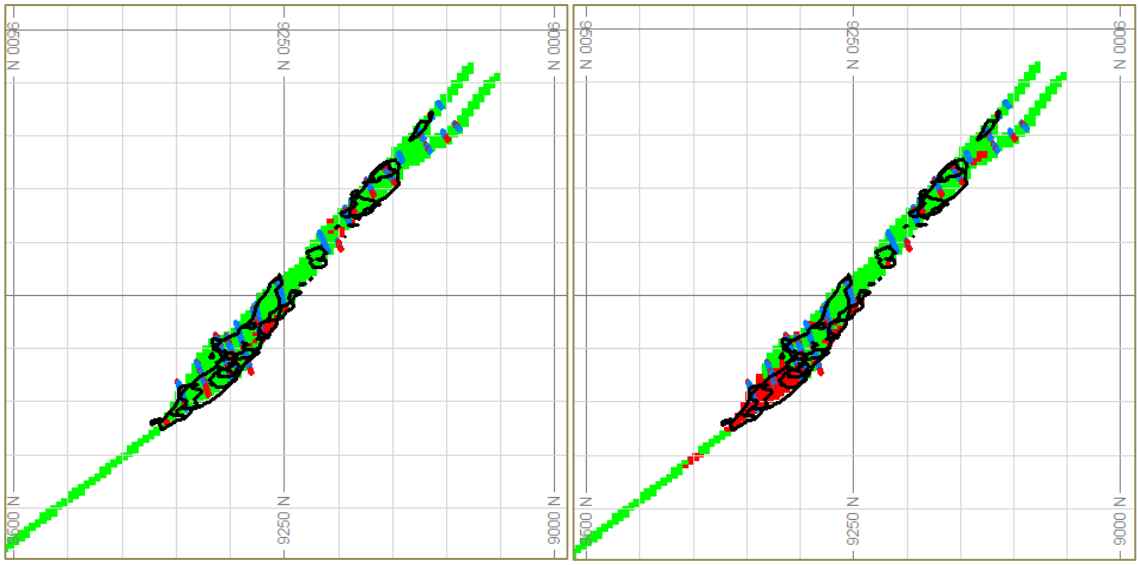


Figure 4-5: Section view (E3) showing the potential downside scenario (left) and upside scenario (right) based on ranked SIS realisations for GHEE using a 5m x 5m x 3,333m simulation grid. IK high grade wireframe for the deposit is depicted by black outlines.

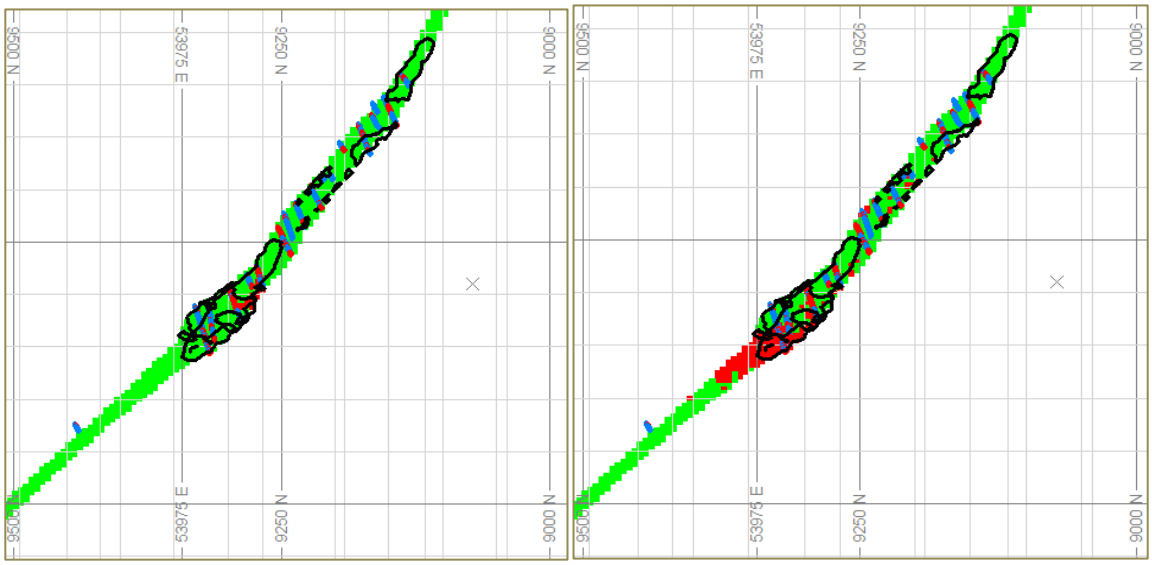


Figure 4-6: Section view (E4) showing the potential downside scenario (left) and upside scenario (right) based on ranked SIS realisations for GHEE using a 5m x 5m x 3,333m simulation grid. IK high grade wireframe for the deposit is depicted by black outlines.

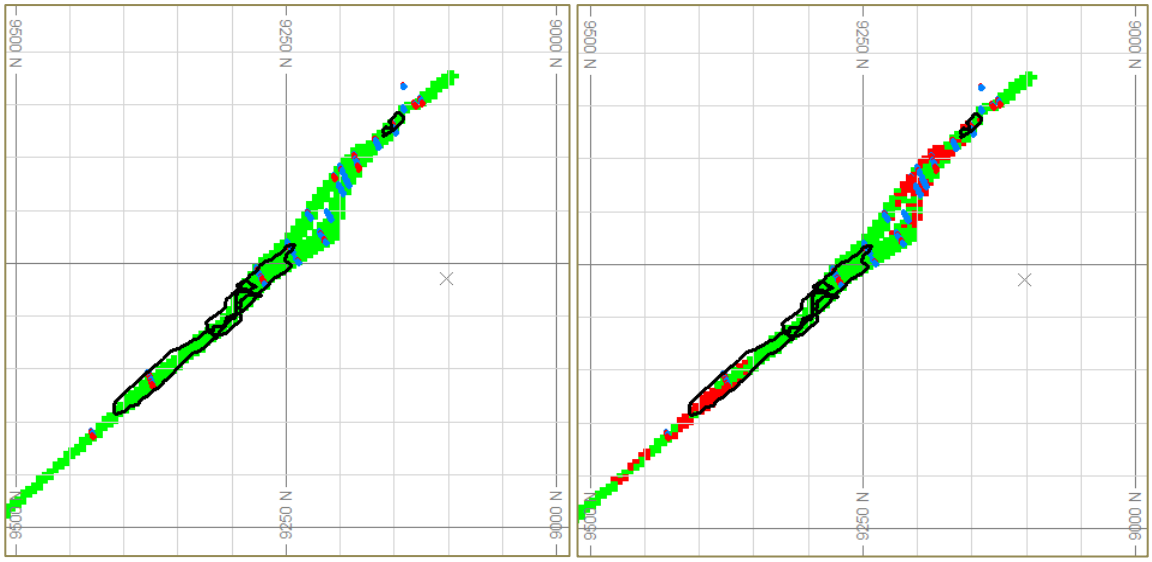


Figure 4-7: Section view (E5) showing the potential downside scenario (left) and upside scenario (right) based on ranked SIS realisations for GHEE using a 5m x 5m x 3,333m simulation grid. IK high grade wireframe for the deposit is depicted by black outlines.

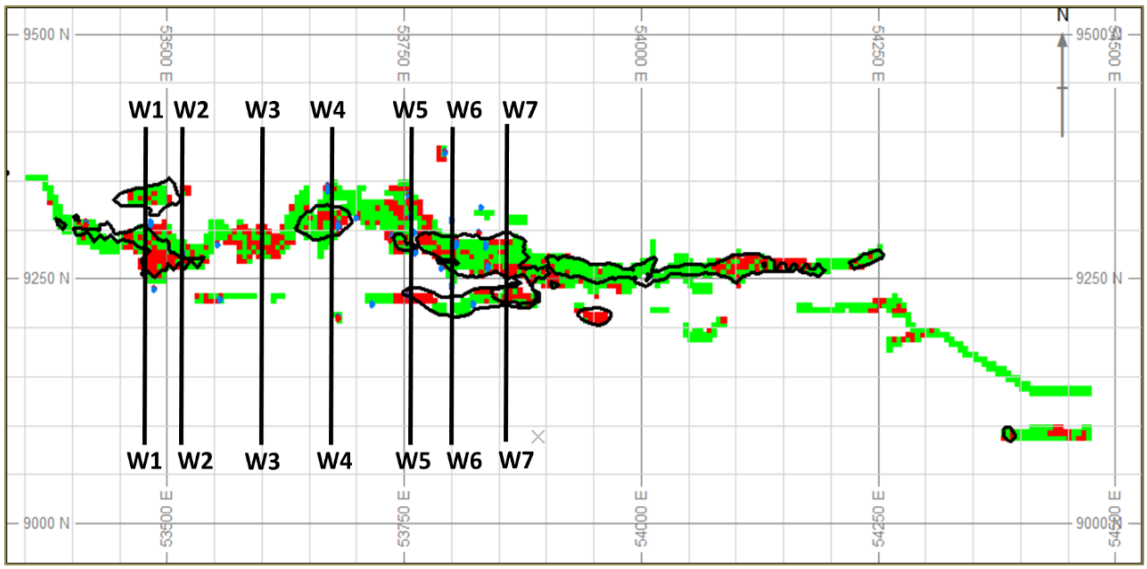


Figure 4-8: Plan view showing the location of cross sections (W1-W7) through GHEW to compare upside and downside scenarios for the SIS realisations on the 5m x 5m x 3,333m simulation grid.

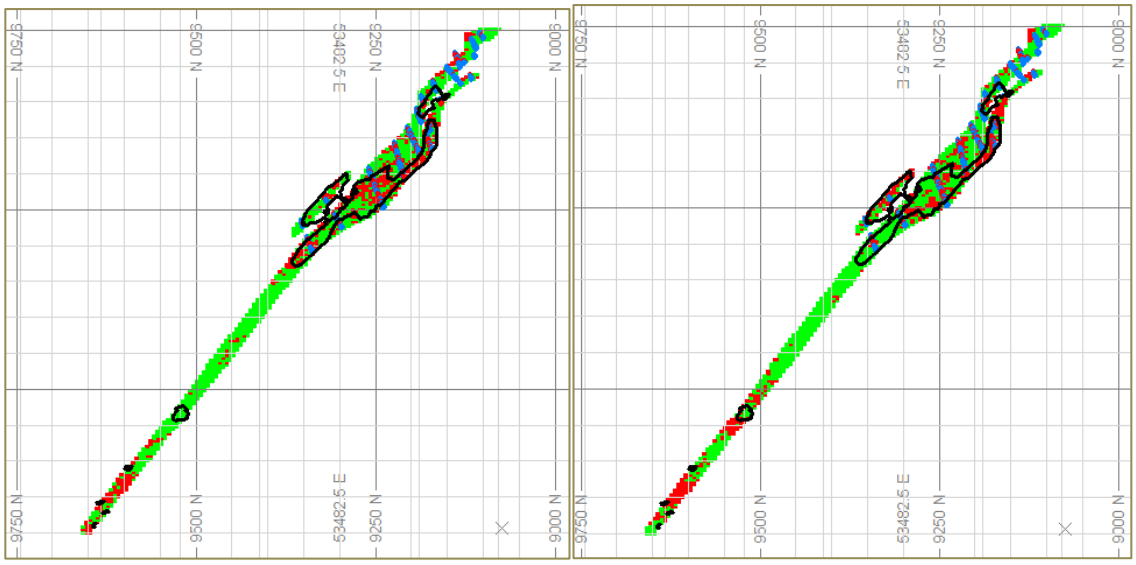


Figure 4-9: Section view (W1) showing the potential downside scenario (left) and upside scenario (right) based on ranked SIS realisations for GHEW using a 5m x 5m x 3,333m simulation grid. IK high grade wireframe for the deposit is depicted by black outlines.

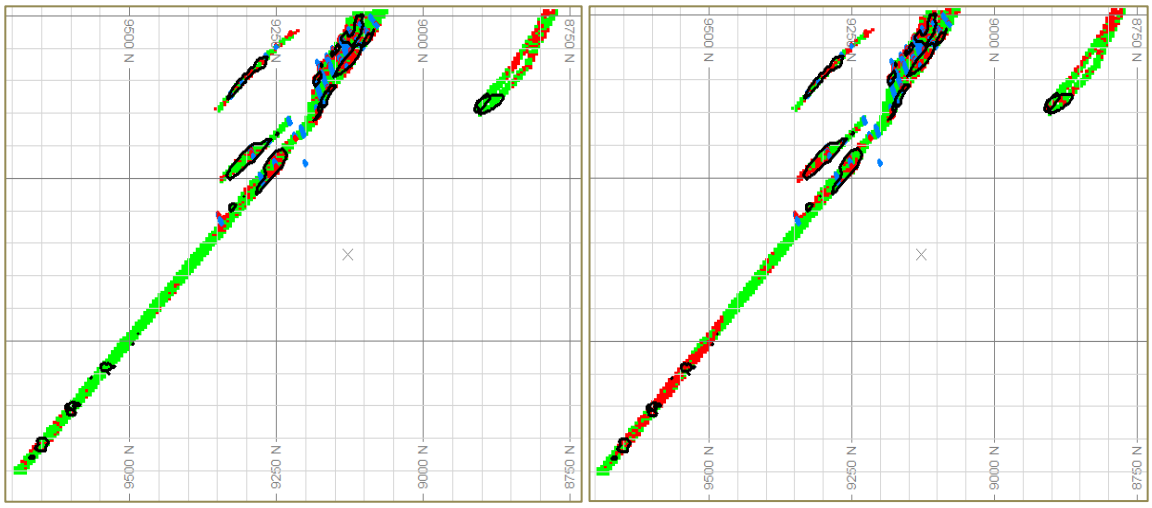


Figure 4-10: Section view (W2) showing the potential downside scenario (left) and upside scenario (right) based on ranked SIS realisations for GHEW using a 5m x 5m x 3,333m simulation grid. IK high grade wireframe for the deposit is depicted by black outlines.

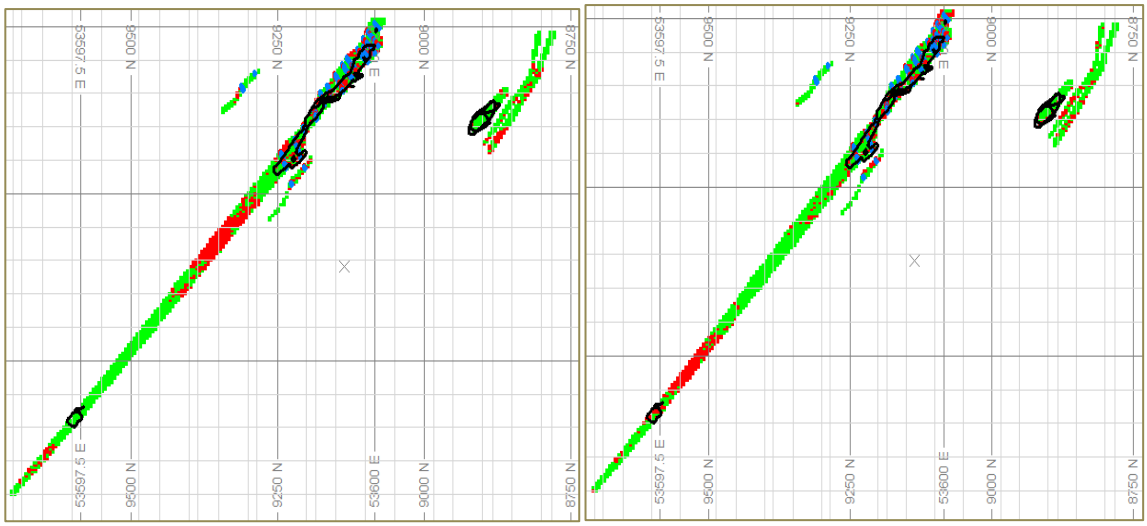


Figure 4-11: Section view (W3) showing the potential downside scenario (left) and upside scenario (right) based on ranked SIS realisations for GHEW using a 5m x 5m x 3,333m simulation grid. IK high grade wireframe for the deposit is depicted by black outlines.

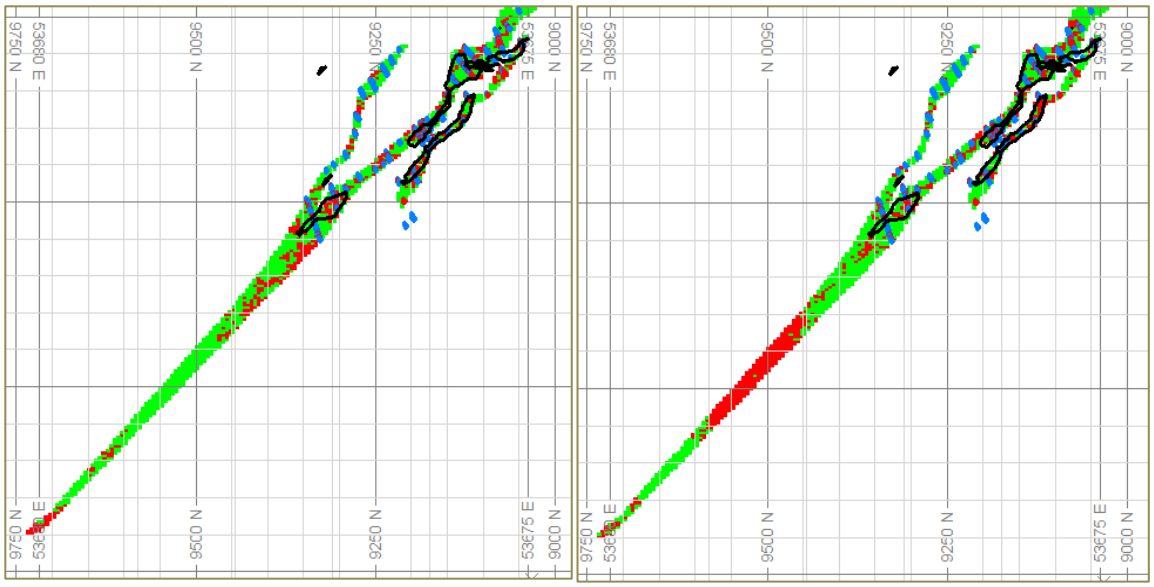


Figure 4-12: Section view (W4) showing the potential downside scenario (left) and upside scenario (right) based on ranked SIS realisations for GHEW using a 5m x 5m x 3,333m simulation grid. IK high grade wireframe for the deposit is depicted by black outlines.

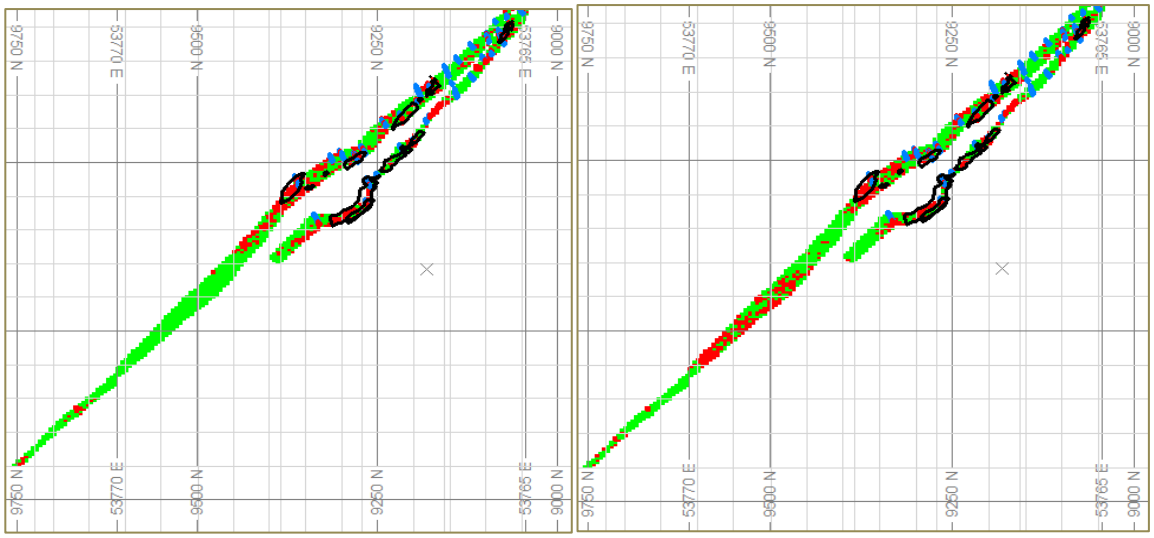


Figure 4-13: Section view (W5) showing the potential downside scenario (left) and upside scenario (right) based on ranked SIS realisations for GHEW using a 5m x 5m x 3,333m simulation grid. IK high grade wireframe for the deposit is depicted by black outlines.

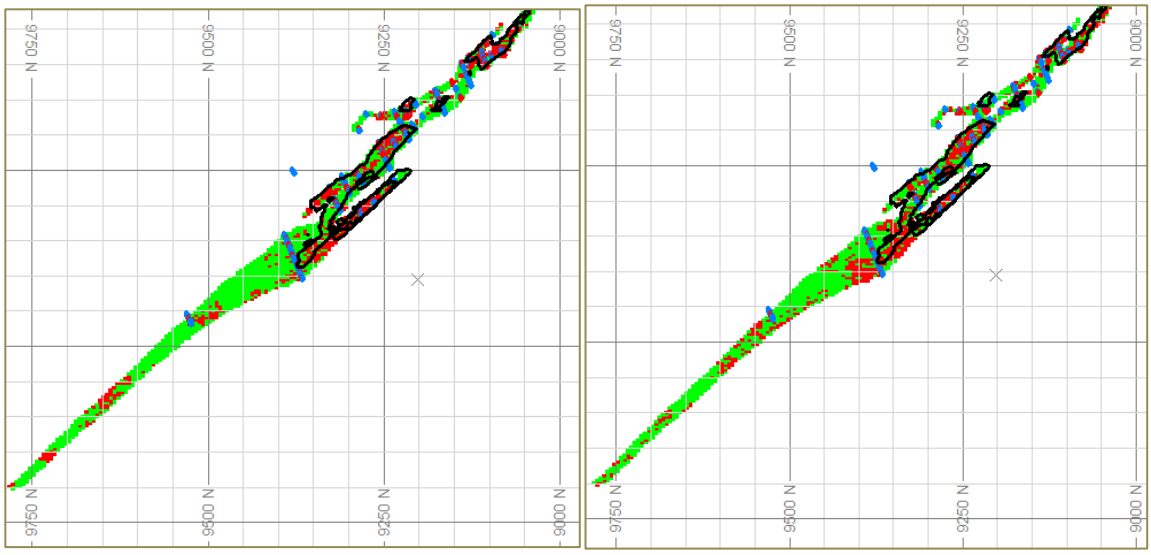


Figure 4-14: Section view (W6) showing the potential downside scenario (left) and upside scenario (right) based on ranked SIS realisations for GHEW using a 5m x 5m x 3,333m simulation grid. IK high grade wireframe for the deposit is depicted by black outlines.

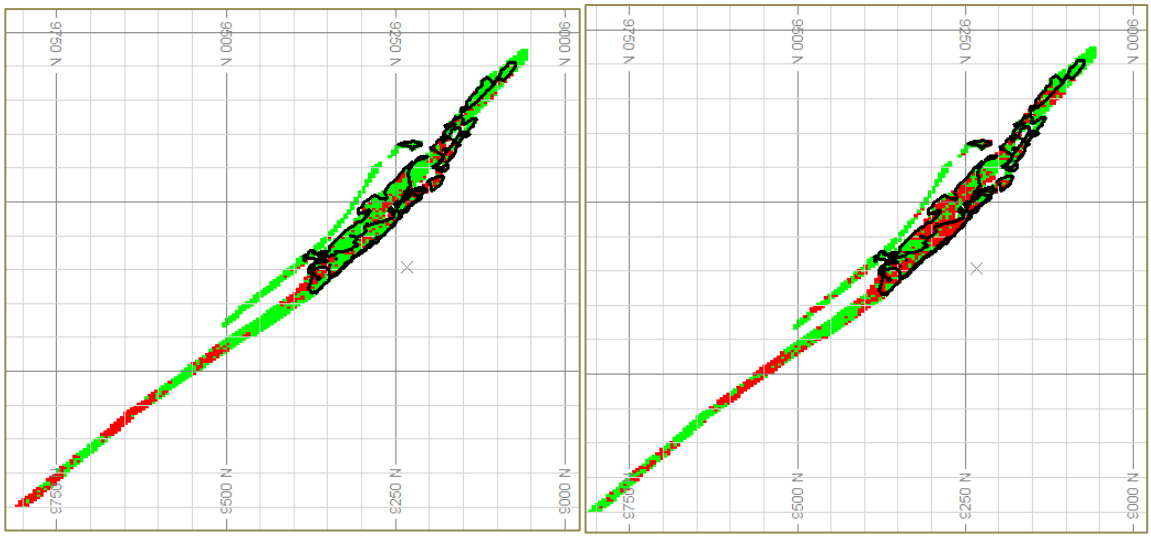


Figure 4-15: Section view (W7) showing the potential downside scenario (left) and upside scenario (right) based on ranked SIS realisations for GHEW using a 5m x 5m x 3,333m simulation grid. IK high grade wireframe for the deposit is depicted by black outlines.

4.2.2 Difference in volumes between simulated results and IK wireframe model

SIS and IK both assist in defining the shape of the high grade lenses. The IK shape is defined on the 50% probability of the material being high grade. As the shapes of the high grade lenses vary between the SIS realisations, so too does the volume of expected high grade material. The potential upside and downside volumes of high grade material are not included due to bias since IK only created high grade shapes in the vicinity of conditioning data whereas SIS simulates over the whole shear area.

4.2.3 Ranking of simulated volumes occuring inside proposed stope designs

The total volume of simulated high grade material occurring inside the proposed stope layout, was ranked in ascending order for all SIS realisations. This was performed to check if the stopes are currently located in areas where the high grade lenses can be well accessed and high volumes are expected. By ranking the volumes inside the stopes, comparisons can also be made to the upside and downside mine planning scenarios. These results could not be included due to confidentiality clauses.

4.3 Results for DBSim

The findings for DBSim will be presented as follows: potential upside and downside scenarios will be compared to the Indicator Kriged high grade wireframe for the deposit to understand the distribution of higher grade values in the deposit.

4.3.1 Comparison between DBSim Upside and Downside Scenarios

The higher and lower Grade DBSim potential upside downside scenarios are presented below as cross sections through the deposit. They are compared against the IK wireframe for the deposit to understand the distribution of higher grades.

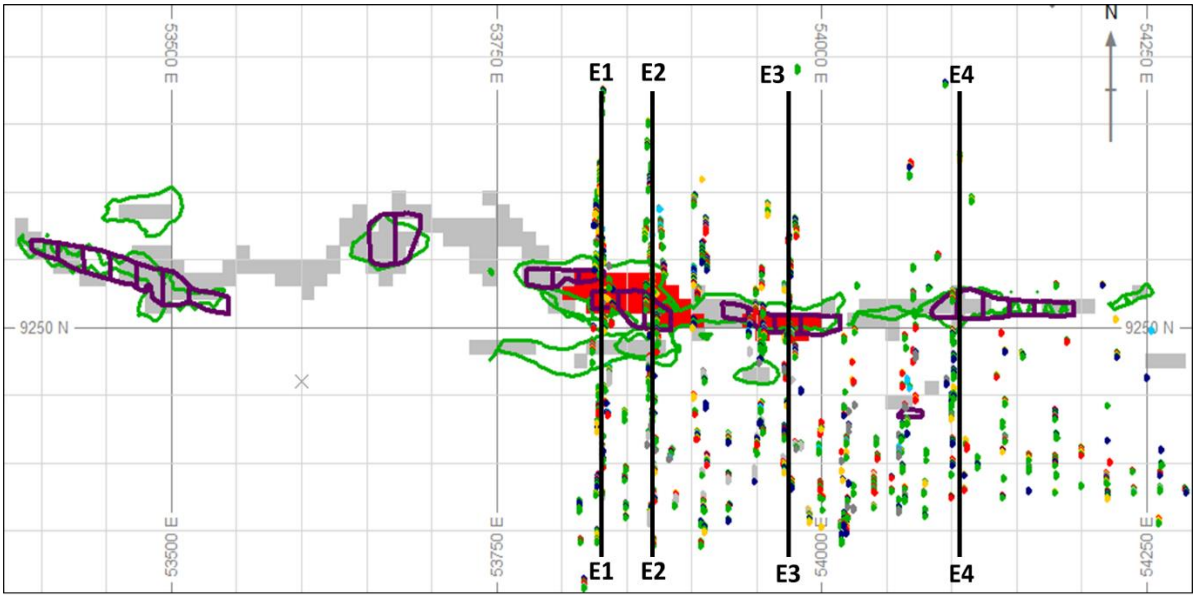


Figure 4-16: Plan view showing the location of cross sections (E1-E4) through GHEE to compare upside and downside scenarios for the High and Low Grade DBSim realisations on a 10m x 10m x 3,333m simulation grid.

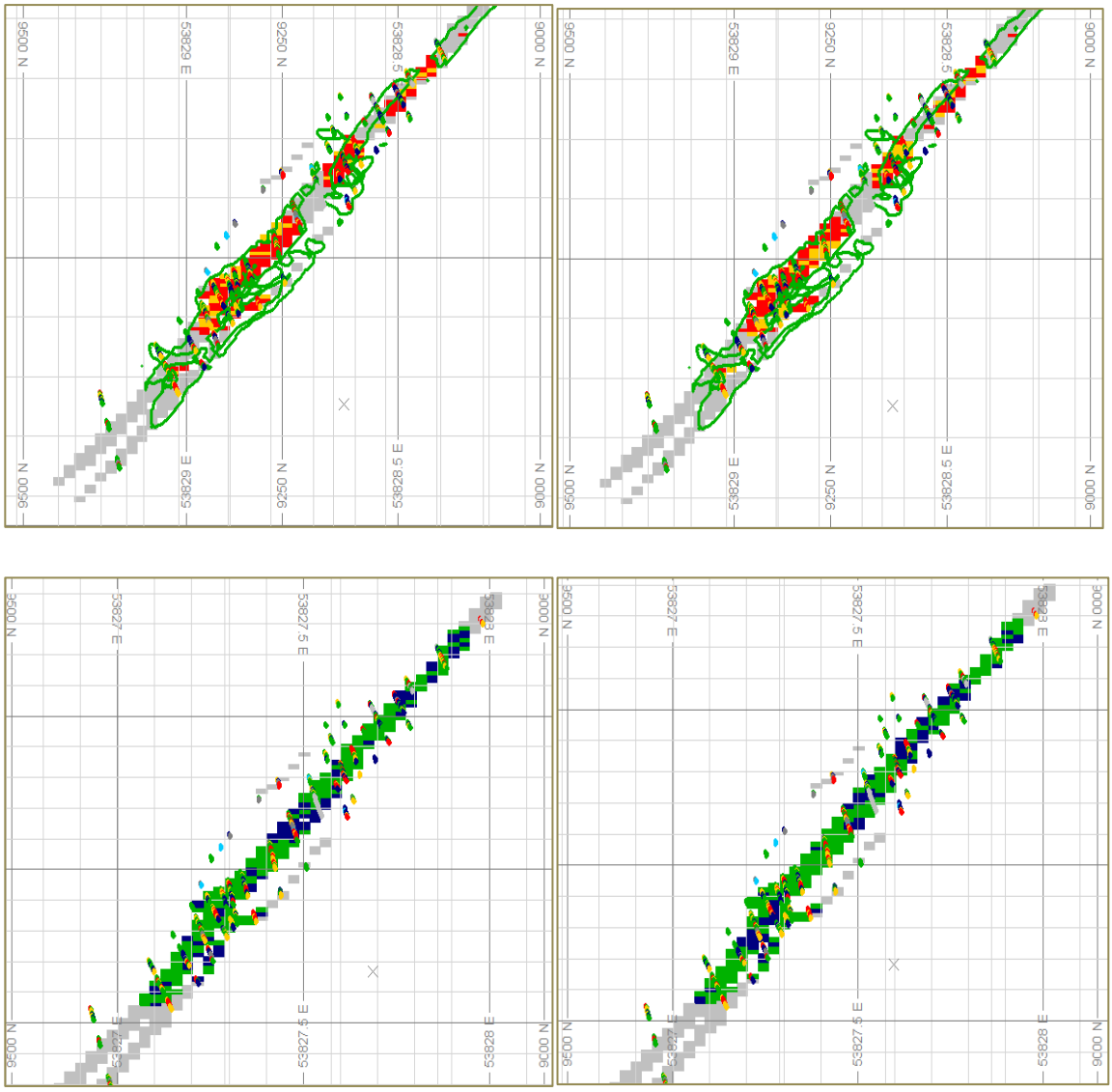


Figure 4-17: Section view (E1) showing the HG potential downside scenario (top left) and upside scenario (top right) and LG potential downside scenario (bottom left) and upside scenario (bottom right) based on ranked DBSim realisations for GHEE using a 10m x 10m x 3,333m simulation grid. IK high grade wireframe for the deposit is depicted by green outlines for the HG simulations.

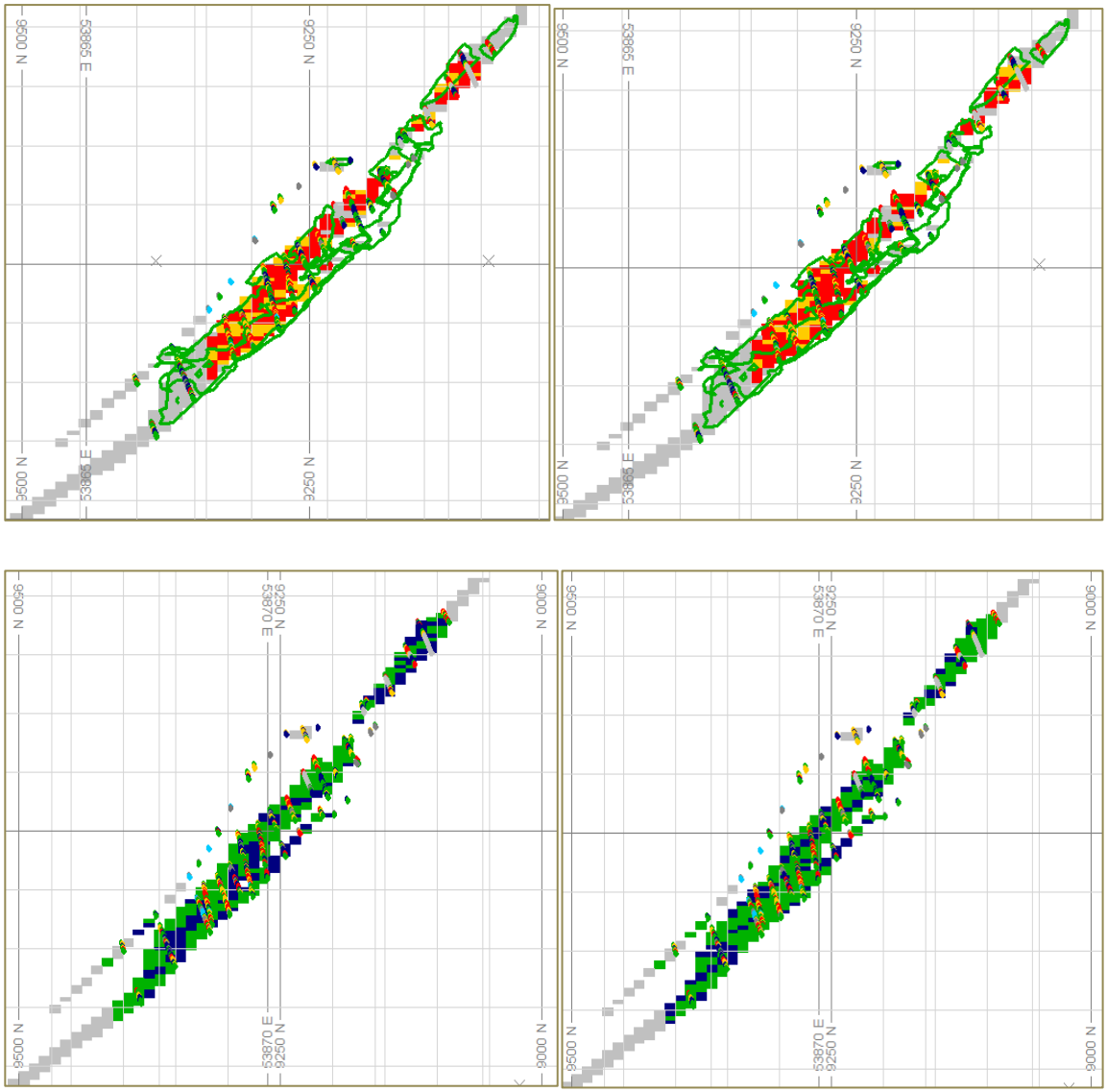


Figure 4-18: Section view (E2) showing the HG potential downside scenario (top left) and upside scenario (top right) and LG potential downside scenario (bottom left) and upside scenario (bottom right) based on ranked DBSim realisations for GHEE using a 10m x 10m x 3,333m simulation grid. IK high grade wireframe for the deposit is depicted by green outlines for the HG simulations

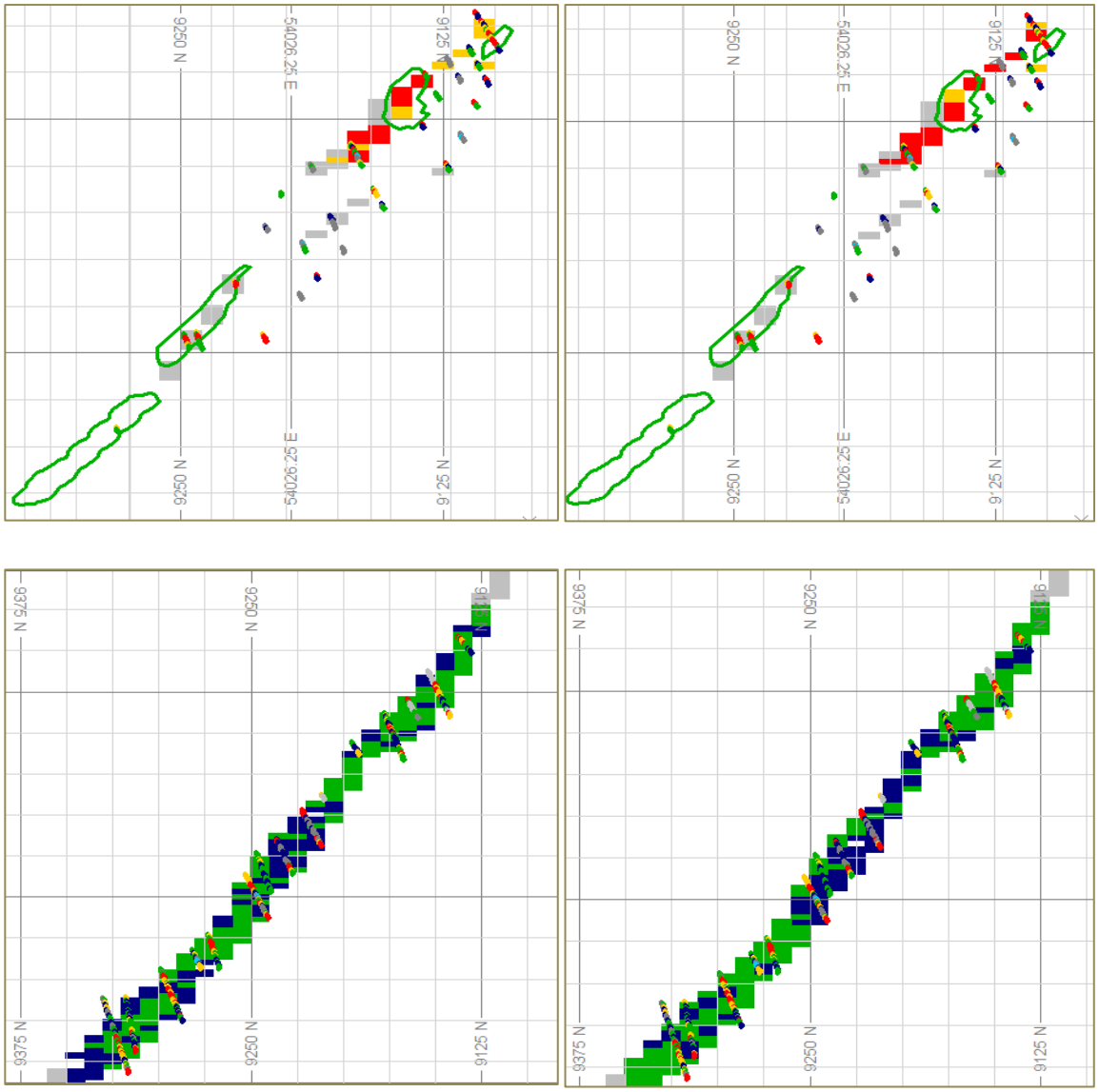


Figure 4-19: Section view (E3) showing the HG potential downside scenario (top left) and upside scenario (top right) and LG potential downside scenario (bottom left) and upside scenario (bottom right) based on ranked DBSim realisations for GHEE using a 10m x 10m x 3,333m simulation grid. IK high grade wireframe for the deposit is depicted by green outlines for the HG simulations

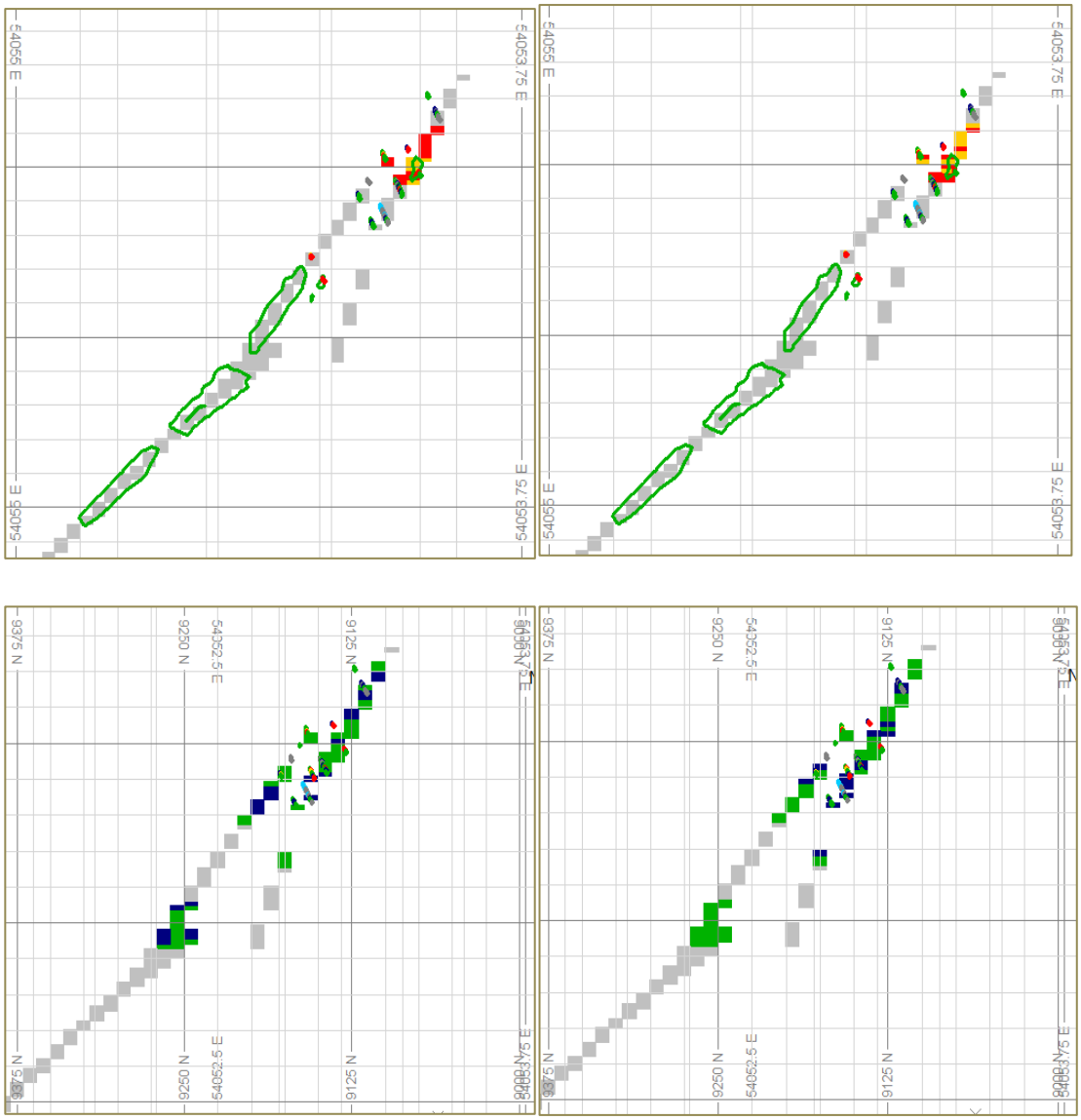


Figure 4-20: Section view (E4) showing the HG potential downside scenario (top left) and upside scenario (top right) and LG potential downside scenario (bottom left) and upside scenario (bottom right) based on ranked DBSim realisations for GHEE using a 10m x 10m x 3,333m simulation grid. IK high grade wireframe for the deposit is depicted by green outlines for the HG simulations

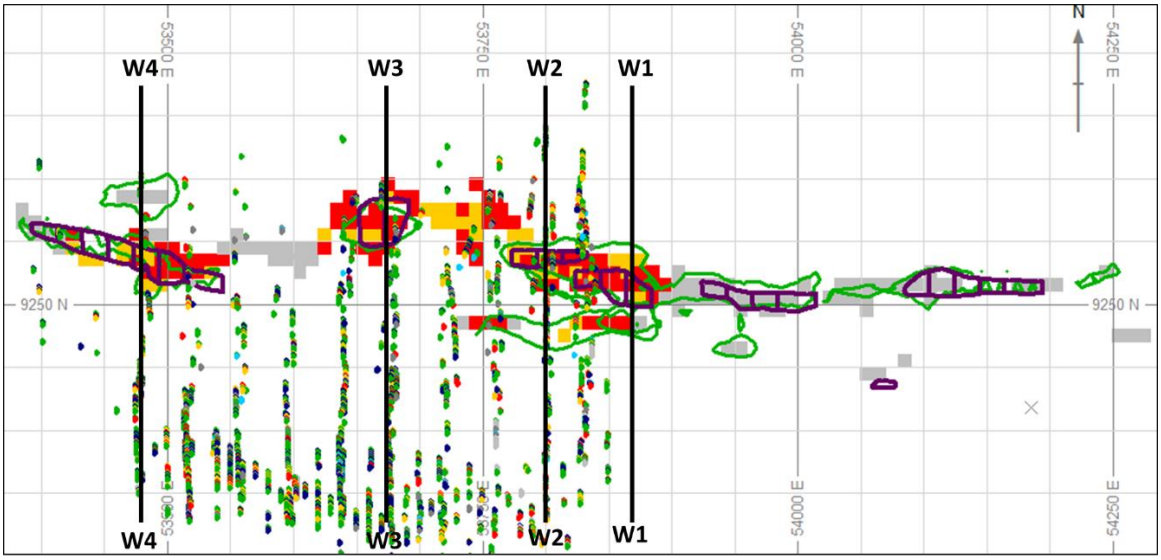


Figure 4-21: Plan view showing the location of cross sections (W1-W4) through GHEW to compare upside and downside scenarios for the High and Low Grade DBSim realisations on a 10m x 10m x 3,333m simulation grid.

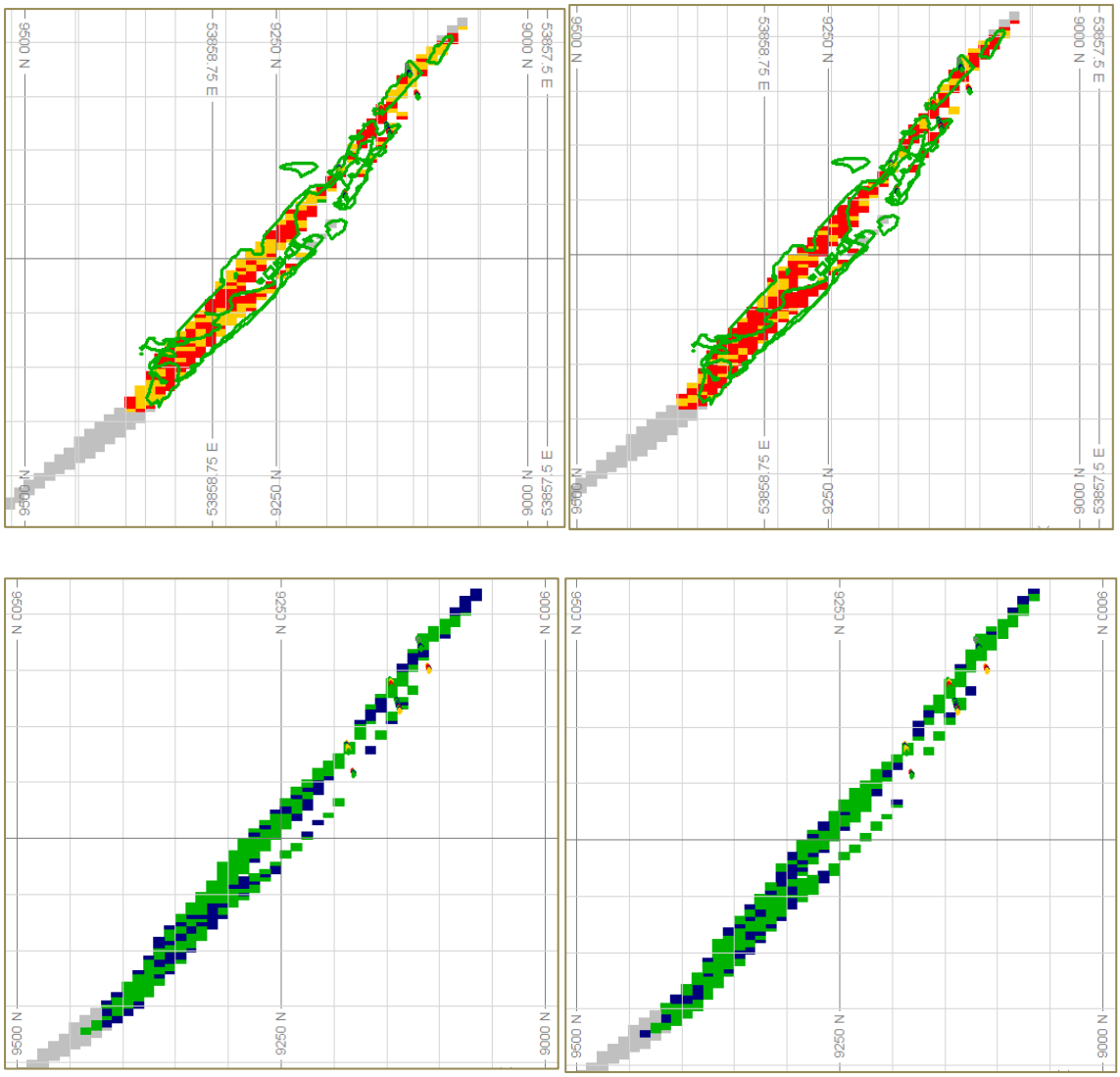


Figure 4-22: Section view (W1) showing the HG potential downside scenario (top left) and upside scenario (top right) and LG potential downside scenario (bottom left) and upside scenario (bottom right) based on ranked DBSim realisations for GHEW using a 10m x 10m x 3,333m simulation grid. IK high grade wireframe for the deposit is depicted by green outlines for the HG simulations

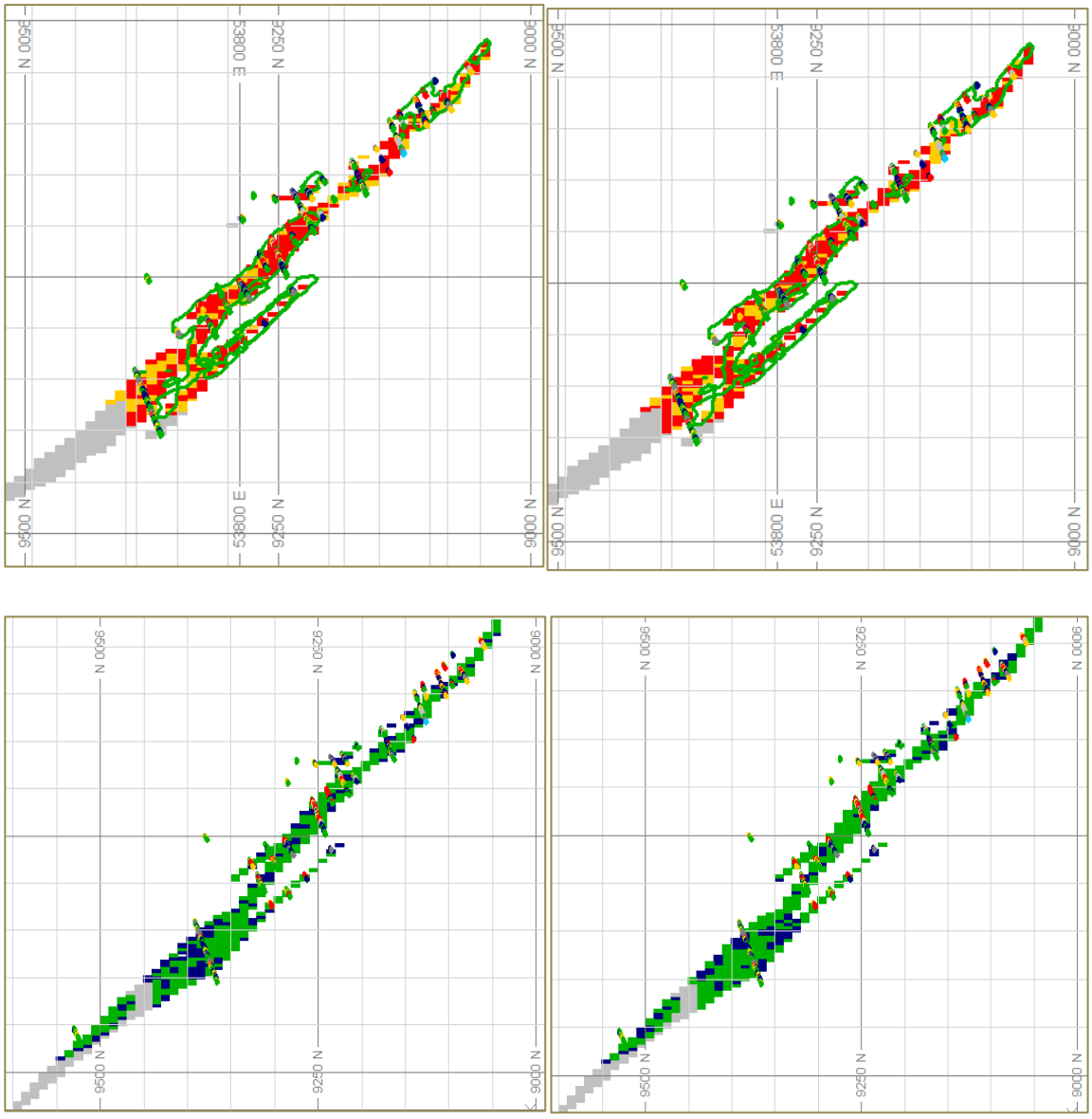


Figure 4-23: Section view (W2) showing the HG potential downside scenario (top left) and upside scenario (top right) and LG potential downside scenario (bottom left) and upside scenario (bottom right) based on ranked DBSim realisations for GHEW using a 10m x 10m x 3,333m simulation grid. IK high grade wireframe for the deposit is depicted by green outlines for the HG simulations

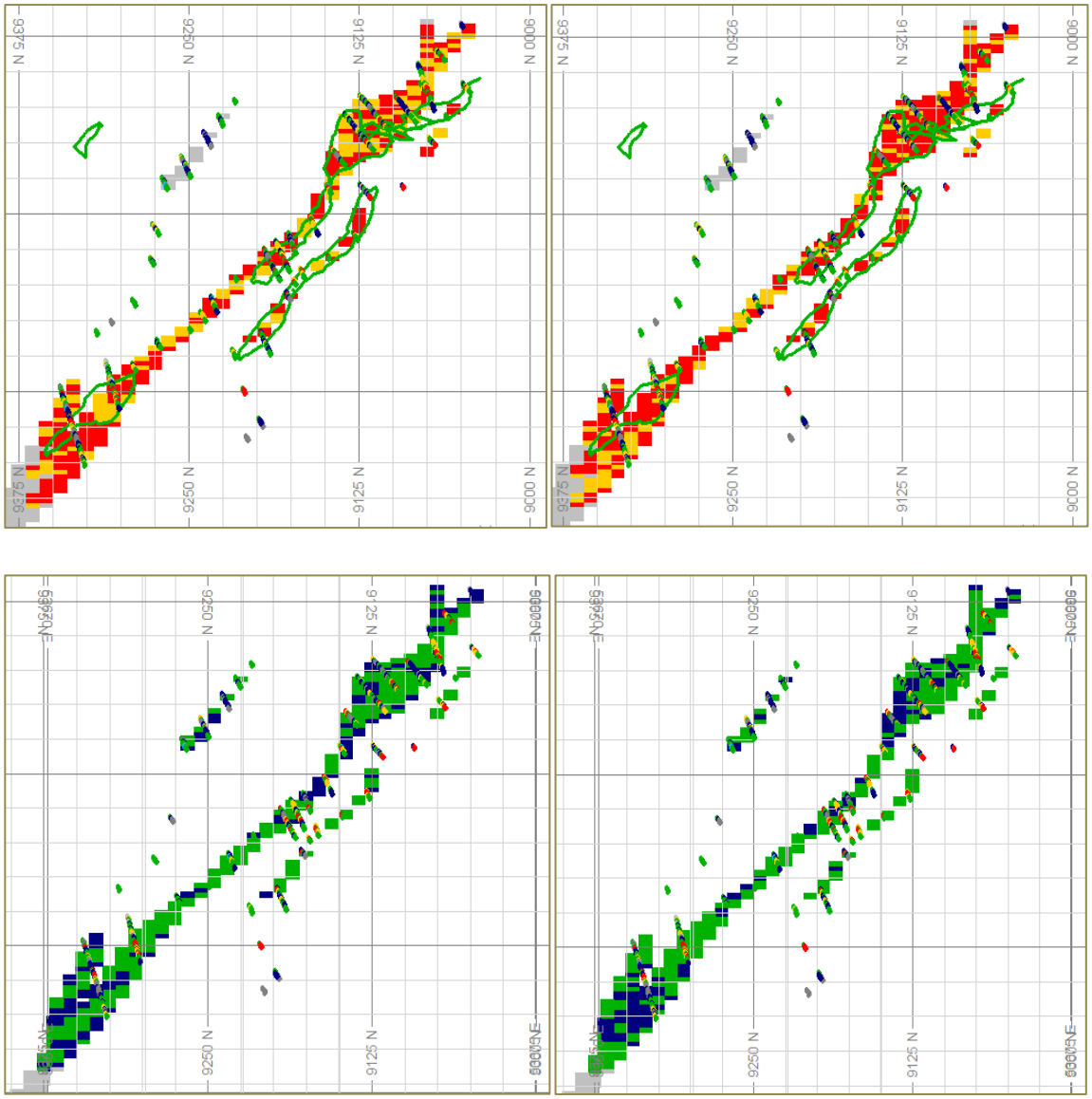


Figure 4-24: Section view (W3) showing the HG potential downside scenario (top left) and upside scenario (top right) and LG potential downside scenario (bottom left) and upside scenario (bottom right) based on ranked DBSim realisations for GHEW using a 10m x 10m x 3,333m simulation grid. IK high grade wireframe for the deposit is depicted by green outlines for the HG simulations

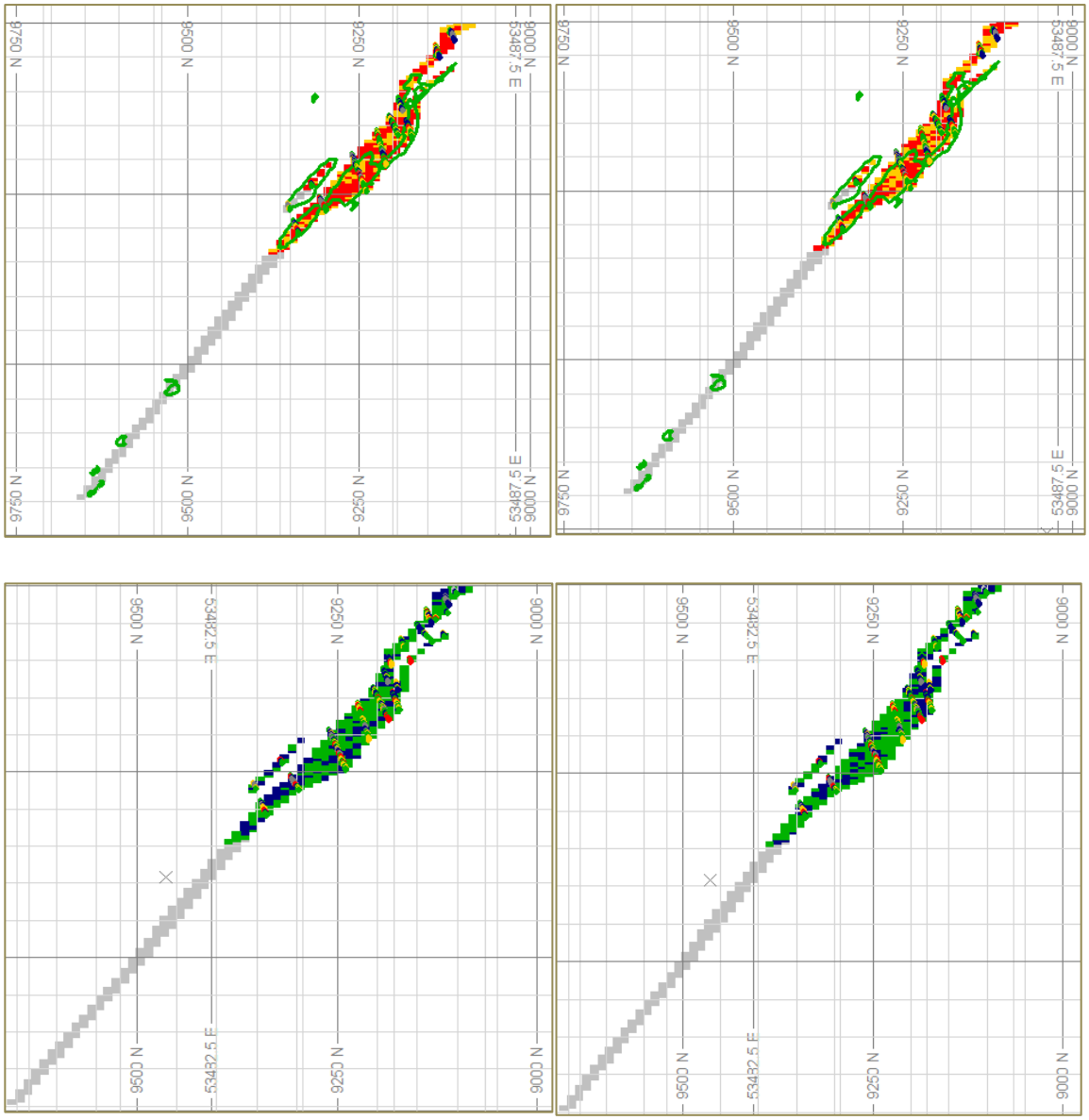


Figure 4-25: Section view (W4) showing the HG potential downside scenario (top left) and upside scenario (top right) and LG potential downside scenario (bottom left) and upside scenario (bottom right) based on ranked DBSim realisations for GHEW using a 10m x 10m x 3,333m simulation grid. IK high grade wireframe for the deposit is depicted by green outlines for the HG simulations

4.4 Results for the Model of Joint Uncertainty

The findings for model of joint uncertainty will be presented as follows:

- potential upside and downside scenarios for DBSim will be compared to the deterministic kriged model for the deposit. The model of joint uncertainty is used for this because of higher and lower grade simulations being generated independently, and
- finally, potential upside and downside scenarios are compared against the proposed stope layout.

4.4.1 Comparison between joint simulation upside and downside scenarios against the deterministic estimated ore model for the deposit

The figures below depict cross sections through the model of joint uncertainty and the deterministic kriged model. The findings were used to compare variations between simulated and deterministic grade and volumes.

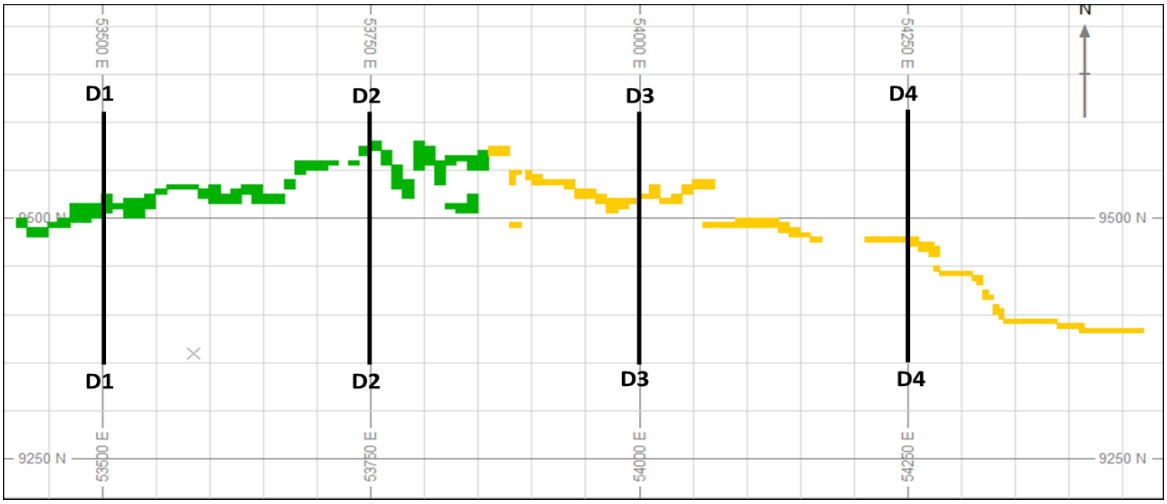


Figure 4-26: Plan view showing the location of cross sections (D1-D4) through GHEW and GHEE to compare upside and downside scenarios for the High Grade DBSim realisations on a 10m x 10m x 3,333m simulation grid against the deterministic estimated model for the study areas.

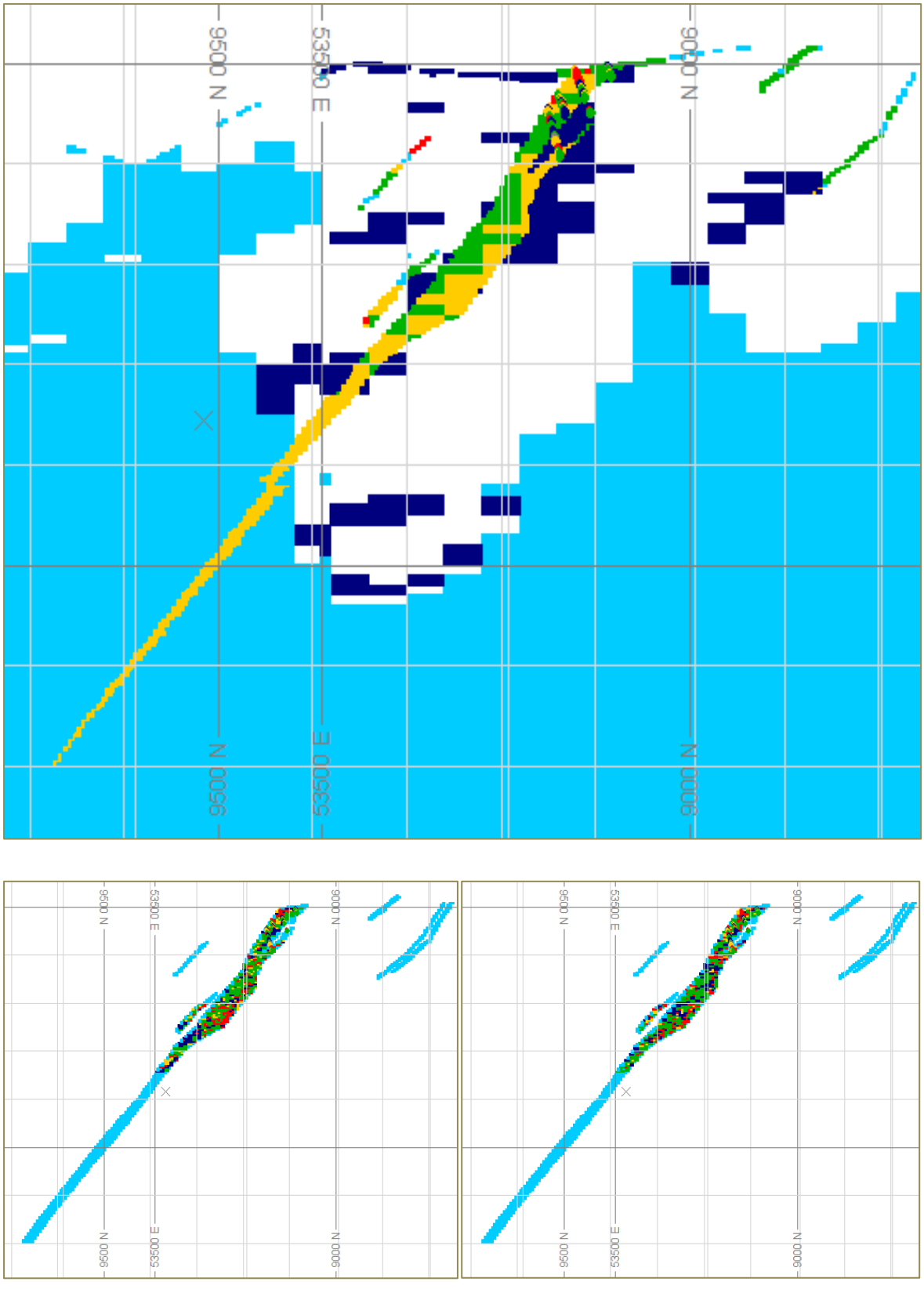


Figure 4-27: The deterministic kriged model for the deposit (top), and section view (D1) showing the potential downside scenario (bottom left) and upside scenario (bottom right) for the joint simulation model

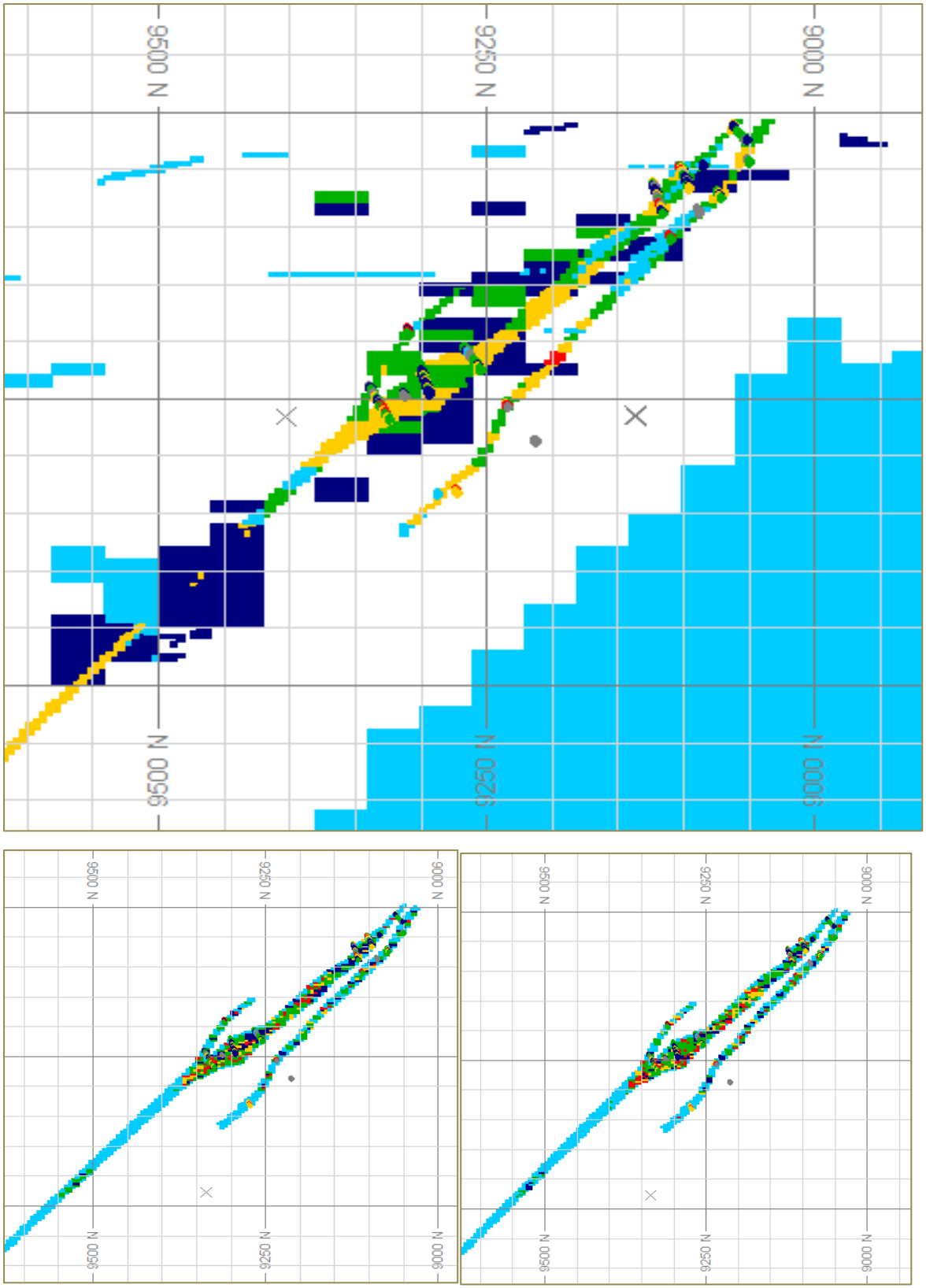


Figure 4-28: The deterministic kriged model for the deposit (top), and section view (D2) showing the potential downside scenario (bottom left) and upside scenario (bottom right) for the joint simulation model

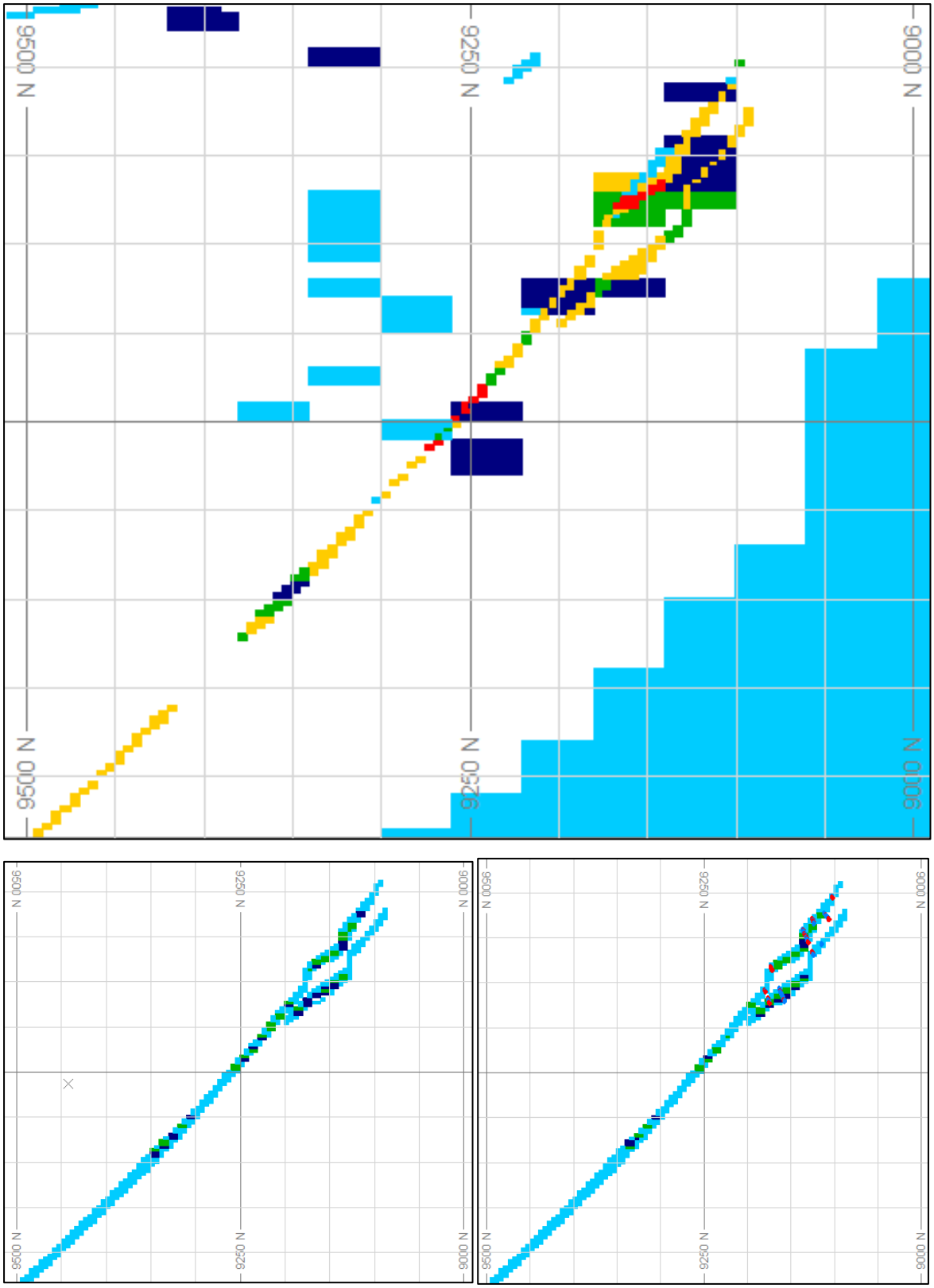


Figure 4-29: The deterministic kriged model for the deposit (top) and section view (D3) showing the potential downside scenario (bottom left) and upside scenario (bottom right) for the joint simulation model

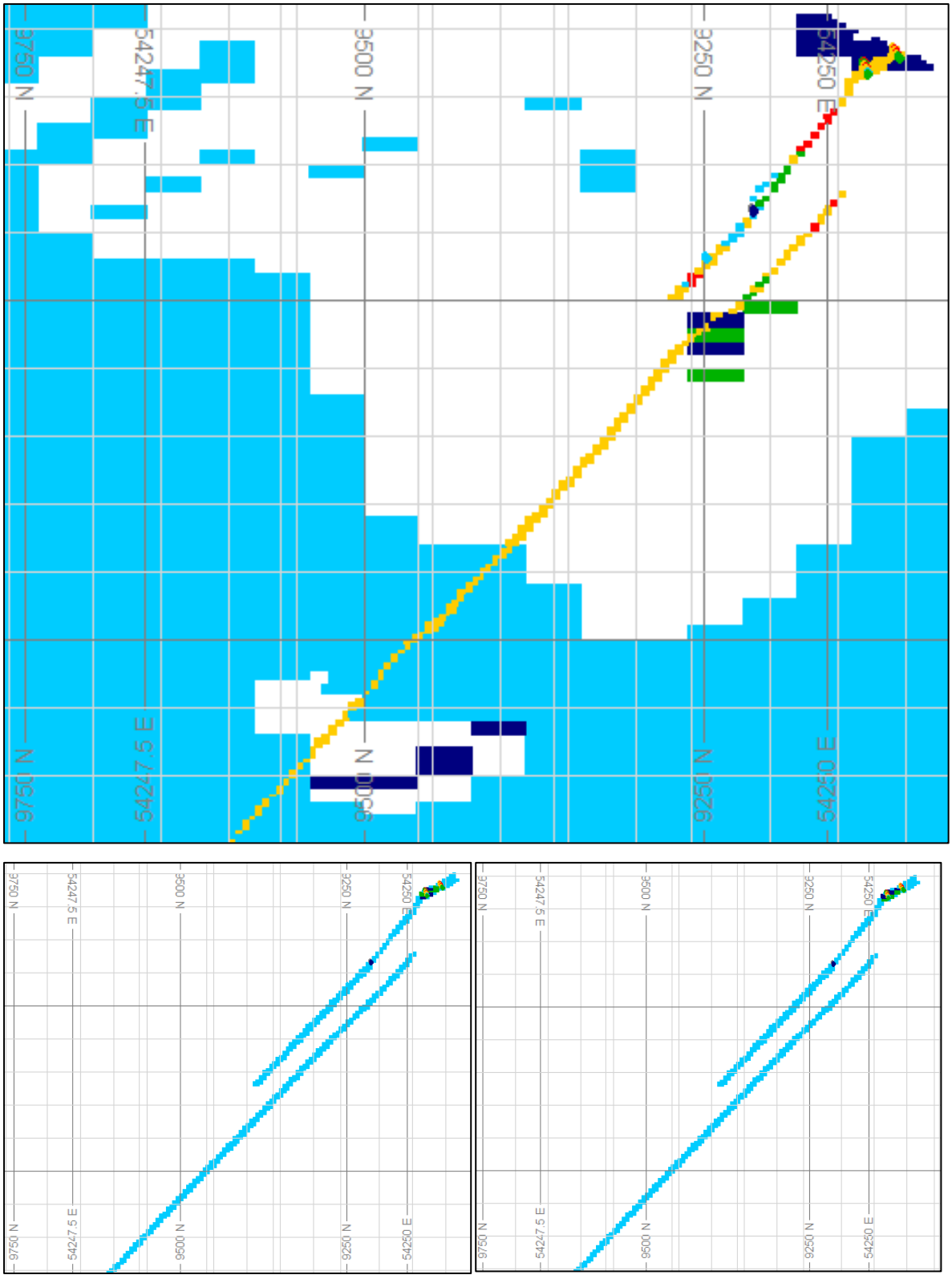


Figure 4-30: The deterministic kriged model for the deposit (top) and section view (D4) showing the potential downside scenario (bottom left) and upside scenario (bottom right) for the joint simulation model

4.4.2 *Comparison between joint simulation upside and downside scenarios against the proposed Stope layout*

The following figures show cross sections through the model of joint uncertainty to compare the simulated ore zones with the location of the proposed stope layouts. These images reveal whether or not the stopes are positioned correctly to target high grade lenses for underground mining.

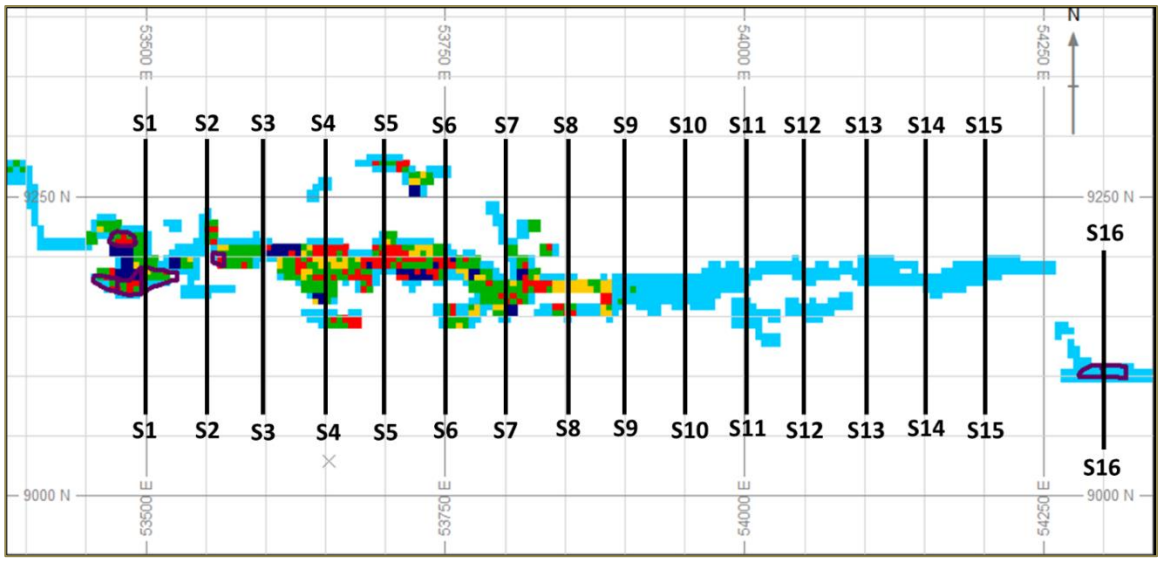


Figure 4-31: Plan view showing the location of cross sections (S1-S16) through GHEW and GHEE to compare upside and downside scenarios for the joint uncertainty models on a 10m x 10m x 3,333m simulation grid.

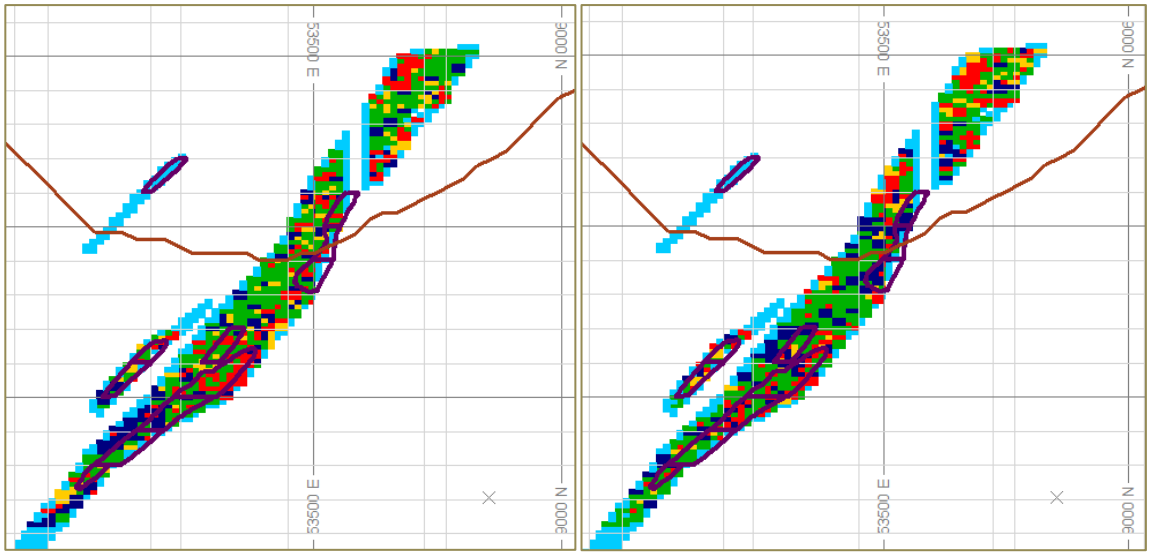


Figure 4-32: Section view (S1) showing the potential grade downside scenario (left) and upside scenario (right) for the joint uncertainty model (10m x 10m x 3,333m grid). Proposed location of stope designs are depicted by purple outlines. Resource pit surface is indicated by the brown line.

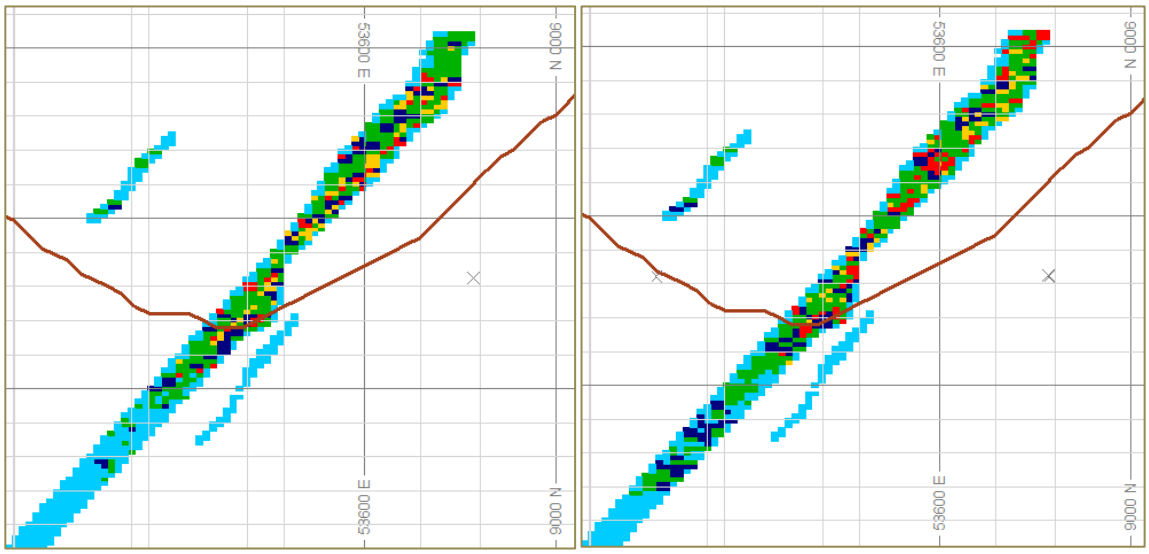


Figure 4-33: Section view (S2) showing the potential grade downside scenario (left) and upside scenario (right) for the joint uncertainty model (10m x 10m x 3,333m grid). Proposed location of stope designs are depicted by purple outlines. Resource pit surface is indicated by the brown line.

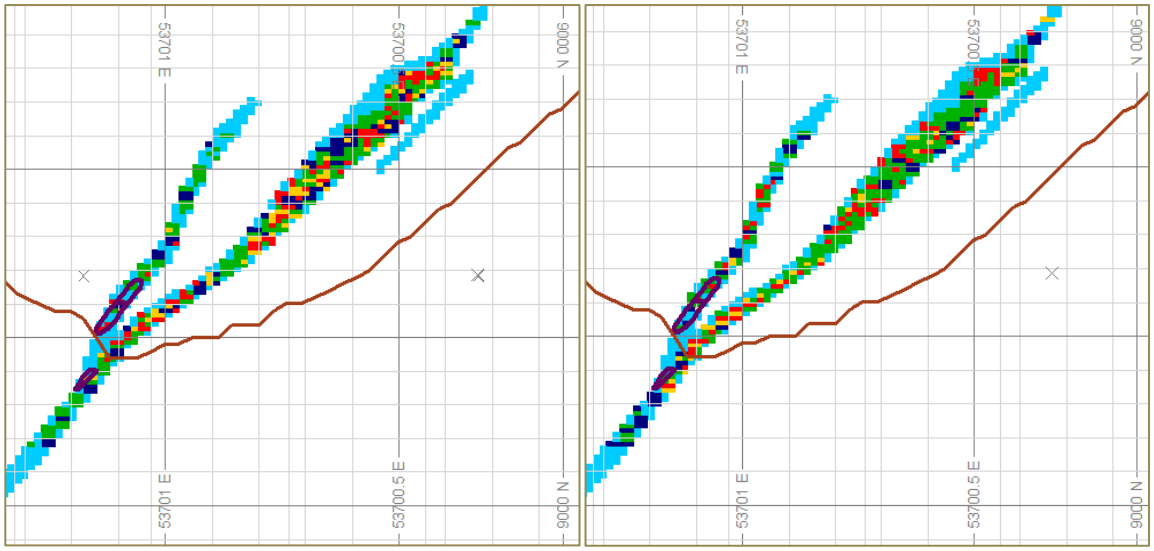


Figure 4-34: Section view (S3) showing the potential grade downside scenario (left) and upside scenario (right) for the joint uncertainty model (10m x 10m x 3,333m grid). Proposed location of stope designs are depicted by purple outlines. Resource pit surface is indicated by the brown line.

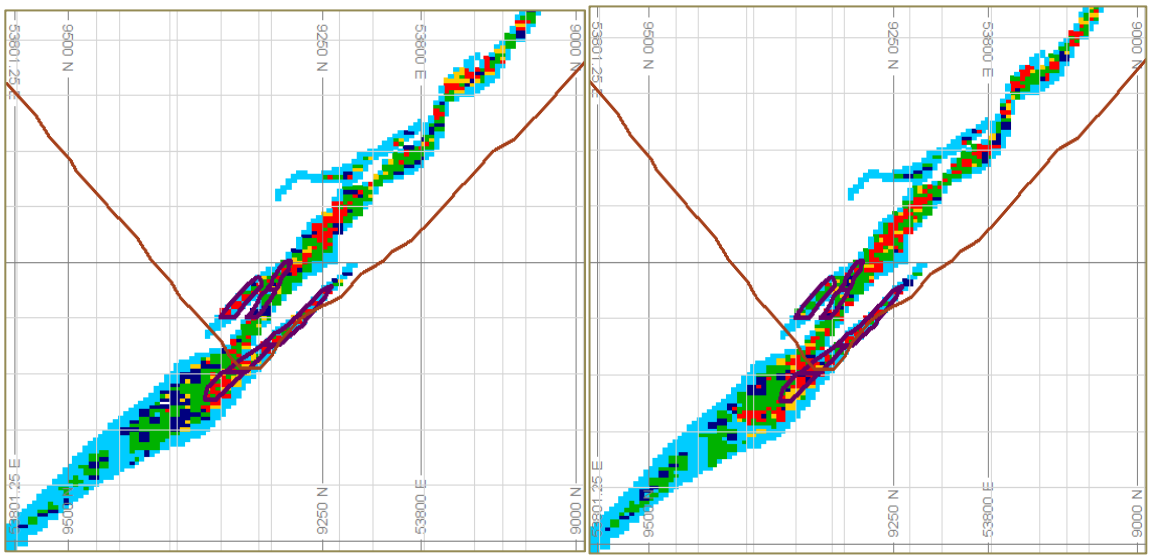


Figure 4-35: Section view (S4) showing the potential grade downside scenario (left) and upside scenario (right) for the joint uncertainty model (10m x 10m x 3,333m grid). Proposed location of stope designs are depicted by purple outlines. Resource pit surface is indicated by the brown line.

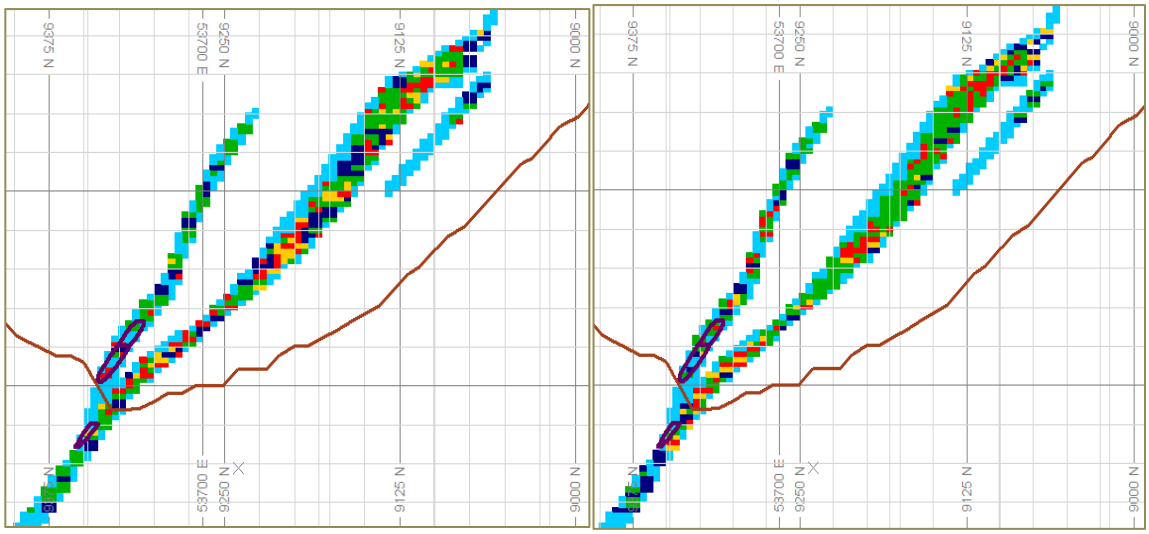


Figure 4-36: Section view (S5) showing the potential grade downside scenario (left) and upside scenario (right) for the joint uncertainty model (10m x 10m x 3,333m grid). Proposed location of stope designs are depicted by purple outlines. Resource pit surface is indicated by the brown line.

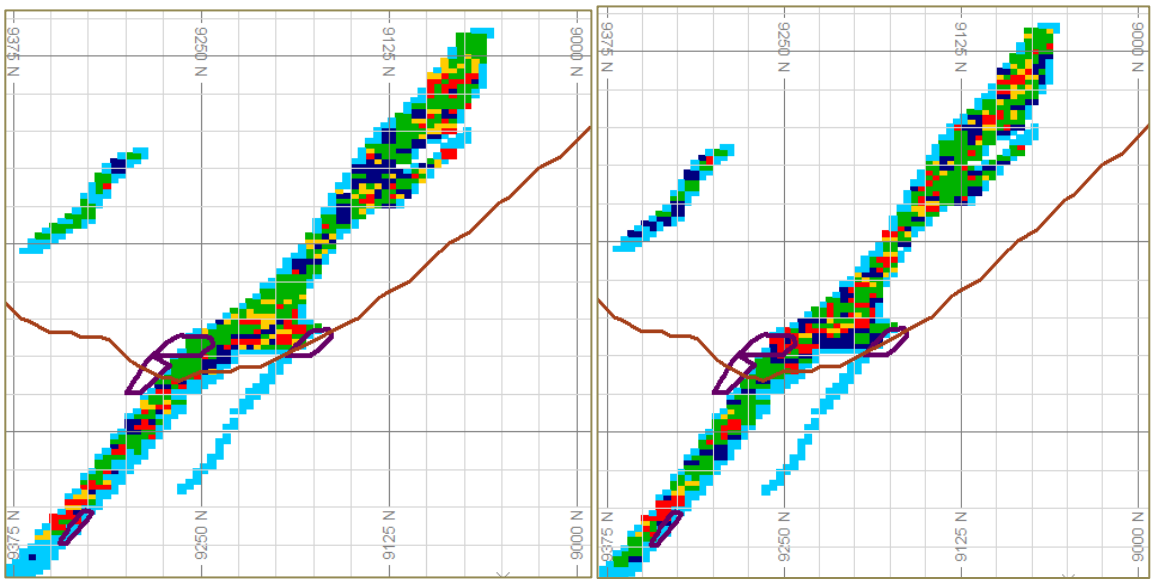


Figure 4-37: Section view (S6) showing the potential grade downside scenario (left) and upside scenario (right) for the joint uncertainty model (10m x 10m x 3,333m grid). Proposed location of stope designs are depicted by purple outlines. Resource pit surface is indicated by the brown line.

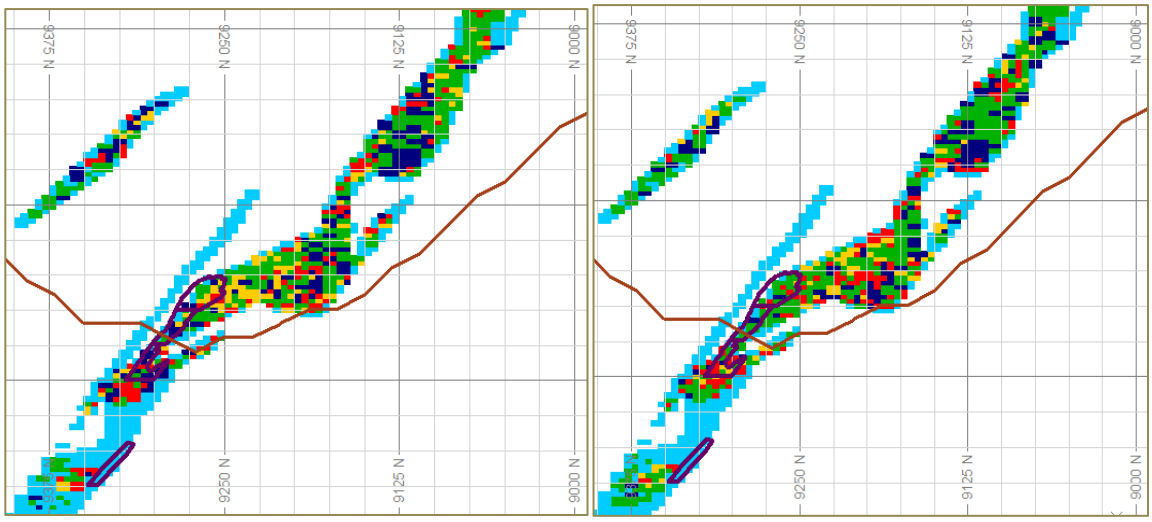


Figure 4-38: Section view (S7) showing the potential grade downside scenario (left) and upside scenario (right) for the joint uncertainty model (10m x 10m x 3,333m grid). Proposed location of stope designs are depicted by purple outlines. Resource pit surface is indicated by the brown line.

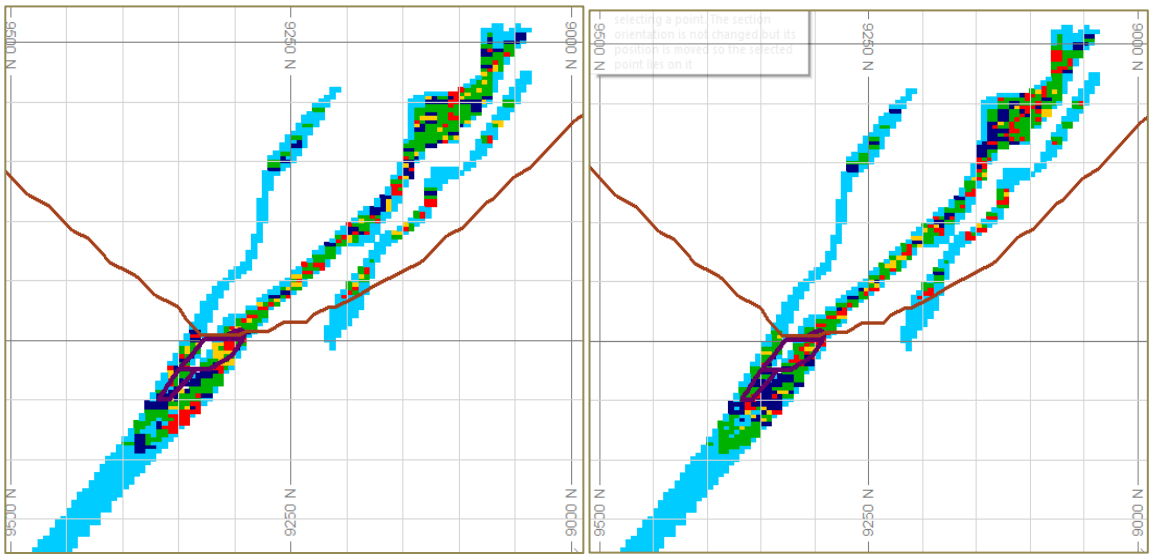


Figure 4-39: Section view (S8) showing the potential grade downside scenario (left) and upside scenario (right) for the joint uncertainty model (10m x 10m x 3,333m grid). Proposed location of stope designs are depicted by purple outlines. Resource pit surface is indicated by the brown line.

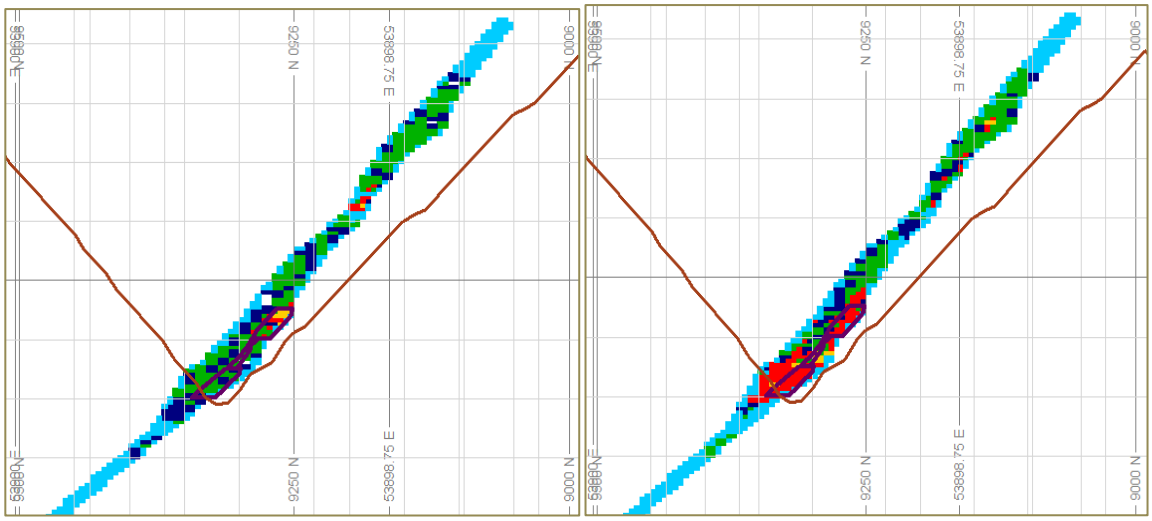


Figure 4-40: Section view (S9) showing the potential grade downside scenario (left) and upside scenario (right) for the joint uncertainty model (10m x 10m x 3,333m grid). Proposed location of stope designs are depicted by purple outlines. Resource pit surface is indicated by the brown line.

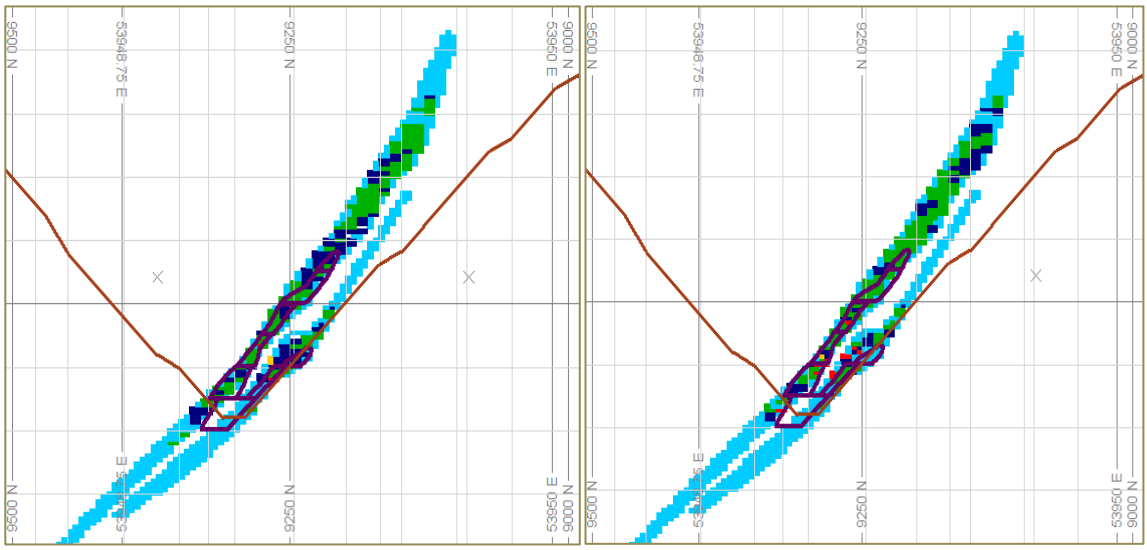


Figure 4-41: Section view (S10) showing the potential grade downside scenario (left) and upside scenario (right) for the joint uncertainty model (10m x 10m x 3,333m grid). Proposed location of stope designs are depicted by purple outlines. Resource pit surface is indicated by the brown line.

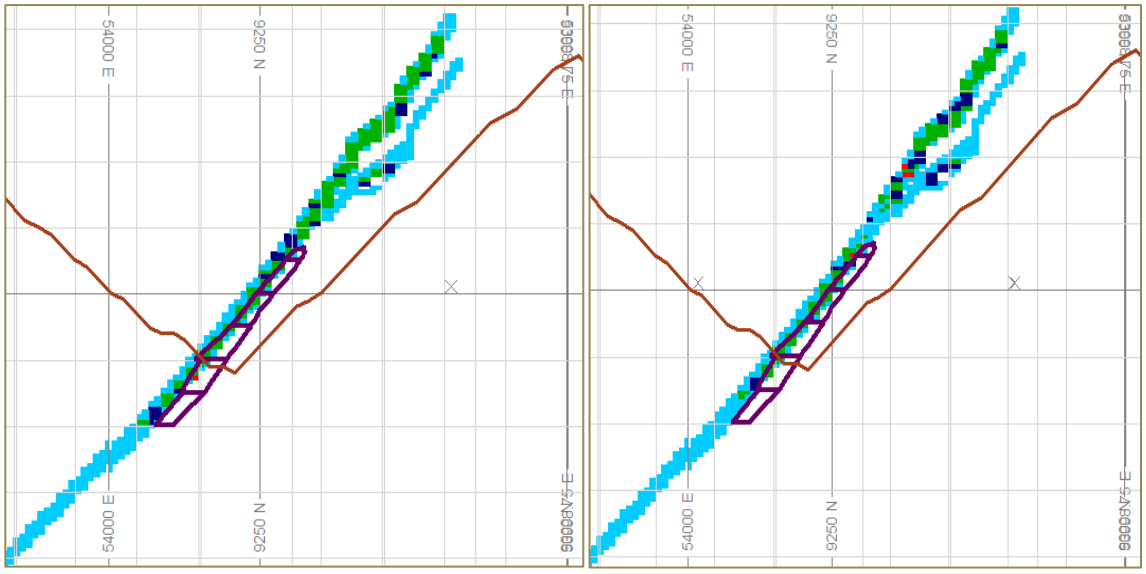


Figure 4-42: Section view (S11) showing the potential grade downside scenario (left) and upside scenario (right) for the joint uncertainty model (10m x 10m x 3,333m grid). Proposed location of stope designs are depicted by purple outlines. Resource pit surface is indicated by the brown line.

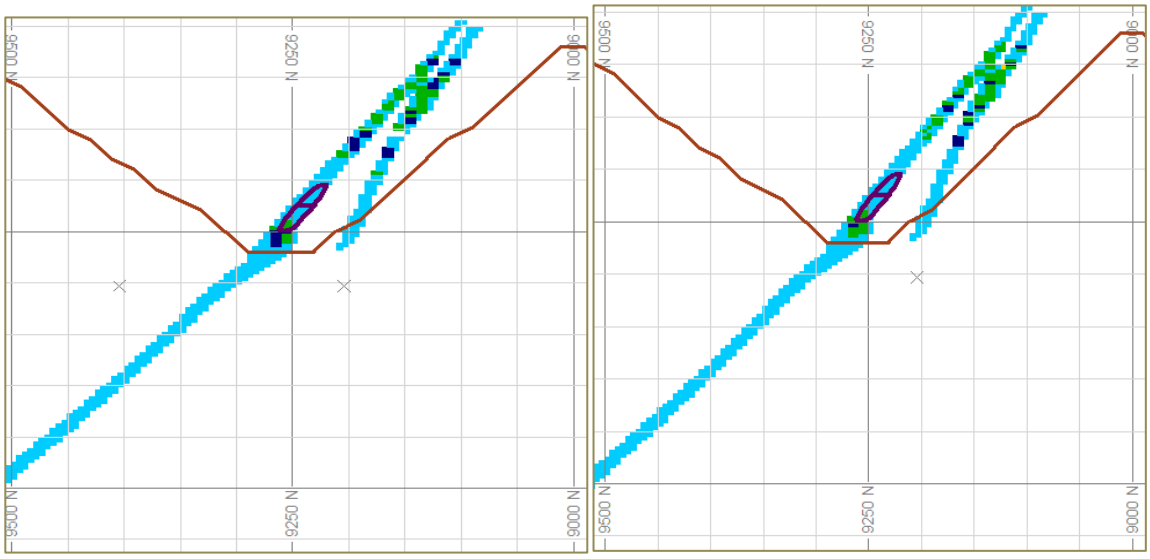


Figure 4-43: Section view (S12) showing the potential grade downside scenario (left) and upside scenario (right) for the joint uncertainty model (10m x 10m x 3,333m grid). Proposed location of stope designs are depicted by purple outlines. Resource pit surface is indicated by the brown line.

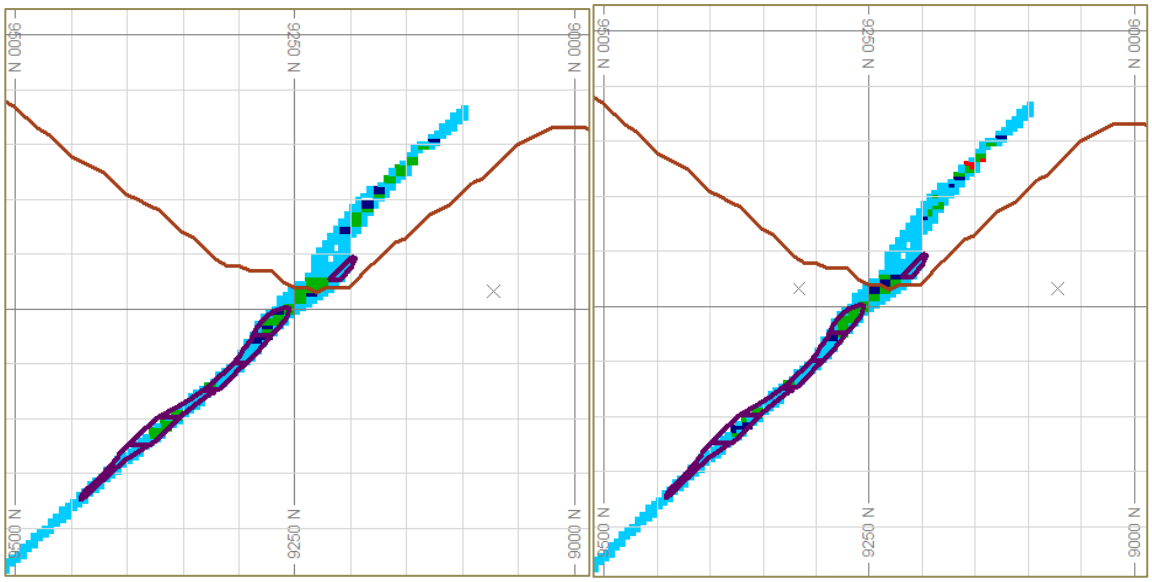


Figure 4-44: Section view (S13) showing the potential grade downside scenario (left) and upside scenario (right) for the joint uncertainty model (10m x 10m x 3,333m grid). Proposed location of stope designs are depicted by purple outlines. Resource pit surface is indicated by the brown line.

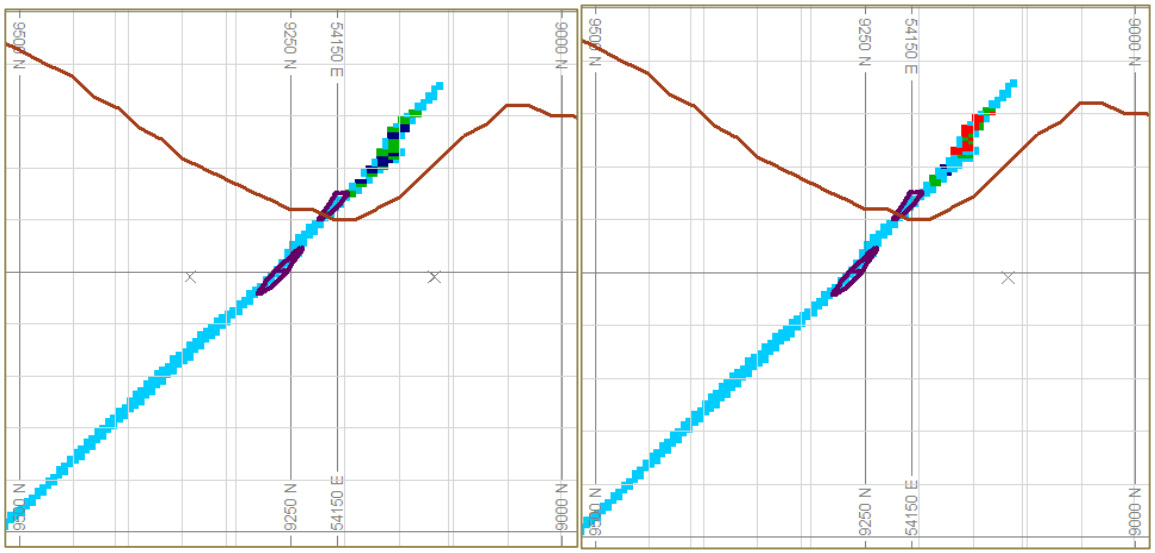


Figure 4-45: Section view (S14) showing the potential grade downside scenario (left) and upside scenario (right) for the joint uncertainty model (10m x 10m x 3,333m grid). Proposed location of stope designs are depicted by purple outlines. Resource pit surface is indicated by the brown line.

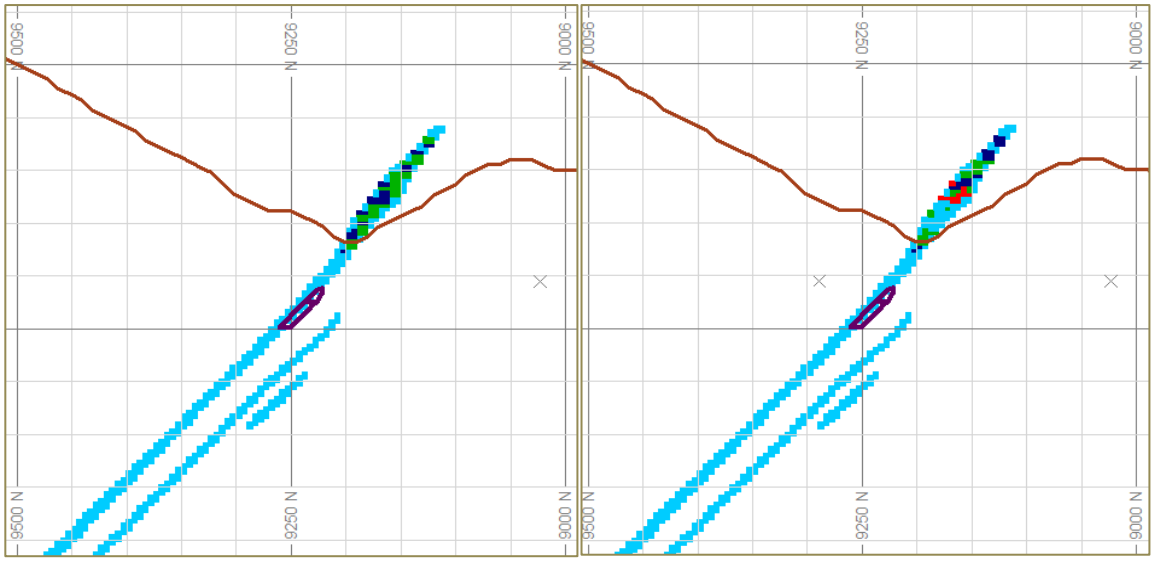


Figure 4-46: Section view (S15) showing the potential grade downside scenario (left) and upside scenario (right) for the joint uncertainty model (10m x 10m x 3,333m grid). Proposed location of stope designs are depicted by purple outlines. Resource pit surface is indicated by the brown line.

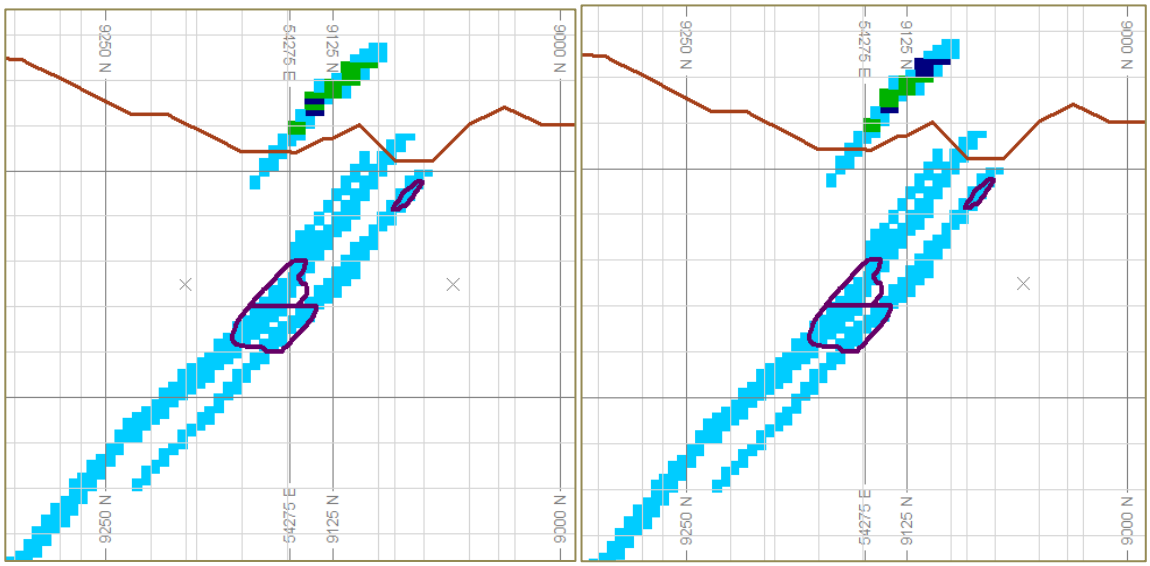


Figure 4-47: Section view (S16) showing the potential grade downside scenario (left) and upside scenario (right) for the joint uncertainty model (10m x 10m x 3,333m grid). Proposed location of stope designs are depicted by purple outlines. Resource pit surface is indicated by the brown line.

4.5 Conclusion

This Chapter highlighted the pertinent results derived from the SIS and DBSim realisations generated. A model of joint uncertainty was also presented to compare variations in simulated grades and to account for the independent simulation of higher and lower grade populations using DBSim. These findings included the identification of potential upside and downside mine planning scenarios for expected volumes and grade. The findings are summarized and discussed in **Chapter 5**.

CHAPTER 5

‘‘Humans may crave absolute certainty; they may aspire to it; they may pretend ... to have attained it. But the history of science—by far the most successful claim to knowledge accessible to humans—teaches that the most we can hope for is successive improvement in our understanding, learning from our mistakes, an asymptotic approach to the Universe, but with the proviso that absolute certainty will always elude us. We will always be mired in error. The most each generation can hope for is to reduce the error bars a little, and to add to the body of data to which error bars apply. The error bar is a pervasive, visible self-assessment of the reliability of our knowledge”

-Carl Sagan

The Demon-Haunted World: Science as a Candle in the Dark (1995), p. 28.

5 DISCUSSION

This chapter discusses the findings of the results presented in Chapter 4. To aid the reader in understanding the results, the research objectives and the statement of the research problem considered are reiterated.The bulk of this chapter is however concerned with summarizing and discussing the results. The discussion will be presented in the same order in which the findings were presented in Chapter 4:

- Discussion on the SIS results including: ranking of realisations, identification of potential upside and downside mine planning scenarios, comparison of simulated results and the IK model and finally calculated volumetric differences in expected higher grade material between the simulated volumes, IK model volumes and stope volumes;
- discussion on the DBSim results including: ranking of realisations, identification of potential upside and downside mine planning scenarios, and comparisons between the simulated gold distributions and the IK model, and
- finally, a discussion on the results for the model of joint uncertainty including: ranking of joint simulations and comparisons between simulated grades and the deterministic kriged model and expected grades using the current stope design.

The Chapter concludes with a summary of the findings. The main and subsidiary research questions will be answered in Chapter 6 based on the assessment of geological uncertainty presented in this Chapter.

5.1 Summary of Research Problem

The aim of the research was to assist Geita in their decisions regarding underground mining. As part of the research, simulations were required to highlight uncertainty in expected grade and tonnes expected for underground operations. Deterministic kriged models are ill-suited to studies requiring an assessment of risk, because only a single outcome value for grade is output. Stochastic simulations were therefore used as an alternative. The results of the study (Chapter 4) will be used by the mine to consider the current business case supporting underground mining, from a risk-informed perspective. These considerations formed the three fundamental research questions addressed in the research. The first of these questions pertained to the applicability of stochastic ore body modelling to studies involving geological uncertainty. Based on the findings of stochastic ore body modelling, the next research question was posed: could the knowledge revealed in realisations assist in highlighting underlying geological risk? And if so, could this information be used to make risk informed mine planning decisions? The final question to be answered involved understanding how to incorporate stochastic ore body models into mine design and planning.

5.2 Assessing geological uncertainty

The SIS result findings suggested that the simulated realisations did not show sufficient ore category allocation consistency in the targeted areas. The findings for the simulated grades, conversely displayed good grade allocation consistency in the targeted areas. The variability revealed in the simulations can be used to improve the current understanding of the deposit and to reduce potential geological risk that may exist in the deterministic model. By incorporating the simulated knowledge into planning decisions, Mining Engineers can get closer to producing optimal mine designs and the likelihood of making an inaccurate statement of expected resources for underground mining can be reduced.

5.3 Assessing volumetric uncertainty using SIS

Underground mine planning requires a well-informed geological model of the geometry of the high-grade lenses. The kriged resource model was developed from manual interpretations of the drill hole data and represent a single deterministic description of the geological controls of the higher grade lenses. The SIS techniques approached this problem probabilistically to produce a stochastic image of the potential geometric shapes of the lenses, as described in Chapter 3. The technique demonstrated multiple ore lense geometrical configurations that were used together with the IK model for the lenses to study the impact of volumetric uncertainty on resource estimates for underground mining.

5.3.1 Ranking of SIS Realisations

The SIS realisations were ranked in ascending order of volumetric ratio of high grade material (indicator=1) relative to low grade ore (indicator=0). The ranking does not consider the 3D configuration of blocks. Instead, the global proportion of higher grade material for each realisation was calculated. Differences in volumes and the uncertainty arising thereof can be assessed in relation to corresponding regions in the simulated and kriged model where conditioning data is available.

5.3.2 Potential upside and downside mine planning scenarios

The realisation having rank=50 was found to contain the largest volume of high grade material, and the smallest volume was found in the realisation having rank=1. In general, the upside potential scenarios identified higher grade lenses GHEE and GHEW inside or in close proximity to the IK wireframe. An exception to this was found in Figure 4-9, where visually the scenario representing the upside potential, contained less higher grade material in the informed area, as compared to the same downside scenario. This highlights the point raised above, that the rankings account for global proportions and that to assess the volumetric uncertainty, both the IK wireframe, available sample data and the kriged model be used in conjunction.

5.3.3 Comparison between the IK model and SIS realisations

Cross sections through the simulated deposit for GHEE (Figure 4-2) and GHEW (Figure 4-8) were drawn in areas with good data coverage. The sections indicated that for both GHEE (Figure 4-3 to Figure 4-7) and GHEW (Figure 4-9 to Figure 4-15), visually, the continuity of the high grade lenses reduced, with occasionally more regular boundaries than displayed by the IK model. The realisations provided a stochastic image of potential lense shapes, whose boundary variability gives an indication of potential volumetric uncertainty.

For GHEE (Figure 4-3 to Figure 4-7), the realisations depicted the connectivity of the high grade lenses as being less continuous along strike, suggesting that the lenses occur as discrete zones. Figure 4-7 indicated that lenses of mineralization can be detected in areas not defined by the IK wireframe. Because simulations do not provide an accurate answer for where the lenses occur, but only the likelihood of occurrence. In parts of the deposit, where simulations failed to detect lenses possibly due to insufficient volumes for definitive shapes, the available drillhole information can be used to confirm the presence of high grade material and to motivate for more drilling.

Similarly for GHEW (Figure 4-3 to Figure 4-7), the lenses were less continuous than the IK wireframe suggests, but with better connectivity. The transitions between the higher grade and lower grade facies were softer and could be the result, of the support of information used being larger for the eastern area. Blocks in the model which lacked drill hole information were not considered with a high degree of confidence because of the absence of conditioning information. They also occur in areas not currently targeted for underground mining.

5.3.4 Calculated volumetric differences

The difference in simulated volumes for the scenarios were compared. The IK wireframe volume covered the extent of both GHEE and GHEW and contained an expected a very large high grade volume (value omitted due to privacy). If the scenarios for GHEW and GHEE are considered together, the tonnage indicated by the IK wireframe can be anticipated. However, caution must be exercised when considering the SIS results, because it accounts for the spatial variation of

observed data at sampled locations as well as the variation in estimates at unsampled locations (Deutsch 2006), which makes it more suited for making an assessment of variations in local rather than global volumes of material. The IK algorithm, on the other hand, provides only a single location of uncertainty which is open to smoothing effects due to the dependence of kriging (Goovaerts, 1997). The results indicate that the poor continuity and connectivity of the high grade lenses could be the reason for expecting smaller volumes of material, but also that where large volumes are expected, this could be because of global volumes used in ranking. The IK wireframe was observed to unrealistically correlate the high grade ore. Therefore, when used in combination, in the areas of interest, it was found that the volumes are potentially less than indicated on the kriged resource model.

5.4 Assessing grade uncertainty using DBSim

A better understanding of the geometry of the high grade lenses can be obtained by examining the distribution of gold grades within them. The kriged resource model represents a single deterministic description of the grades and may be open to smoothing effects of Kriging, described in Chapter 2. The SIS technique generated multiple realisations for higher and lower grades independently, because of the decision to separate the conditioning data into lower and higher grade populations. This was done to reduce possible smoothing relating to the Gaussian assumptions required for DBSim. Therefore, grade uncertainty was assessed from the model of joint uncertainty that considers the higher and lower grade realisations simultaneously.

The resultant realisations were used to study the impact of grade uncertainty on resource estimates for underground mining.

5.4.1 Ranking of DBSim Realisations

The DBSim realisations were ranked in ascending order of total metal content. This was done for higher and lower grade simulations for each domain. As with SIS, the ranking did not consider the 3D configuration of simulated blocks. However, in the case of the grade simulations, each realisation generated a

simulated grade for common areas in the model making the results more meaningful.

5.4.2 Potential upside and downside mine planning scenarios

The differences in scenarios for GHEE higher and lower grade realisations was small. The same is noted for the upside and downside scenarios for GHEW realisations for higher and lower grades. However, when comparing the results between higher and lower grade simulations for each domain, the effect of grade uncertainty is highlighted. By only considering higher grades, the realisations may predict many more millions of ounces of gold compared to the lower grade realisations. This shows how sensitive the models can be to grade uncertainty, especially if results are biased toward the lower or higher grades.

5.4.3 Comparison between the IK model and DBSim realisations

The higher and lower grade, potential upside and downside scenarios were presented as cross sections through the deposit for GHEE (Figure 4-16) and GHEW (Figure 4-21). The higher grade simulations were also displayed against the IK wireframe for the deposit to understand the distribution of higher grades. For GHEE (Figure 4-17 to Figure 4-20), visually, it was noticed that the distribution of the simulated high grades, were less extensive than indicated by the IK wireframe. The simulations did not smooth results between neighboring drillholes. In the case of GHEW (Figure 4-22 to Figure 4-25), the distribution of the simulated high grades tended toward being more extensive than indicated by the IK wireframe. The lower grade simulations showed the same behavior as their higher grade counterparts. All realisations picked up the in-situ variability of the conditioning data and illustrated that variations in grade distributions makes it necessary to consider geological uncertainty. To assess the actual grade uncertainty, the ranked lower and higher grade simulations need to be considered together. This is discussed in the next section.

5.5 Assessing grade uncertainty from the model of joint uncertainty

To fully characterise potential risk from geological uncertainty, it is best practice to simultaneously assess ore category and grade simulations. However, this may

involve incorrect constraining of grade simulations based on the results of ore category realisations. The model of joint uncertainty presented may also be prone to such problems, because it depends on the ability of the SIS realisations to realistically represent the underlying spatial patterns observed in the deposit. Despite this, models of joint uncertainty are necessary to be able to assess the higher and lower grade simulations in a single model, and to also allow for more informed grade allocation to simulated blocks. The joint model considers the multiple ore lense geometrical configurations obtained through SIS, to assign simulated grades from the higher and lower grade DBSim realisations. This model provides a simple way to study the impact of geological uncertainty on resource estimates for underground mining.

5.5.1 Ranking of Joint Realisations

To combine the SIS and DBSim realisations, the SIS simulation grid was upscaled to fit into the 10m x 10m x 3,33m grid blocks established for DBSim. The DBSim realisations for lower and higher grades were combined according to order of rank for GHEE and GHEW. Next the models were linked to the ranked SIS realisations for the relevant study areas. Final grades were then assigned to the model based on the ranking.

5.5.2 Comparison between potential upside and downside mine planning scenarios and deterministic kriged model

Due to the manner in which the realisations were combined, it was not necessary to compare upside and downside scenarios for SIS. Arbitrary cross sections were selected through the deposit (Figure 4-26) to compare the simulations with the kriged model. The results (Figure 4-26 to Figure 4-30) showed that in comparison to the kriged model, the simulations were able to capture the in-situ grade variability. The distribution of grades in the kriged model was smoothed, with higher grades occurring as large continuous zones. The effect of smoothing in the kriged model was also evident in areas that did not contain any sample data. In contrast, the simulations did not smear out the higher grades in uninformed areas (Figure 4-27 to Figure 4-30). The results suggest that any mine planning based

on the kriged model, will present a high degree of risk due to smoothed estimates that potentially over-represent the higher grade populations in the deposit.

5.5.3 Comparison between potential upside and downside mine planning scenarios and proposed stope layout

The proposed stope layouts are designed around the high grade areas in the kriged model. As discussed above, the kriged model overstates the continuity of the higher grades. A comparison between the simulated grades and planned stopes was presented using sections through the model of joint uncertainty (Figure 4-31). The cross sections presented for GHEE (Figure 4-40 to Figure 4-47), suggested that the stopes were incorrectly situated to access higher grade ore. This however, was deemed as a result of the grade allocation being restricted to the SIS realisations for GHEE, which did not show good connectivity. In light of the DBSim realisations for the same areas, it is noted that the stopes are adequately located. For GHEW (Figure 4-32 to Figure 4-39), the stopes show adequate coverage to access high grade material. It is therefore repeated here, that all simulations be regarded in conjunction to avoid basing decisions on partial truth - The stopes are designed to access the lenses, and if the designs are informed by the simulations, care should be taken do not consider the SIS and DBSim realisations in isolation. The reason for this is that if only the SIS realisations are considered, stopes may not be designed large enough to access the lenses. Conversely, if only the DBSim realisations are considered the stopes may be designed too wide. In those areas where adequate sample information is available, and the simulations and kriged model show comparable grades, the mine may consider with higher confidence for planning purposes.

5.5.4 General research findings

Journel, A.G., 1985, pp 1, states: “A model choice and its properties must be judged on its efficiency in capturing and solving the problem at hand”. This applies strongly to the decisions that need to be made when selecting conditioning data. By definition, conditional simulations require input of all the available data. However, the simulations were found to be highly sensitive to data domaining. The research showed that separating the data into its higher and lower grade

populations was necessary to better constrain the high grade lenses. The simulated realisations honoured the data values at their respective locations and the data domaining prevented smoothing that result from the Gaussian assumptions necessary for DBSim.

Another observation that warrants discussion regards the choice of variogram models and support of data. To correctly simulate any deposit, substantial testing is required to ensure that conditioning data and variogram models used, are appropriate to meet the needs of the study. After transforming gold grades into indicator variables, the variogram models for SIS were calculated in ISATIS. When the theoretical variogram models were fitted to the experimental variograms, the ranges were too short to capture the connectivity of the high grade lenses. Despite passing the validation process (Section 3.5.1.2), the realisations were found to be noisy and meaningless (Figure 3-14). The experimental data was then fitted with model variograms that did not model the calculated data well, but instead honoured the knowledge of the geology of the deposit. The spatial correlation captured in the realisations improved, but the data connectivity in the Z direction remained poor. Attempts to adjust the simulation parameters, specifically through modification of the search applied in the Z direction, still did not reduce the noise in the realisations (Figure 3-15). SIS doesn't account for the support of data used, therefore it cannot make necessary changes in support as performed in DBSim. The difference in support here, specifically deals with the difference in sample size and simulation grid size. To overcome this, different composite lengths were tested for the data using the modified model variograms. The adjustment in composite length for GHEE, from 1m to 3m, produced more representative simulations. For GHEW, the change in composite length from 1m to 3m, left insufficient information to inform the simulations resulting in poor connectivity in the Z direction. As a result, a 1m composite was used together with the modified variogram model and produced more representative results.

5.6 Conclusion

Simulations are a proven way to assess geological uncertainty, but do not replace useful additional data nor the need for common sense. DBSim can be used for mapping grade distributions whereas SIS and IK are useful tools for describing the geometry of the feature of interest. The results indicated that the volume and total metal of high grade material expected for underground mining, is more discontinuous than that represented by the current business case high grade wireframes. The stope layout was found to be largely well positioned to access the high grade lenses. It should be noted that the support size used in the simulation is smaller than the kriged panel size but equal to the support as used in the Uniform conditioned models that the company employed in the final business case . Using the summary of findings presented in this Chapter, final research conclusions will be given in Chapter 6.

CHAPTER 6

"All knowledge resolves itself into probability. ... In every judgment, which we can form concerning probability, as well as concerning knowledge, we ought always to correct the first judgment deriv'd from the nature of the object, by another judgment, deriv'd from the nature of the understanding"

-David Hume

In A treatise of Human Nature (1888), p. 181-182.

6 CONCLUSIONS AND RECOMMENDATIONS

The aim of this study was to identify suitable stochastic orebody modelling techniques that can be used to assess geological volume and grade uncertainty at the Geita gold reef deposit in Tanzania. Stochastic simulations of grade and lithology formed part of the pre-feasibility studies regarding underground mining at Geita. The current business case supporting underground mining is centred around the interpretation of high grade lenses in the deterministic kriged model for the deposit. This estimate is then post processed to yield a UC estimate into a 10m x 10m x3.33m smu size. The results for the ore category and grade simulations were used in conjunction to help the mine evaluate the business case for the development of an underground mine from a risk-informed perspective. The workflow proposed in the research, is the first application of stochastic orebody modelling at Geita Hill and involves the use of Sequential Indicator Simulations and Direct Block Simulations to quantify volumetric and grade uncertainty respectively. The workflow can however be adapted to any similar deposits to produce more realistic models that account for geological uncertainty to allow for risk-informed decision making. This Chapter provides answers to the three fundamental research questions facing the mine outlined in Chapter 1.

These objectives are presented according to their original formulation in separate subsections. The Chapter provides appropriate recommendations and conclusions, in light of the theoretical subject matter presented (Chapter 1-3), as well as the findings made in the research results and discussion (Chapter 4 and Chapter 5). The chapter is concluded with suggestions for further research.

6.1 Research question 1: “Can stochasticsimulations of the geological ore body modelbe used to assess the uncertainty associated with identifying high grade lenses within the known lower grade mineralisation at Geita Mine?”

Yes. The gap in knowledge about geological uncertainty in deterministic models as a result of using conventional risk analysis at Geita Hill, was addressed in this study using stochastic simulations. Kriged models cannot account for geological uncertainty because they are unable to capture the true complexity and in-situ variability of the geological phenomena under study, resulting in misleading MREs and poorly informed mine planning expectations. Unless a deposit is drilled sufficiently to provide adequate confidence in terms of grade distribution and the position of geological contacts, there may be manyinterpretationsof the data and geological models of the ore body as there are geologists. Furthermore, a single, often smoothedversion of grade distribution is produced from kriged models which by definition cannot account for geological uncertainty. Such models pose risk to mine planning decisions. The research applied stochastic simulation techniques that use all the geological information from drill holes in a recursive manner to produce multiple equiprobable orebody realisations of the spatial arrangement of the geology, each conditioned by the same data. Like conventional estimation methods, it was found that simulations also require sufficient data to be accurate. The choice of stochastic algorithm and its success require a good practical and theoretical understanding of the underlying assumptions and mathematics of the available methods as well as their applicability to the geology. But unlike the deterministic kriged model of the deposit, simulations enhanced the variability of the data (deposit) allowing for an assessment of geological uncertainty.

In this way it was possible to assess the uncertainty associated with the spatial distribution of grades of the high grade lenses. Underground mine planning requires a well-informed geological model of the geometry of the high-grade lenses. The kriged resource model was developed from manual interpretations of the drill hole data and represent a single deterministic description of the geological controls of the higher grade lenses. The SIS techniques approached this problem probabilistically to produce a stochastic image of the potential geometric shapes of the lenses. The technique demonstrated multiple ore lenses geometrical

configurations that were used together with the IK model for the lenses to study the impact of volumetric uncertainty on resource estimates for underground mining. The simulated results indicated that the connectivity of the high grade lenses was less continuous along strike but due to the poor reproduction of variograms along strike it cannot be conclusively deducted that the lenses terminate abruptly. Rather than occurring as large continuous zones as shown by the IK wireframe, which was observed to unrealistically lump together the high grade ore. Therefore, when used in combination, in the areas of interest, it was found that visually the volumes are less than indicated in the kriged resource model.

In addition to better understanding the geometry of the high grade lenses, Direct Block Simulations were used to characterise the uncertainty of the distribution of grades within the lenses. Multiple realisations for higher and lower grades were generated independently and grade uncertainty assessed from a model of joint uncertainty. The results showed that in comparison to kriged model, the simulations were able to capture the in-situ grade variability. The distribution of grades in the kriged model was smoothed, with higher grades depicted as occurring in large continuous zones. The effect of smoothing in the kriged model was also evident in areas that did not contain any sample data. In contrast, the simulations did not smear out the higher grades in uninformed areas. The results suggested that any mine planning based on the kriged model, will be present a high degree of risk due to smoothed estimates that over-represent the higher grade populations in the deposit.

Therefore, stochastic simulations of the geological ore body model canbe used to quantify the uncertainty associated with identifying high grade lenses within the known lower grade mineralisation at Geita Mine.

6.2 Research question 2: “Can this knowledge (from 6.1) be used to make a risk-informed decision on whether or not to develop an underground mining operation?”

Yes. The current business case for underground mining is based on a kriged model for the deposit. The kriged model is a deterministic mathematical model that outputs a single prediction for values at unsampled locations, ignoring random

variation i.e. in-situ grade variability and material type distribution. Since random variation is not incorporated in the model, the risk associated with the uncertainty embedded in the interpretation of geological boundaries and estimated grades, cannot be assessed using deterministic methods.Any geological uncertainty in the model because of incomplete knowledge about the deposit, erodes the validity of the model if incorrect assumptions are drawn from the availabledrilling data. Since deterministic models provide a single, possibly incorrect model, of the true distribution of the deposit, it is not possible to use deterministic models in studies involving risk. The SIS and DBSim realisations provided alternative versions of reality to describethepossiblenature of the same deposit, which allows for risk-informed decision making. This was achieved in the research through identification of potential upside and downside mine planning scenarios for volume and total metal. Through the assessment of the scenarios, relative to the kriged model, it was possible to consider worst and best case scenarios, and thus allow for risk informed decision making.

The improved understanding of the deposit, from stochastic simulations, can be used to make risk-informed decisions. The ultimate decision is based on the mine's appetite for risk. Rather than a single deterministic value, the simulations provided a range of estimated grades and volumes that reflect the geological uncertainty. In this way expectations about potential upside and downside scenarios were accounted for and allowed the problem of associated risk to be quantified. Using this knowledge, the mine can make risk informed decisions.

6.3 Research question 3: "Can uncertainty about the ore body model be incorporated in planning and designing stope layouts to access the high grade lenses in the underground mine?

Yes. Failure to meet production targets is strongly linked to over-estimation of metal grades and volumes derived from kriged resource models on which mine designs, production schedules and expectations about NPV are based. The problem of constructing accurate geological models with which to constrain mineral resource estimates is compounded because of geological uncertainty. Where the deterministic resource model carries a high degree of geological uncertainty, geological risk is introduced into mine designs, production schedules

and predictions of NPV, resulting in unrealistic expectations about the rates of production. Stochastic simulations were used to represent the in-situ variability of metal grades and potential production volumes. The study compared the use of SIS to establish the shapes and locations of high grade lensesoccurring within the known low grade mineralisation and DBSim to assess their associated grade variability. The results indicated that the volumes expected for underground mining is less than stated in the current business case for underground mining based on the deterministic model. The simulated realisations were evaluated relative to stope layouts. The research found that the simulated grades and volume of higher grade material, occur close to, or within the current stope designs, indicating that the location of the proposed stopes is suitably positioned to access the high grade lenses.

In terms of incorporating uncertainty into the stope designs, one would need to consider SIS and DBSim realisations jointly to avoid laying out stopes that are too large (if only using DBSim) or too conservative (if only using SIS). The uncertainty can be evaluated to improve stope layouts to avoid understating or overstating the potential value of the project, hence losing the opportunity to support an underground mine.

6.4 Limitations and Recommendations

This research was conducted as part of the COSMO scholarship using data supplied by AngloGold Ashanti. The understanding of simulation software and applicability of the algorithms to the deposit required considerable time for testing. As a result, only those algorithms deemed to provide meaningful results, in the limited time in which to conduct a study of this nature, were considered. As such, more representative techniques such as Multiple-point statistics may be used but require considerable time for testing. It is therefore recommended that this approach be followed up in future work to better delineate the shapes and locations of the high grade lenses.

It is also recommended that a sensitivity analysis be conducted on the support of conditioning data used, because of the observed effects on the connectivity and continuity in resultant realisations. A final recommendation is to repeat the study without using deterministic (modelled) shapes for the high grade lenses as these

could bias the results. Although the study focused on highlighting the risk involved with Geita Mine using a deterministic model for mine planning, the business case at the time of completion of the research was based on a Uniform Conditioned (UC) model. Since the Uniform Conditioned model cannot quantify risk, the approach in this research provides a risk based model alternative. It is therefore recommended that further work involve comparing the joint simulations with grade-tonnage curves for the UC model.

6.5 Conclusion

Mining companies have traditionally used deterministic kriged models for mine planning. However, these models provide only a single, and often incorrect description of the characteristics of the spatial patterns in a deposit, because they do not account for in-situ material type and grade variability. As an alternative to the conventional kriged models which do not provide any insights into the uncertainty of estimates, stochastic simulation techniquescanassist and guide mine planning under geological uncertainty,by providing a means for quantifying the uncertainty associated with planning decisions.

To apply simulation techniques correctly, it is critical that the user understand the fundamentals underlying the algorithm. However, the field of stochastic simulations tends to be dominated by academics, computer programmers, operations research specialists and mathematicians, who are not the main users on mine sites. This is most likely the why many mines still using deterministic models in decision making.The true value of this areas of research, lies in the ability to firstly, successfully apply stochastic techniques to real deposits in the mining industry. Secondly, they need to be presented in a way that Resource Geologists and Mining Engineers can apply easily and meaningfully.

From a practical standpoint, the research highlighted that implementation of the techniques, using real datasets, requires the knowledge of a geologist to get admissible and appropriate stochastic realisations. The workflow developed in the dissertation focused more on the understanding of the geostatistical modelling choices rather than the mathematics underlying the algorithms. The research is the first application of SIS and DBSim for stochastic orebody modelling at Geita Mine. The framework established, allows for a practical application of stochastic

simulations to make risk-qualified decisions that consider the underlying geological risk allowing forimproved mine designs, production planning and valuation of mining projects.The contributions made by this study, will therefore be of interest to mining companies with similar deposit types, who require a simple workflow to undertake similar studies involving geological uncertainty.

APPENDIX A: HISTOGRAM VALIDATION

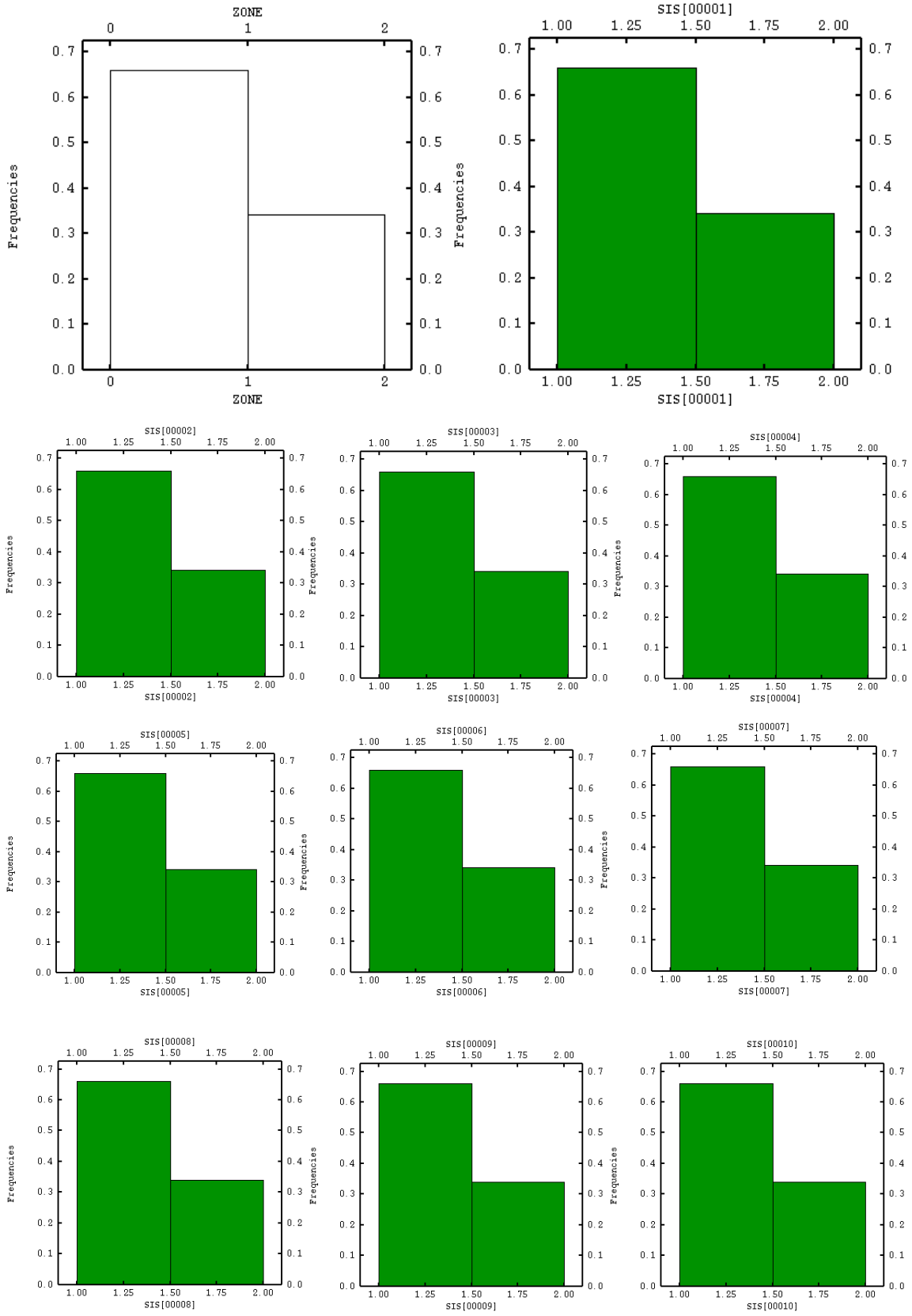


Figure A-1: East SIS histogram reproduction

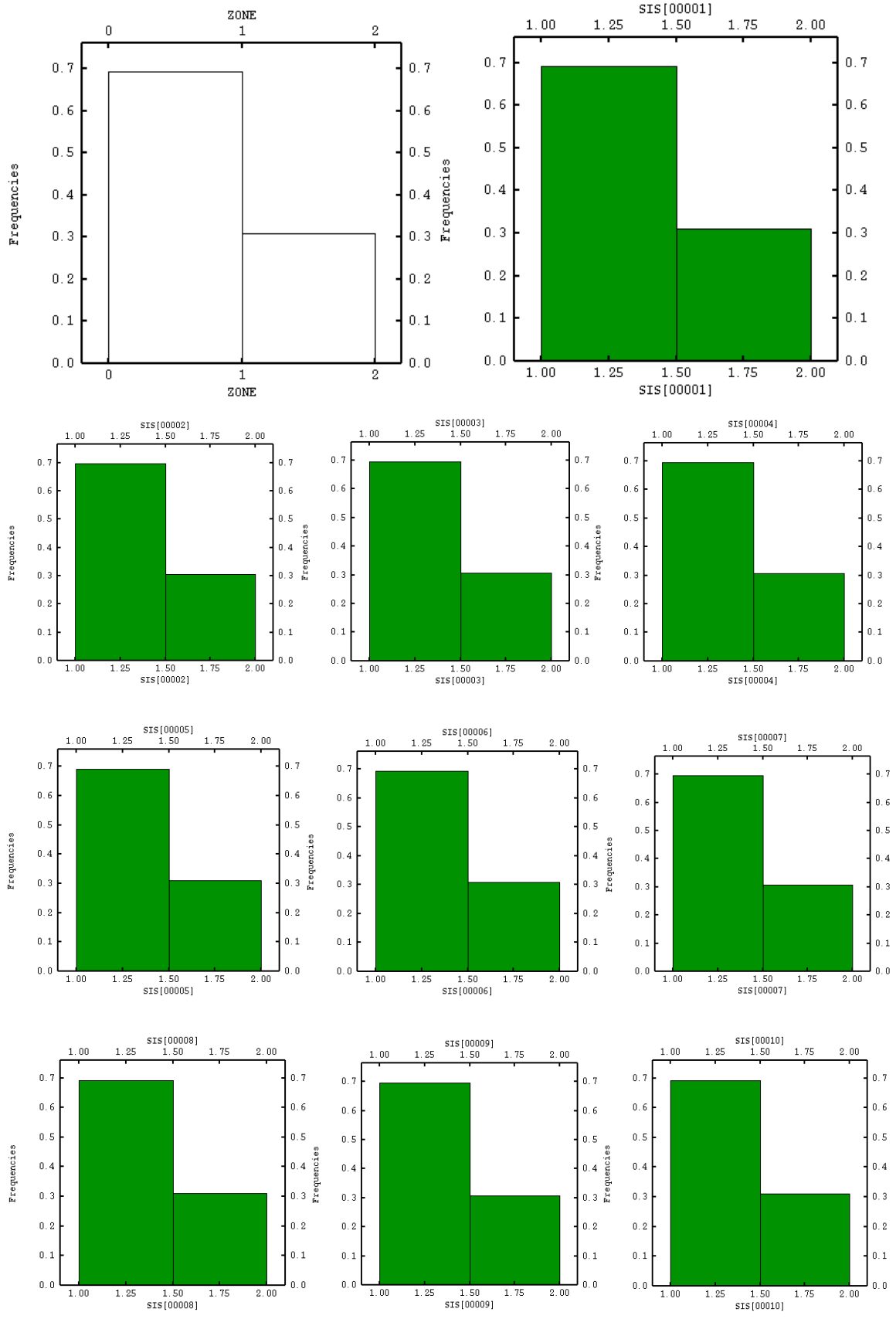


Figure A-2: West SIS histogram reproduction

REFERENCES

Boucher, A., & Dimitrakopoulos, R. (2009). Block simulation of Multiple Corrrelated Variables. *Mathematical Geosciences, 41*, 215-237.

Boucher, A., Felipe Costa, J., Gustavo Rasera, L., & Motta, E. (2014). Simulation of Geological Contacts from Interpreted Geological Model Using Multiple-Point Statistics. *Mathematical Geoscience, 46*, 561-572.

Caers, J., & Arpat, B. (2007). Conditional Simulation with Patterns. *Mathematical Geology, 39*(2), 177-201.

Caers, J., & Journel, A. (1998). Stochastic reservoir simulation using neural networks trained on outcrop data: Society of Petroleum Engineers Annual Technical Conference and Exhibition, New Orleans (September 27-30), SPR Paper 49026, 16p

Chanderman, L. (2015). *3D Geological Modelling and Mineral Resource Estimate for the FE2 Deposit - Sadiola Mine, Mali.* Johannesburg: Masters Thesis submitted to the School of Mining Engineering University of Witwatersrand.

Chiles, J.-P., & Delfiner, P. (1999). *Geostatistics: Modeling Spatial Uncertainty.* New York: Wiley-Interscience Publication.

Coombes, J., Thomas, G., Glacken, I., & Snowden, V. (2016, October 10). *http://citeseerx.ist.psu.edu.* Retrieved from citeseerx: http://citeseerx.ist.psu.edu/viewdoc/download?doi=10.1.1.115.6973&rep=rep1&type=pdf

Costa, J. F., Zingano, A. C., & Koppe, C. J. (2000). Simulation — An Approach to Risk Analysis in Coal Mining. *Exploration Mining Geology, 9*(1), 43-49.

Cressie, N. (1990). The Origins of Kriging. *Mathematical Geology, 22*(3), 239-252.

Deloitte. (2015). *www.deloitte.com/mining.* Retrieved May 05, 2016, from https://www2.deloitte.com/content/dam/Deloitte/global/Documents/Energy-and-Resources/gx-er-tracking-the-trends-2016.pdf

Deraisme, J., Rivoirard, J., & Castelli, P. C. (2008). Multivariate Uniform Conditioning and Block Simulations with Discrete Gaussian Model: Application to Chuquicamata Deposit. *Geostats .* Santiago, Chile.

Deutsch, C. V. (1992). PhD Thesis: Annealing techniques applied to reservoir modeling and the integration of geological and engineering (well test) data. Retrieved January 11, 2016, from http://citeseerx.ist.psu.edu/viewdoc/download?doi=10.1.1.330.7685&rep=rep1&type=pdf

Deutsch, C. V. (2006). A sequential indicator simulation program for categorical variables with point and block data: BlockSIS. *Elsevier, Computers and Geosciences 32*, 1669-1681.

Deutsch, C. V. (2006). A sequential indicator simulation program for categorical variables with point and block data: BlockSIS. *Computers and Geosciences*, 1669-1681. Retrieved October 31, 2016

Deutsch, C. V., & Journel, A. G. (1998). *GSLIB: Geostatistical Software Library and User's Guide.* New York: Oxford University Press.

Deutsch, C., Askari-Nasab, H., & Koushavand, B. (2009). *Transfer of Geological Uncertainty through Mine Planning.* CCG Annual Report 11.

Dimitrakopoulos, R. (1990). Conditional Simulation of Intrinsic Random Functions of Order k. *Mathematical Geology, 22*(3), 361-380.

Dimitrakopoulos, R. (1998). Conditional Simulation Algorithms for Modelling Orebody Uncertainty in Open Pit Optimisation. *International Journal of Surface Mining, 12*(4), 173-178.

Dimitrakopoulos, R. (2011). Stochastic Optimisation for Strategic Mine Planning: A Decade of Developments. *Journal of Mining Science, 47*(2), 138-150.

Dimitrakopoulos, R., & Benndorf, J. (2005). New Efficient Methods for Conditional Simulation of Large Orebodies. *Orebody Modelling and Strategic Mine Planning, 14*, 61-67.

Dimitrakopoulos, R., & Luo, X. (2004, July). Generalized Sequential Gaussian Simulation on Group size v and Screen-effect Approximations for Large Field Simulations. *Mathematical Geology, 36*(5), 567-591.

Dimitrakopoulos, R., Mustapha, H., & Gloaguen, E. (2010). High-order Statistics of Spatial Random Fields: Exploring Spatial Cumulants for Modeling Complex Non-Gaussian and Non-linear Phenomena. *Mathematical Geosciences, 42*, 65-99.

Emery, X. (2008). Change of Support for Estimating Local Block Grade Distributions. *Mathematical Geosciences, 40*(6), 671-688. Retrieved from http://repositorio.uchile.cl/bitstream/handle/2250/125161/Emery_Xavie.pdf?sequence=1

Goodfellow, R. (2012, February). Quantifying multi-element and volumetric uncertainty, Coleman McCreedy deposit, Ontario, Canada. *Computers & Geosciencs*, pp. 71-78.

Goovaerts, P. (1997). *Geostatistics for natural resources evaluation.* USA: Oxford University Press.

Guardiano, F., & Srivastava, M. (n.d.). Multivariate geostatistics: beyond bivariate moments. In *Geostatistics-Troia.* (pp. 133-144). Amsterdam: Kluwer Academic.

Hansen, K. M. (1992). *The Use of Sequential Indicator Simulation to Characterise Geostatistical Uncertainty.* Albuquerque: Sandia National Laboratories.

He, Y., Chen, D., Li, B. G., Huang, Y. F., Hu, K. L., Li, Y., & Willett, I. R. (2009). Sequential indicator simulation and indicator kriging estimation of 3-dimensional soil textures. *Australian Journal of Soil Research, 47*, 622–631. doi:10.1071/SR08218

Isaaks, H. E., & Srivastava, M. (1989). *Applied Geostatistics.* Oxford University Press

Journel, A. (1983). Nonparametric Estimation of Spatial Distributions. *Mathematical Geology, 15*(3), 445-468.

Journel, A. (1985). The Deterministic Side of Geostatistics. *Mathematical Geology, 17*(1), 1-15.

Journel, A. (1993). Geostatistics: Roadblocks and challenges. *Geostatistics Troia '92, vol 1*, 179-199

Kleingeld, W., & Ossterveld, M. (1989). Researching Local Reserve Estimates for a Sporadic, Discrete Particles Deposit. In M. Amstrong, & D. M. Armstrong (Ed.), *Geostatistics: Proceedings of the Third International Geostatistics Congress September 5–9, 1988, Avignon, France* (Vol. 4, pp. 347-358). Fontainebleau, France: Springer Netherlands. doi:10.1007/978-94-015-6844-9_26

Lindsay, M., Jessell, M., De Kemp, E., Betts, P., & Ailleres, L. (2010). Integrating geological uncertainty into combined geological and potential field inversions. Orleans.

Liu, Y. (2006). Using the Snesim program for multiple-point statistical simulation. *Computers and Geosciences, 32*, 1544-1563.

Matheron, G. (1973). The Intrinsic Random Functions and their Applications. *Advanced Applied Probability, 5*, 439-468.

Matheron, G., & Kleingeld, W. (1987). The Evolution of Geostatistics. *South African Institute of Mining and Metallurgy, 3*, 9-12.

McNeil, J. (2015). MSc. Thesis: A stochastic optimization formulation for the transition from open-pit to underground mining. Montreal.

mining-technology.com. (2015). *www.mining-technology.com*. Retrieved January 12, 2015, from http://www.mining-technology.com/projects/sadiola-gold-mine-mali/

Mirowski, P. W., Tetzlaff, D. M., Davies, R. C., McCormick, D. S., Williams, N., & Signer, C. (2009). Stationarity Scores on Training Images for Multipoint Geostatistics. *Mathematical Geosciences, 41*, 447-474.

Mustapha, H., & Dimitrkopoulos, R. (2010). A new approach for geological pattern recognition using high-order spatial cumulants. *Computers & Geosciences, 36*, 313-334.

Myers, D. E. (2016, 06 12). *Choosing and Using Simulation Algorithms*. Retrieved from www.scholar.google.co.za: http://www.fs.fed.us/rm/pubs_rm/rm_gtr277/rm_gtr277_023_029.pdf

Sanislav, I. V., Brayshaw, M., Kolling, S. L., Dirks, P. H., Cook, Y. A., & Blenkinsop, T. G. (2016, May 24). *The structural history and mineralization controls of the world-class Geita Hill gold deposit, Geita Greenstone Belt, Tanzania.* Retrieved September 9, 2016, from www.researchgate.net: https://www.researchgate.net/publication/303507191_The_structural_history_and_mineralization_controls_of_the_world-class_Geita_Hill_gold_deposit_Geita_Greenstone_Belt_Tanzania

Strategic Mine Planning under Uncertainty: A D. (n.d.).

Strebelle, S. (2002). Conditional Simulation of Complex Geological Structures Using Multiple-Point Statistics. *Mathematical Geology, 34*(1), 1-21.

Strebelle, S. (2002). Conditional Simulation of Complex Geological Structures Using Multiple-Point Statistics. *Mathematical Geology, 34*(1), 1-20.

Strebelle, S. (2012). Multiple-Point Geostatistics: from Theory to Practice. Oslo, Norway: Ninth International Geostatistics Congress.

Srivastava, M. (2013). Geostatistics: A toolkit for data analysis, spatial prediction and risk. *International Journal of Coal Geology, 112*, 2-13.

Tran, T. T. (1994). Improving variogram production on dense simulation grids. *Computers and Geosciences, 20*(7/8), 1161-1168.

Van den Boogaart, K. (2006). Some theory for Multiple Point Statistics: Fitting, checking and optimally exploiting the training image. Belgium: Int. Assoc. for Mathematical Geology.

Vann, J., Bertoli, O., & Jackson, S. (2002). An Overview of Geostatistical Simulation for Quantifying Risk. Western Australia: Geostatistical Association of Australasia symposium.

Webster, R., & Oliver, M. (2014). A tutorial guide to geostatistics: Computing and modelling variograms. *Catena, 113*, 56-69.

Yamamoto , J. K., Landim, P. M., Kikuda, A. T., Leite, C. B., & Lopez, S. D. (2015). Post-processing of sequential indicator simulation realizations for modeling geologic bodies. *Computers and Geosciences, 19*, 257-266. doi: 10.1007/s10596-014-9465-4